Torque Transfer System for offshore Turret Production System

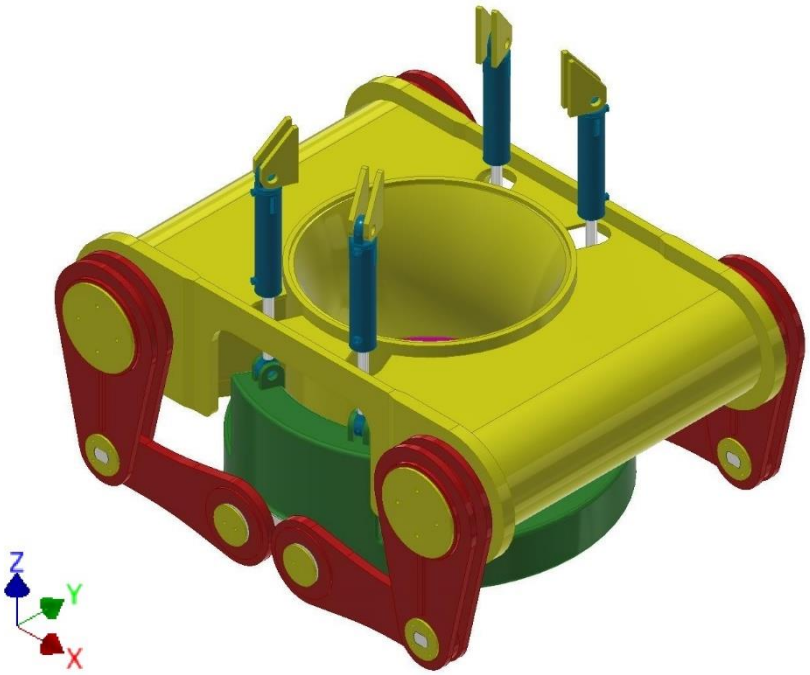

(BW Offshore, 2019a)

Odd-Gunnar Valborgland

Spring of 2020

Page left blank intentionally.

University of Stavanger

FACULTY OF SCIENCE AND TECHNOLOGY

MASTER'S THESIS

Study programme/specialization: Engineering Structures and Materials with specialization in Mechanical Systems	Spring semester, 2020 Open
Author: Valborgland, Odd-Gunnar	Odd-Gunnar Valborgland
Programme coordinator: Teigen Giljarhus, Knut Erik Faculty supervisor: Lemu, Hirpa Gelgele External supervisor: Holm, Espen	
Title of master's thesis: Torque Transfer System for offshore Turret Production System	
Credits: 30 ECTS	
Keywords: - Floating, Production, Storage and Offloading - Turret Production System - Torsional transmission - Finite Element Analysis - Ultimate Limit State - Fatigue Limit State - Accidental Limit State	Number of pages: 133 + supplemental material/other: 20 Grimstad, 12th of June 2020

Title page for Master's Thesis
Faculty of Science and Technology

Page left blank intentionally.

Preface

This thesis represents the final part of the master's degree in Engineering Structures and Materials with specialization in Mechanical Systems at the University of Stavanger. The thesis is written during the spring of 2020 in cooperation with BW Offshore, a company that provides floating production services for the oil and gas industry.

I would like to express my deepest gratitude to my faculty supervisor Professor Hirpa Gelgele Lemu for his support and guidance.

A huge thanks to BW Offshore supervisor Espen Holm for constructive advice and comments on my work. A special thanks to Vidar Berg Pedersen in BW Offshore for technical consultation and productive discussions. I would also like to express my appreciation to Morten Kilen, Hans Høegh-Omdal and Anders Lia, in BW Offshore.

For matters regarding Ansys software, I would like to thank Senior Engineer Adugna Deressa Akessa at the University of Stavanger. In addition, thanks to the IT department at the University of Stavanger, for being especially helpful setting up off-campus Ansys license on my personal computer, during the special times of the Covid-19 pandemic.

Finally, I would like to express gratitude to my family, friends and fellow students, for encouragement and rewarding discussions regarding my work.

I sincerely hope and believe that this work shall benefit BW Offshore in developing the torque transfer system for offshore turret production system.

Grimstad, 12th of June 2020

Odd-Gunnar Valborgland

Abstract

Turret production systems allow Floating Production Storage and Offloading (FPSO) units to weathervane and thus significantly reduce environmental loads on the mooring system. There are several different variants of such mooring systems, and some can be disconnected in case of ice bergs or cyclones coming into proximity of the FPSO. BW Offshore have developed a new solution, called the torque transfer system, for connecting and transferring rotational movement from the disconnectable buoy/turret to the production system inside the FPSO. The torque transfer system shall also transfer frictional torque from the production system, release all other Degrees of Freedom (DoF) and accommodate all inherent tolerances.

This thesis aimed to determine if structural integrity is fulfilled based on the applicable standard, considering Ultimate Limit State (ULS), Fatigue Limit State (FLS) and Accidental Limit State (ALS) conditions.

Comprehensive principal and technical description of the system were conducted to fully comprehend the functionality. Static assessment of the system formed the basis for the analyses. Components, system activation, redundancy system, maintenance and allowable positional adjustments, are also described in detail.

Through Finite Element Analysis (FEA) and hand calculations, the initial torque transfer system was found to fulfill ULS condition. However, two regions with stress concentration close to material strength capacity were identified. Hence, implementing geometry optimization was proposed that proved to reduce the stress concentrations. This optimized geometry was consequently used in the rest of the thesis work, as ULS forms the basis for FLS, ALS and sensitivity study. FLS condition was also fulfilled and fatigue fracture shall not occur during operational lifetime of the system. The system was found to withstand maximum ALS loading of 1.5 times the ULS design torque. The sensitivity study proved that positional adjustment of the components, leading to an unsymmetrical system, still resulted in ULS condition to be fulfilled.

As a result of the analyses, a few improvements to the system were recommenced. And it is believed that the optimized torque transfer system will fulfill all applicable demands for offshore steel structures and ease operation of turret production systems in FPSO units.

Table of Contents

List of Figures

List of Tables

Abbreviations

The following abbreviations are used in this thesis:

ALS	Accidental Limit State
CAD	Computer Aided Design
CFD	Computational Fluid Dynamics
DFF	Design Fatigue Factor
DoF	Degree of Freedom
ESD	Emergency Shutdown
FBD	Free-Body Diagram
FEA	Finite Element Analysis
FLS	Fatigue Limit State
FPSO	Floating Production Storage and Offloading
FSO	Floating Storage and Offloading
Hex20	20-node hexagonal
LRFD	Load and Resistance Factor Design
PLEM	Pipeline End Manifold
PTFE	Polytetrafluoroethylene
SLS	Serviceability Limit State
STEP	Standard for the Exchange of Product Data
SURF	Subsea Umbilical Riser Flowline
SUTA	Subsea Umbilical Termination Assembly
Tet10	10-node tetrahedron
ULS	Ultimate Limit State
WBS	Work Breakdown Structure
Wed15	15-node pentagonal/wedge

Nomenclature

The following symbols are used in the calculations in this thesis:

A_A	Axle cross-sectional area
A_{CF}	Contact face area in torsion ring
A_H	Cross-sectional area of central pipe section of shaft
A_H	Cross-sectional area of hub
A_{HA}	Tear-out area in horizontal arms
A_{HC}	Internal bore area of hydraulic cylinders
A_{TR_A}	Cross-sectional area of connection joint for horizontal arms in torsion ring
A_{VA}	Cross-sectional area of vertical arm below hub
B_{VA}	Width of vertical arm cross-section
b_{VA}	Combined flange width of vertical arm cross-section
c	Maximum distance to outer surface
c_H	Maximum distance to outer surface of hub
c_S	Maximum distance to outer surface of shaft
D	Deformation load
d	Size of member exposed to fatigue
d_A	Axle diameter
d_B	Inner diameter of shaft bearing
DFF	Design Fatigue Factor
D_H	Spline hub outer diameter
d_H	Spline hub inner diameter
D_H	Outer diameter of hub
d_H	Inner diameter of hub
d_{HC}	Internal bore diameter of hydraulic cylinders
D_L	Bearing race diameter
d_S	Inner diameter of central pipe section in shaft
D_S	Outer diameter of central pipe section in shaft
D_S	Outer diameter of shaft
d_S	Inner diameter of shaft
d_{TR}	Inner diameter of contact face in torsion ring
d_{TR_A}	Diameter of connection joint for horizontal arms in torsion ring
E	Environmental load or Young's modulus/modulus of elasticity

F	Reaction force
F_a	Axial load
F_d	Design load
F_{g_HC}	Total force capacity of hydraulic cylinders
F_k	Characteristic load
F_r	Radial load
F_{TR}	Applied load in torsion ring
F_x	X-component reaction force
F_{x_A}	Reaction x-component force in torque transfer arms
F_{x_B}	Reaction x-component force in shaft bearings
F_{x_S}	Reaction x-component force in round bars (spline connections)
G	Permanent load or shear modulus/modulus of rigidity
H_{VA}	Height of vertical arm cross-section
h_{VA}	Height between flanges of vertical arm cross-section
I_H	Second-area moment of spline hub
I_H	Second-area moment of hub
I_S	Second-area moment of shaft
J_H	Polar second moment of area in spline hub
J_H	Polar second moment of area in hub
J_S	Polar second moment of area
J_S	Polar second moment of area in shaft
k	Combined modification factor
k_a	Surface modification factor
k_b	Size modification factor
L	Length exposed to torque/torsion
l_B	Length of shaft bearing
l_{VA_w}	Web length of vertical arm cross-section
M	Reaction moment
M_k	Resulting tilting moment
M_r	Starting moment
M_y	Reaction moment around y-axis
M_{y_S}	Reaction moment around y-axis in round bars (spline connections)
M_z	Reaction moment around z-axis

M_{z_B}	Reaction moment around z-axis in shaft bearings
M_{z_D}	Design moment around z-axis applied to the torque transfer system
M_{z_S}	Reaction moment around z-axis in round bars (spline connections)
n_d	Fatigue design cycles
n_{YR}	Number of full loading cycles per year
P_{HC}	Pressure capacity of hydraulic cylinders
P_{TR}	Applied pressure at contact face in torsion ring
P_{TR_FLS}	Applied pressure for FLS in torsion ring
Q	Variable functional load
R_d	Design resistance
R_H	Hub radius in vertical arm
R_{HA_r}	Outer radius of rear horizontal arms
S_d	Design load effect
T	Applied torque/torsion
t_{HA}	Horizontal arms thickness
t_{VA_f}	Flange length of vertical arm cross-section
t_{VA_w}	Web thickness of vertical arm cross-section
t_{YR}	Number of design years of operational service
u_A	Utilization of tear-off shear stress capacity in axle
u_H	Utilization of equivalent stress capacity in spline hub
u_H	Utilization of equivalent stress capacity in hub
u_{HA}	Utilization of shear stress capacity in horizontal arms
u_{HA_a}	Utilization of equivalent stress capacity in horizontal arms
u_S	Utilization of equivalent stress capacity in shaft
u_{TR_A}	Utilization of shear stress capacity in connection joint for horizontal arms in torsion ring
u_{VA}	Utilization of equivalent stress capacity in vertical arm below hub
W_{gm}	Geostationary module weight
W_s	Swivel core weight
W_{y_VA}	Section modulus of cross-section in vertical arm below hub
x_A	X-distance between connection joints of horizontal arm
x_{def_S}	Relative deformation in shaft
y_B	Y-distance between shaft bearings and round bars (spline connections)

y_S	Y-distance between shaft bearings
y_{TR}	Y-distance between torsion ring connection joints
z_A	Z-distance between connection joints of vertical arm
z_{VA_H}	Distance from load to max. stress location at cross-section in vertical arm
γ_f	Load factor
γ_M	Material factor
θ_S	Angle of twist in shaft
μ	Friction coefficient
ν	Poisson's ratio
σ_B	Shaft bearing pressure
σ_{cap}	Equivalent stress capacity
σ_{HA}	Axial stress in horizontal arm
σ_{max_H}	Maximum bending stress in spline hub
σ_{max_H}	Maximum bending stress in hub
σ_{max_S}	Maximum bending stress in shaft
σ_{UTS}	Material ultimate tensile strength
σ_{VA}	Bending stress in vertical arm below hub
σ_{VM}	Equivalent Von Mises stress for uniaxial state
σ_{VM_H}	Equivalent Von Mises stress in spline hub
σ_{VM_H}	Equivalent Von Mises stress in hub
σ_{VM_S}	Equivalent Von Mises stress in shaft
σ_{VM_VA}	Equivalent Von Mises stress in vertical arm below hub
σ_x	Rectangular x-component of stress
σ_{YS}	Material yield strength
τ_A	Axle tear-off shear stress
τ_{cap}	Shear stress capacity
τ_H	Shear stress from shear force in spline hub
τ_H	Shear stress from shear force in hub
τ_{HA}	Tear-out shear stress in horizontal arms
τ_{max_H}	Maximum shear stress from applied torsion in spline hub
τ_{max_H}	Maximum shear stress from applied torsion in hub
τ_{max_S}	Maximum shear stress from applied torsion in shaft
τ_{tot_S}	Total shear stress in spline hub

τ_{TR_A}	Shear stress in connection joint for horizontal arms in torsion ring
τ_{VA}	Shear stress in vertical arm below hub
τ_{xy}	Rectangular xy-component of shear stress
φ	Resistance factor

1 Introduction

Background information on turret production system, torque transfer system, BW Offshore and FPSO units, are described in order comprehend the functionality and need for floating production solutions. Further, the specific objectives addressed in the thesis are stated. Lastly, the thesis structure is described.

1.1 Background

BW Offshore have conducted concept engineering for a buoy, turret, mooring, swivel and Subsea Umbilical Riser Flowline (SURF) system for a new FPSO unit. This is called the turret production system, and a new design for a torque transfer system is now being developed into this system. Hence, fully structural verification analyses need to be conducted to assure structural integrity.

The complete swivel and geostationary module, including the torque transfer system, will be installed and integrated into the FPSO at the shipyard in Singapore. The term "geostationary" means in this context at rest in relation to the Earth's surface as opposite to the systems fixed to the vessel, which revolves relative to the Earth.

The buoy/turret/mooring system and the SURF system will be pre-installed on the field. Once the FPSO arrives the field the buoy/turret will be pulled into the ship cone, locked off and connected to the vessel's turret production system.

1.1.1 Turret Production System

The buoy, turret and risers are connected to a swivel unit to permit weathervaning of the FPSO. The concept of weathervaning can be visualized in *Figure 1* (Bluewater, n.d.). Weathervaning is a process of allowing rotation around a pivoting point/axis for a floating structure to adjust the heading in response to shifting environmental loads. Most production systems weathervane passively, i.e. without consuming energy (SBM Offshore, 2020). The entire mooring system including buoy, turret and risers can be disconnected in case of ice bergs or cyclones coming into proximity of the FPSO. This kind of solution is often referred to as a disconnectable internal turret production mooring system. To simplify phrasing, it will only be referred to as "the turret production system" in the rest of the thesis.

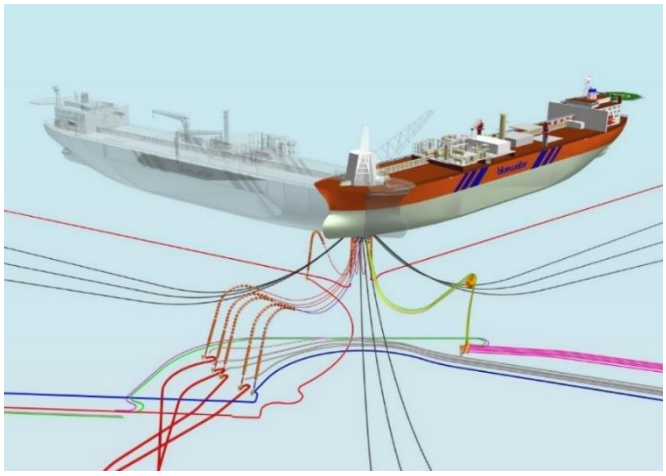

Figure 1 The concept of weathervaning for a FPSO.

During normal operation the turret (with its risers and umbilical), the torque transfer system, the geostationary module and the swivel core, are all rotationally connected to the mooring system and therefore "geostationary" while the rest of the vessel rotates around this system, as seen in *Figure 2*.

The buoy surrounds the turret structure. Dynamic bearing between these two structures allows the turret to rotate relative to the buoy which is fixed to the vessel in the ship cone. Similarly, the geostationary module and the swivel stack is supported on a dynamic bearing, allowing the weight to be transferred to the ship structure and at the same time allow relative rotation between the structures.

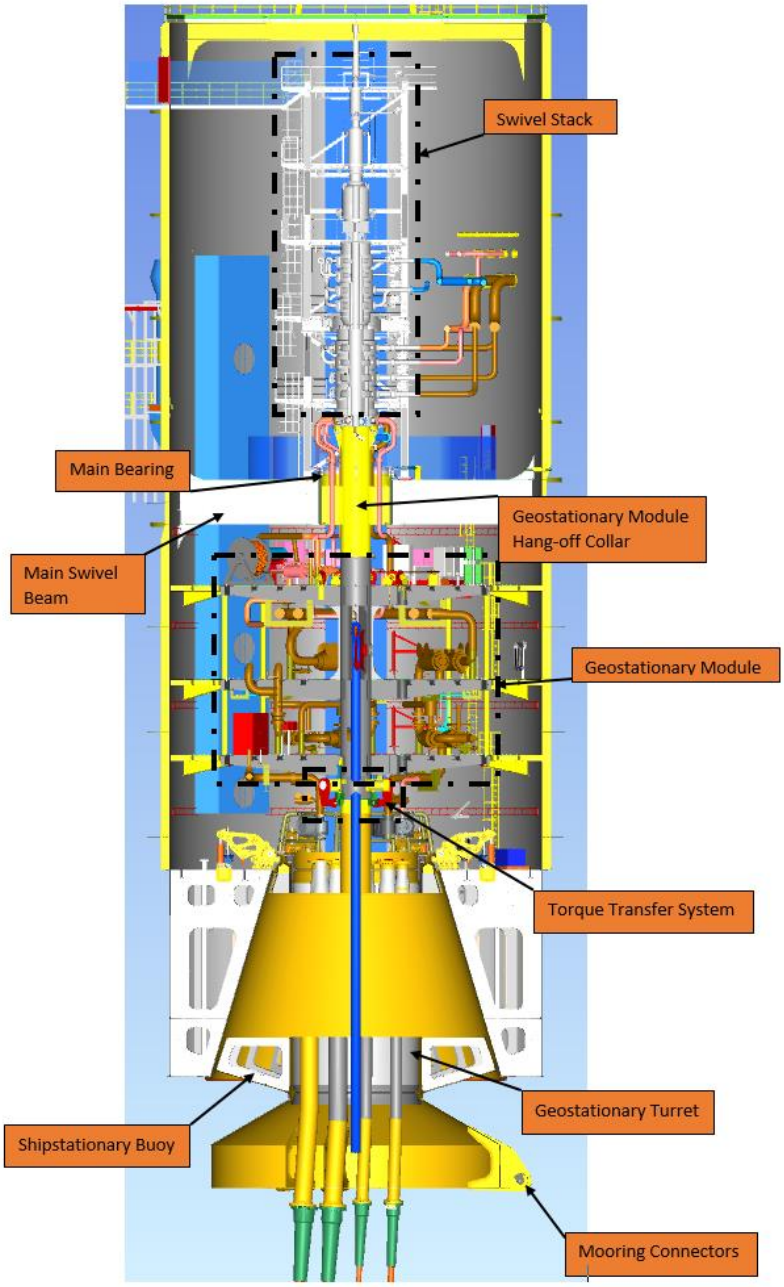

Figure 2 Cross-section of the Turret Production System viewed from the side of the FPSO[1].

[1] Courtesy of BW Offshore.

1.1.2 Torque Transfer System

The torque transfer system is a relatively small, but important part of this turret production system. The purpose of the torque transfer system is to:

1. Transfer the rotational movement from the buoy/turret to the geostationary parts above, i.e. the geostationary module and the swivel unit.
2. Transfer the torque from the friction in the main dynamic roller bearing and the swivel bearing rings.
3. Release all other DoF between the buoy/turret and the geostationary parts above.
4. Accommodate all inherent tolerances in the system from construction and mating of the buoy/turret into the ship cone at the field.

As seen in *Figure 3* the torque transfer system will be located at the bottom of the tube from the geostationary structure and be connected to the buoy/turret torque tube when activated.

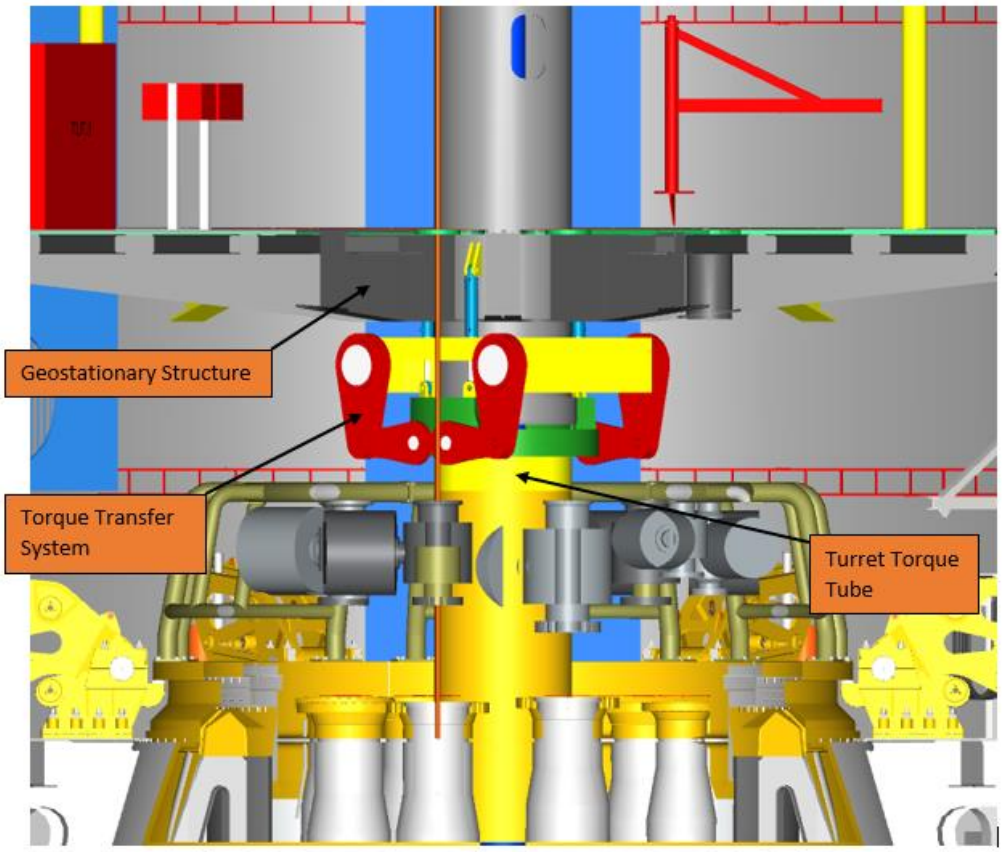

Figure 3 Torque Transfer System placement in offshore Turret Production System[2].

The torque transfer system structure is an assembly of several mechanical parts as seen in *Figure 4*. It shall fulfill the four main purposes that are required for the device. Additionally, the coordinate system in *Figure 4* will remain consistent throughout the thesis.

[2] Courtesy of BW Offshore.

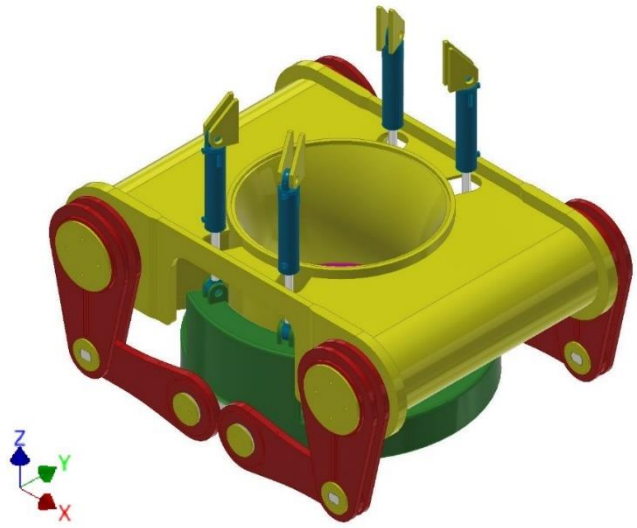

Figure 4 Torque Transfer System structure assembly.

In earlier similar turret production systems, the geostationary module was bolted directly on top of the buoy/turret system. There were two disadvantages with this solution:

1. The geostationary module and swivel had to be skidded a side before pulling the buoy/turret into the ship cone, due to the routing of the pull-in wire.
2. The weight and acceleration load from the geostationary module and swivel were transferred to the buoy/turret, and thus to the locking devices holding it in place, resulting in an increased number of locking devices required.

1.1.3 BW Offshore

This thesis is written in cooperation with the Arendal office of BW Offshore.

BW Offshore Ltd. is a company that provides floating production services for the oil and gas industry. It includes design, fabrication, installation and operation of these FPSOs. Both of new units and conversion of tankers are used for this purpose. The company is represented world-wide with a fleet of 15 owned FPSOs, which is the second largest fleet in the world of such vessels. Since the 1980s, the company have executed 30 FPSO and 10 Floating Storage and Offloading (FSO) projects, with a production track record of more than 30 years. BW Offshore is listed on the Oslo Stock Exchange (BW Offshore, 2020).

The Arendal office of BW Offshore is mainly an in-house specialized team responsible for the mooring, turret, swivel, SURF and installation of these systems. A typical turret production system with mooring and SURF for a FPSO, is illustrated in *Figure 5* (BW Offshore, 2019a). Their services involve projects of spread mooring or turret mooring and permanent or disconnectable. Previously, BW Offshore held the record for the deepest moored FPSO. The BW Pioneer, located in the Gulf of Mexico, is a disconnectable turret moored FPSO at a depth around 2,600 meters (BW Offshore, 2019a).

Figure 5 Internal turret production system, mooring and SURF for a FPSO.

1.1.4 Floating Production Storage and Offloading units

FPSO units are ship-shaped offshore floating oil platforms. They are popular production platforms since they have the main advantage of flexibility, especially with regard to installation, relocation and storage (Lin et al., 2019).

An advantage of floating production systems is that they favor minor or medium size fields, due to reduced upfront investments and less decommissioning cost than for fixed structures. In addition, the vessels can retain some of their value because they can relocate to other fields. For remote, harsh and deep waters, where installation of pipeline can prove to be costly and difficult, usage of a FPSO can be an appropriate alternative. On the other hand, the need for offloading shuttle tankers is a disadvantage with respect to possible oil spill, and production shutdown if the shuttle tankers are unable to offload a vessel's storage. Another advantage using FPSO concepts is that execution schedules are normally shorter than for fixed platform projects, especially so when converting tankers. It is common to convert tankers into FPSOs. However, designing specific FPSO vessels from scratch tend to be more favorable for space utilization. The hull is often made wider to fit bigger crude oil tanks. The topside production facility can also be divided more easily into practical segments optimal for production and maintenance.

A FPSO will receive fluids from a reservoir through flexible risers to allow for offset in positioning movement. The topside production facility will separate water and gas from the oil. Crude oil is then stored in large tanks inside the hull of the FPSO and later offloaded onto shuttle tankers that transport the product onshore for further refining. Unprocessed natural gas and water will be re-injected back into the reservoir to increase the recovery rate. Today, there are approximately 180 FPSOs and 100 FSOs units in operation worldwide (Modec Inc., 2020).

One of the first projects involving floating production and storage solutions was in the early 1970s, when Hamilton Bros. utilized a converted mobile offshore drilling unit to produce oil in the UK sector of the North Sea. However, it is the Brazilian oil company Petrobras that gets the credit for the widespread utilization of these systems in the late 1970s. Lower oil prices and advances in subsea production technology in this period made floating production systems more

economically viable. FPSOs can have several different mooring systems. The first FPSO systems were deployed in shallow and calm waters with taut spread mooring systems (Chakrabarti, 2005).

Taut spread mooring systems

In taut spread mooring, the mooring lines are tensioned and restoring force is provided by the elasticity from the mooring line material. In the latest years, polyester mooring lines are being frequently used since they are more elastic and lighter than the traditional chain mooring lines. Taut spread mooring systems are normally connected at the "four corners" on the vessel's hull and can only be used for vessels with fixed heading. The SURF system is connected to the vessel through a so called "balcony" located on the ship side.

BW Adolo is located at the Dassafu oilfield in Gabon, Africa. It is visualized through a schematic in *Figure 6* (BW Offshore, 2019b), that shows the layout of the subsea installations and mooring system. It is permanently taut spread moored with 4 x 3 mooring lines. Taut spread mooring is used for this vessel since there are favorable environmental conditions offshore West Africa. This solution is less expensive than a turret solution, since it is no requirement to separate the vessel movements form the mooring and subsea systems. Subsea installations are shown, including Pipeline End Manifold (PLEM) and Subsea Umbilical Termination Assembly (SUTA), for the BW Adolo.

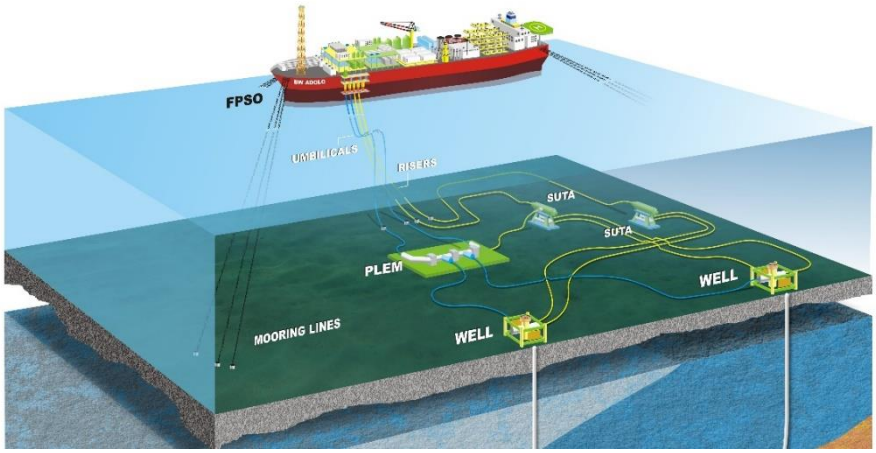

Figure 6 Schematic of BW Adolo FPSO with taut spread mooring system.

More effective mooring systems were developed as FPSOs were designed and constructed for deep water, ultra-deep water (> 1,500 meters depth) and more harsh environments (Chakrabarti, 2005).

Spread catenary mooring systems

Traditionally spread catenary mooring systems are also connected at the "four corners" on the vessel's hull. A catenary configuration means that the mooring line will be slack, in contrary to the tensioned taut spread mooring lines. Chains were first used as mooring lines, but wires soon replaced the free-hanging line to reduce weight and thus loads on the system. Catenary mooring systems provides great stability for the floating structure due to the restoring force through the weight of the catenary. However, large loads on the mooring system occur in harsh

environmental conditions. To overcome these effects, single point mooring solutions were developed (Chakrabarti, 2005).

External turret systems

External turret systems were the first systems to allow weathervaning of FPSOs. In *Figure 7* (NOV APL, 2020) the BW Offshore vessel Berge Helene is shown with a permanent external turret solution. Such a solution is normally less expensive than an internal turret system.

Figure 7 Berge Helene FPSO moored with permanent external turret solution.

However, there are several disadvantages by having the turret externally at the FPSO. The installation process is quite challenging, as the FPSO unit is required to reach the field before installing the mooring lines. The SURF system must then be installed after the vessel is securely moored at site. In addition, shallow water leads to possible mooring line interference with the vessel's bow. Some external turret solutions can be disconnected, and some are permanently moored.

Internal turret systems

Too simplify the installation process and furthermore reduce loads on the vessel, internal turret systems were developed. These permanent systems are both suitable for shallow and deep water. Installation of the mooring and SURF system are also conducted before the FPSO arrives the field, since the turret is surrounded by a buoy and can be pulled into the shipcone. Maintenance and inspection are also easier to conduct inside the vessel, sheltered from environmental conditions.

Disconnectable internal turret systems

In the harshest environmental conditions, solutions for disconnection of the buoy/turret are necessary, to move the FPSO away in case of hurricanes or ice bergs coming into proximity. Disconnectable systems are more expensive than other turret and spread mooring systems. The turret production system featured in this thesis is a disconnectable internal turret system.

To summarize, there exist a vast variety of mooring solutions for FPSOs. As discussed, some allow for weathervaning and some gives geostationary fixed vessels. Some systems are designed for shallow water and some for deep water. The systems can either be located

externally or internally in the vessels. Some are permanently moored, and some can be disconnected. Other solutions also include towers or columns as mooring system (SBM Offshore, 2020).

1.2 Objective

Given the background information the objective of this thesis is to perform a structural integrity analysis with respect to strength, of the torque transfer system for offshore turret production system.

The following three specific objectives will be addressed in the thesis:

1. Conducting principal description of the system
    - Overview
    - Torsional transmission principle
2. Working out the technical description of the system and its components
    - Component description
    - System activation/reactivation
    - Redundancy system: double systems, splines, etc.
3. Conducting strength calculations
    - Design basis: loads, tolerances, etc.
    - FEA
        - ULS
        - FLS
        - ALS
        - Sensitivity study
    - Hand calculations (to support ULS FEA)

Due to the complexity of the system, it is necessary to fully understand and explain the functionality before conducting the strength analyses of the structure. ULS, FLS, ALS and sensitivity study, must all be considered in these analyses.

1.3 Thesis structure

Following this introduction section, which provided background and objective, the thesis is organized as follows. Chapter 2 presents a literature study on similar solutions for turret production systems, two similar FEA theses and one journal article. Chapter 3 gives the principal description with overview, static equilibrium, and torsional transmission principle of the torque transfer system. Chapter 4 explains the rules and regulation, components, activation of the system, redundancy system, maintenance and positional adjustments. Chapter 5 performs design basis for supporting the strength calculations. Chapter 6 defines the approach for each limit state FEA. It involves setup, boundary conditions and other relevant formulations. Results are presented and discussed in chapter 7. Deformation and equivalent stress are examined to determine if each limit states are fulfilled. To finish, the general conclusion and further work are drawn. Finally, appendix is included containing monthly status reports, full Mathcad calculation sheets, Work Breakdown Structure (WBS) and Gantt chart, and assembly drawing of the torque transfer system.

2 Literature study

The oil and gas industry are surrounded by more secrecy and confidentiality than other industries. It means that detailed information regarding similar solutions are more difficult to obtain. In addition, the torque transfer system is believed to be a completely new system, although similar systems are integrated into the swivel. Competitors to BW Offshore in the business of design and construction of disconnectable internal turret production systems, are examined to check for similar solutions. Other structural analysis verifications are also examined, to get an idea of how to structure the thesis. Three brochures, two master theses and one article are reviewed in this chapter.

SBM Offshore supplies systems where the buoy is connected to the internal structure via a collet-type connector or several distributed structural connectors. Collet-type connectors are especially suited to withstand bending stress and separating forces. It seems like their connectors function as the torque transfer system. However, instead of providing allowable movement and accommodate tolerances between buoy/turret and geostationary module, the connection is designed to withstand the large forces (SBM Offshore, 2020).

SOFEC Inc. provides a solution with the geostationary module directly connected to the buoy/turret with a so-called connector with same size as buoy/turret. Hence, it seems like the geostationary system and swivel must be skidded and bolted directly on top of the buoy/turret. The connector have to withstand the large forces and does not seem to accommodate positional movements (SOFEC Inc., 2020).

NOV APL provide a similar solution of a disconnectable offshore turret production system for FPSOs as the previous solution from BW Offshore. However, the geostationary module and swivel is mounted directly on top of the buoy/turret. Hence, the geostationary module and swivel requires to be skidded and bolted in place (NOV APL, 2020).

It seems like most of competitive products still requires the geostationary module and swivel to be mounted directly on top of the buoy/turret and skidded aside, prior to pull in. As a result, the solution holding the system in place must be heavily dimensioned compared to the new solution from BW Offshore. Additionally, none of the examined solutions appear to accommodate positional adjustments of the connection joint. This literature study confirms that the torque transfer system is a new product that some companies seem to not have developed yet.

Helland Andersen (Helland Andersen, 2015) used FEA and Computational Fluid Dynamics (CFD) to verify loads and displacements originating from pressure and temperature differences in tie-in spool pipelines connected to seabed installations during installation and operation. The work reported in this master thesis emphasizes the importance of proper procedure explanation prior to analyzing. Inserting key values into tables and stress distribution screenshots, also provides a clear overview of the findings and should also be applied to this thesis.

Myhre Bøe (Myhre Bøe, 2014) used FEA to examine impact on fatigue life by applying bend stiffeners on mooring lines subjected to bending close to their end terminations. Work conducted in the master thesis shows the importance of proper work before conducting analyses. Thorough simulation setup, model mesh and boundary conditions provide clear

examples on how to perform a well written thesis. Tables of key values and screenshots of stress distribution are also applicable for this thesis.

Lin and colleagues (Lin et al., 2019) used FEA to improve the efficiency and optimization of the hull structure surrounding the turret compartment in the FPSO, which was aimed to find optimal thickness distribution of the turret compartment plate configuration to minimize weight. The work reported in the article shows the importance of explaining general FPSO technology to get a better understanding of how it works and why it is needed. The different load cases supported by hand calculations used in the article is applicable for this thesis.

3 Principal description

The torque transfer system acts as a connection joint and transfer torque between the turret torque tube and the geostationary parts. Torque transfer between the two systems allows for weathervaning of the FPSO while producing hydrocarbons. The torque transfer system consists of two equal and independent systems, which are both designed to withstand the design load single handedly. One system is present in the analyses to verify the structural integrity with respect to the applicable standard (DNV GL, 2019).

This chapter will involve an overview of the applied torque the torque transfer system requires to withstand. Further, a short section on naming of components is included to follow the elaborated descriptions in *Chapter 4.2*. The torsional transmission principle is generally proved through static equilibrium. Finally, specific values are found through these general equations for later use in hand calculations under *Chapter 7.1*.

3.1 Overview

There is 50 mm separation distance between the turret torque tube and geostationary tube, when the buoy/turret are locked off in the ship cone as seen in *Figure 8*.

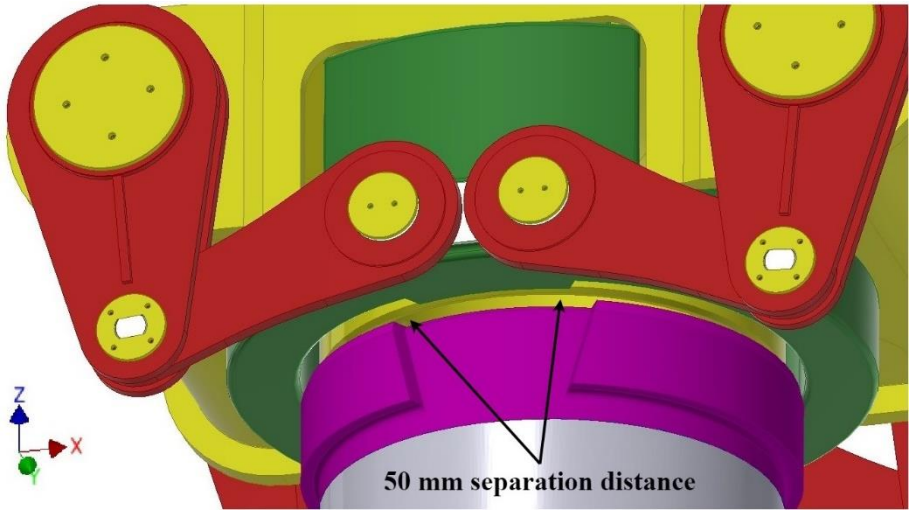

Figure 8 Separation distance between turret torque tube and geostationary module tube.

Before activating the torque transfer system, the two wedges in the torsion ring and turret torque tube must be aligned as seen in *Figure 9 (a)*. When the torsion ring goes over the turret torque tube, the tolerances will be accommodated due to the wedge. It will guide itself in place due to the geometry of the wedge. Finally, the system will be connected and activated as seen in *Figure 9 (b)*.

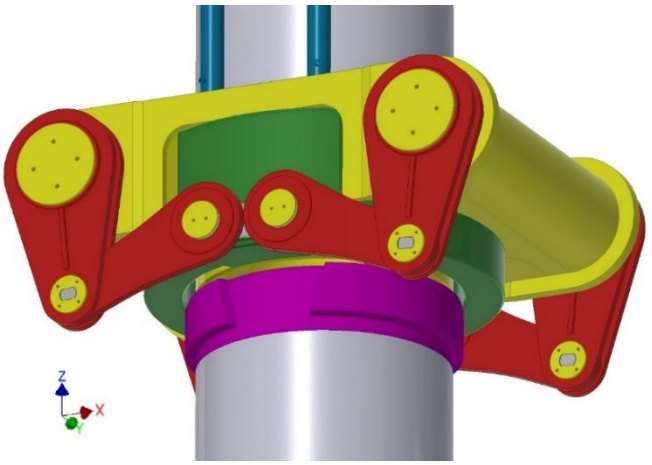

(a)

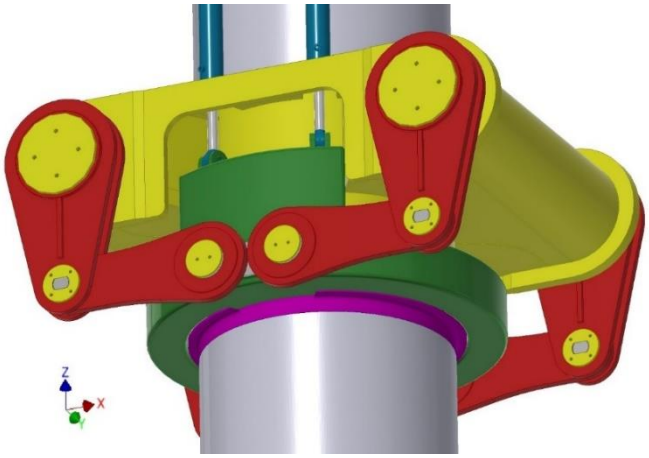

(b)

Figure 9 Torque transfer system when (a) deactivated and (b) activated.

Naming of components is described using figures to clearly state location and name of each component in the torque transfer system. *Figure 10 (a)* shows naming of the visible main components in the system. While *Figure 10 (b)* shows naming for the hidden components with one active system present. The components are more extensively described under *Chapter 4.2*.

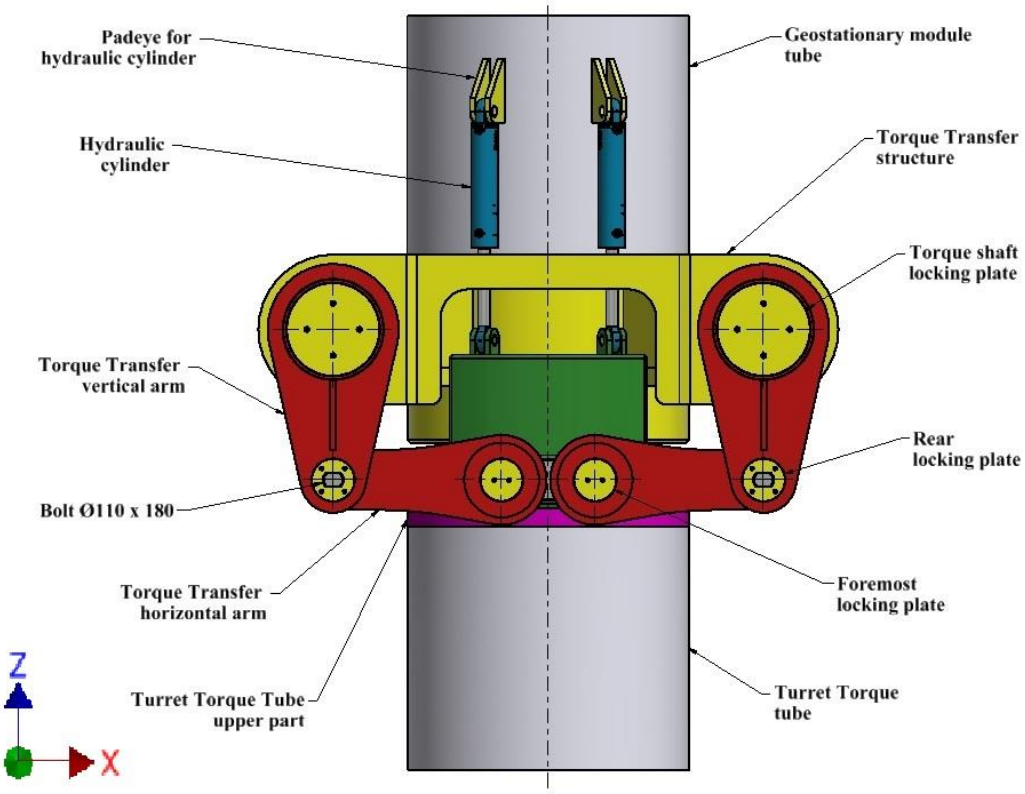

(a)

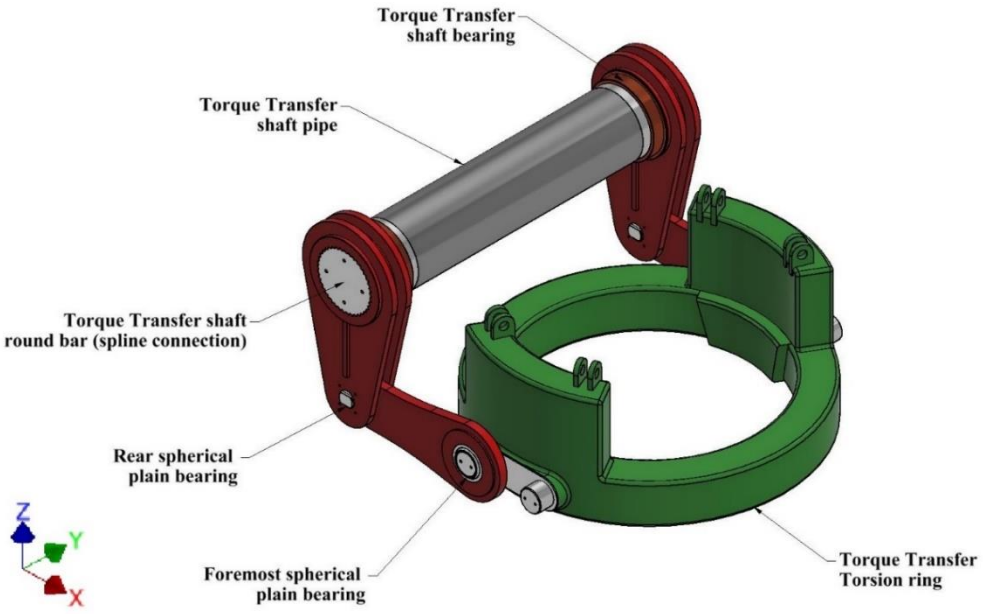

(b)

Figure 10 Component naming in (a) from side and (b) for hidden components with one system.

The torque transfer system with the turret torque tube and geostationary module is presented in *Figure 11*. When the system is activated, the turret torque tube will be connected to the torque transfer torsion ring. Thus, the turret torque tube will become geostationary and provide a torque

transfer to the geostationary parts above. Once activated the risers and umbilicals will be connected to the production system on the geostationary module.

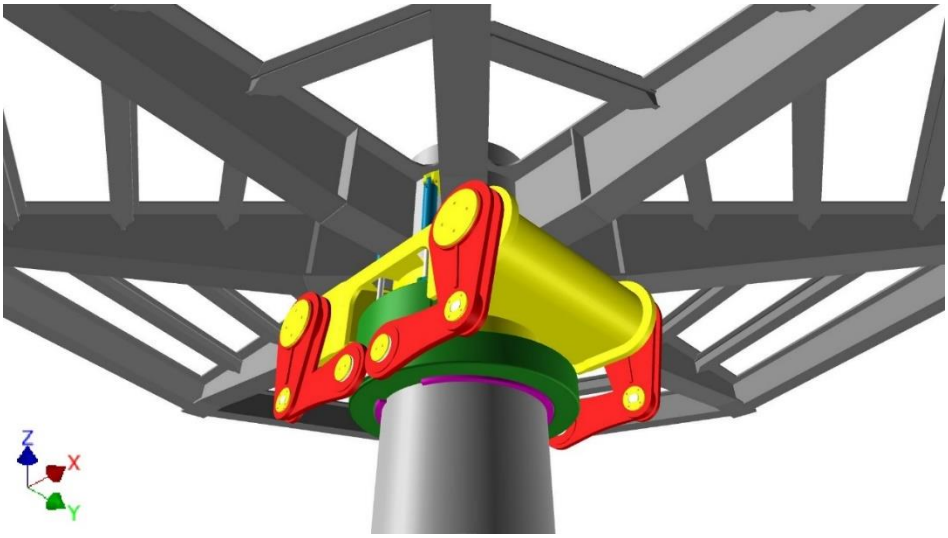

Figure 11 Torque transfer system with turret torque tube and geostationary module.

An overview drawing and description of the turret production system are presented in *Figure 12*. All the red components will be geostationary when the torque transfer system is activated. All the black components will be stationary relative to the FPSO, i.e. ship stationary. The entire vessel will rotate around the central axis. It is also observed that the main swivel beam will take the entire load of the geostationary system, since it will rest on the main bearing.

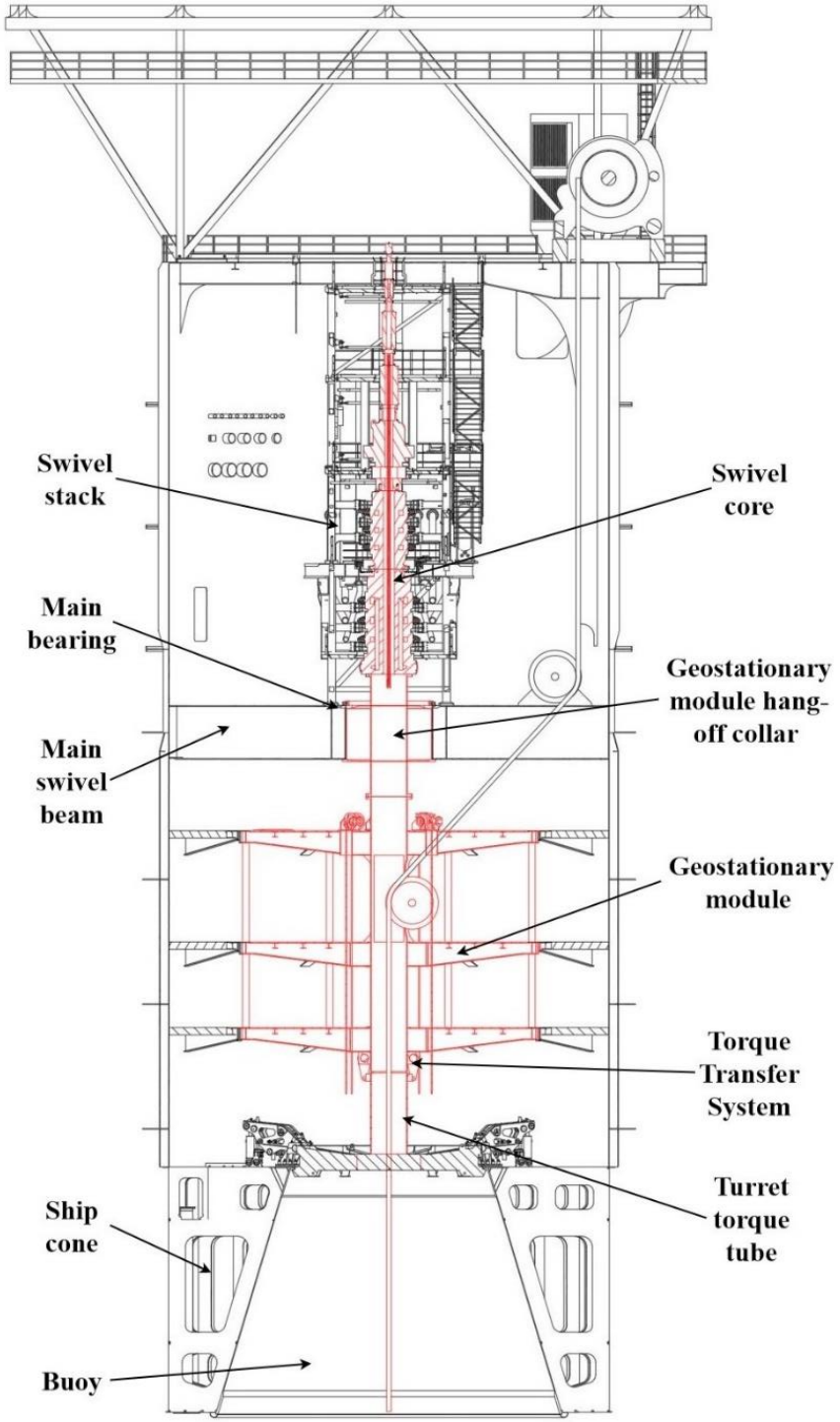

Figure 12 Turret production system description; geostationary parts in red and ship stationary in black.

The entire geostationary system will rest on the main bearing to allow rotation. In addition, the swivel core will provide frictional moments from the swivel stack. The swivel stack will hold the geostationary core with swivel rings connected to arms. Hence, the torque transfer system shall resist a torsional moment of all frictional moments above it, as seen in *Table 1*. Design moment applied to the torque transfer system, M_{z_D}, is 2,400 kNm in total and is calculated based on the following[3]:

[3] Courtesy of BW Offshore.

Table 1 Design moment effect.

Description	Moment (ULS) [kNm]	Moment (ALS) [kNm]	Note
Friction moment from fluid transfer swivel rings	2,000	HOLD	ULS moment provided by swivel supplier
Friction moment from swivel and geostationary module support bearing	200	HOLD	Weight geostationary module: W_{gm} = 4,750 kN (~484 tonnes) Weight swivel core (supported by main bearing): W_s = 1,619 kN (~165 tonnes)
Mass rotational inertia forces from stick slip effect in bearing	200	HOLD	Included as a Dynamic Amplification Factor (DAF) = 1.1
Total torsion moment	**2,400**	HOLD	

Friction moment from the support bearing is calculated from the weight it supports. It is based on theoretical and empirical knowledge provided by the bearing supplier. The support bearing is more precisely defined as a roller bearing slewing ring, and starting torque, M_r, is defined as follows:

$$M_r = \frac{\mu}{2} \bullet (4.1 \bullet M_k + F_a \bullet D_L + 2.2 \bullet F_r \bullet D_L \bullet 1.73) \qquad (1)$$

where μ is friction coefficient, M_k is resulting tilting moment, F_a is axial load, D_L is bearing race diameter and F_r is radial load.

Resulting tilting moment, M_k, and radial load, F_r, are negligible. Hence, only a section of the equation will remain. μ = 0.006 is applicable for this bearing type, D_L = 3,600 mm and F_a = $W_{gm} + W_s$ = 6,369 kN. Inserting the values into equation (1), starting torque will become:

$$M_r = \frac{\mu}{2} \bullet (F_a \bullet D_L) \qquad (2)$$

$$\rightarrow M_r = \frac{0.006}{2} \bullet (6{,}369\ kN \bullet 3{,}600\ mm)$$

$$\rightarrow M_r = 68.8\ kNm$$

Frictional moment from the support bearing will be below 68.8 kNm, but BW Offshore sets it to 200 kNm, just in case.

Friction moment from fluid transfer swivel and mass inertia forces from stick slip effect in bearing, is not specified further then the resulting moments presented in *Table 1*. The applicable values are given by the swivel supplier and bearing supplier. The stick slip effect can be compared to the jerking movement when moving a finger hard across a tablecloth. In similar manner, the geostationary parts will rotate with a start and stop motion, due to the heavy weight of the system and the friction in the main roller bearing.

The torque transfer system has two identical systems, each designed to transfer the entire applied torsional moment. This will allow one of the systems to be disconnected for maintenance and repair, while the turret production system can remain operational and produce hydrocarbons. The two systems will ensure full redundancy of torque transfer. It is difficult to predict the load transfer between the two identical systems due to the fine tolerances in the system. Thus, this is an additional reason for one system being capable of taking the entire applied torque. Frictional moments between the buoy and turret will not be transferred through the torque transfer system.

3.2 Static equilibrium

When studying mechanical systems, it is desirable to study it motionless or have constant velocity, i.e. when the system has zero acceleration. Under this condition the system can be considered as equilibrium state. The term “static equilibrium” is normally used to describe that the system is at rest. To achieve equilibrium, the sum of force vectors and moment vectors in all three dimensional directions acting on the system, needs to be zero (Budyans and Nisbett, 2015).

Complex structures are usually simplified to Free-Body Diagram (FBD) or “stick models”. By isolating each component, it can be examined using these models. However, it is important to evaluate the structure with adequate boundary conditions. The objective is to break complicated problems into manageable subsegments and evaluate them in broader context at a later stage. They must also simplify the complexity and explain the thoughts clearly and unambiguously to the receiver of the information. In addition, the diagrams shall set up mathematical relations and show all forces, so the receiver follows the reasoning (Budyans and Nisbett, 2015).

In a dynamic system, a node’s DoF allow for movements of elements relative to one another. DoF can be present at nodes where independent translational and/or rotational motions exist. A node can maximum have six DoF; three translational and three rotational. If no DoF is present in a certain translational or rotational direction, it will rather result in a reaction force (Budyans and Nisbett, 2015).

3.3 Torsional transmission principle

This chapter will feature static equilibrium in general terms, while *Chapter 3.3.1* will calculate the exact reaction force and moment values for later use in *Chapter 7.1* for hand calculations. The horizontal arm, vertical arm and shaft are also considered in general terms before concluding the combined system. The spherical bearings in the horizontal arms will transfer the torque moment into approximately pure axial reaction forces with associated arms as seen in *Figure 13*. The movable components will be supported at the shaft bearings.

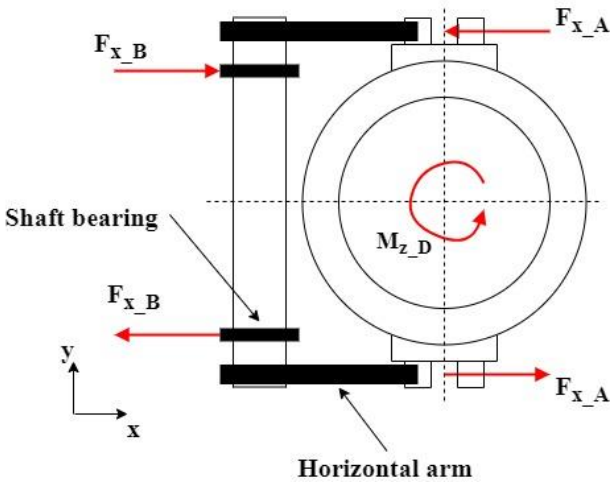

Figure 13 Support forces in shaft bearings and reaction forces in horizontal arms seen from above.

The torque transfer system can be considered as a simple stick model, to illustrate the transmission principle and prove static equilibrium. The simplification in *Figure 14* shows the nodes/joints, i.e. spherical bearings, spline connection and shaft bearings, and elements, i.e. arms, shaft and torsion ring. The torsion ring is visualized as a line to simplify the geometry, but still provide connectiveness between the horizontal arms. Both material elasticity and symmetry are assumed in static equilibrium.

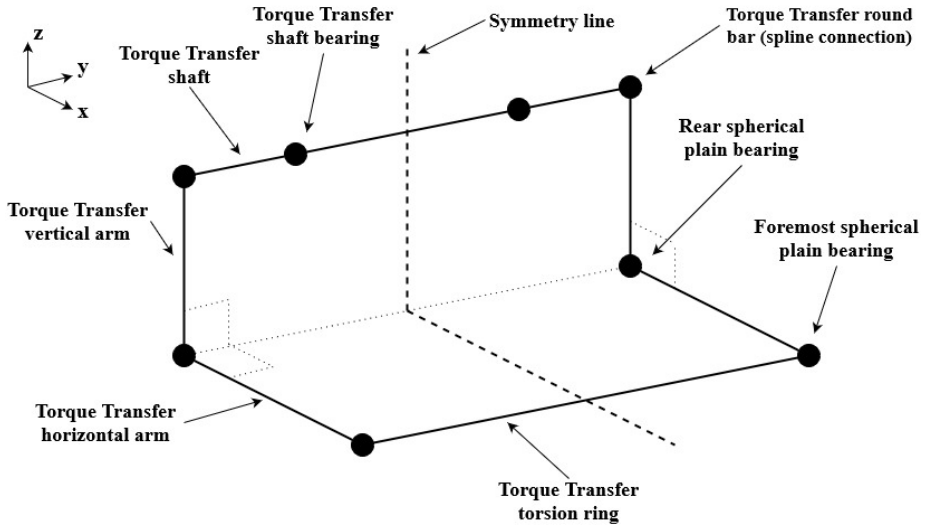

Figure 14 Torque Transfer System FBD explanation.

The hydraulic cylinders at the torsion ring move in z-direction to activate the system and adjust for tolerances. They will only support the self-weight of some of the parts and hold them in position. Hence, the hydraulic supports are negligible in terms of the static equilibrium and are considered disconnected. Thus, gravity is also negligible when proving static equilibrium.

The spherical plain bearings located in both sides of the horizontal arms will provide DoF in all three rotational directions. It means that they can provide reaction forces in all three translation directions.

The two shaft bearings only have one DoF, in rotation about the y-axis. It means that the two other rotational directions, in addition to all three translational directions, can provide reaction forces.

The shaft round bar (spline connection) will be considered as fixed to the shaft. Hence, it will have no DoF. Reaction forces can be present in all three rotational and all three translational directions at that connection point.

Torque transfer horizontal arm

There is no moment present in the horizontal arm as it is only exposed to pure axial force in x-direction from the applied torque as seen in *Figure 15*. One of the sides containing a horizontal arm is visualized in the figure, whereas the other arm will have reaction force in opposite direction and be exposed to compression.

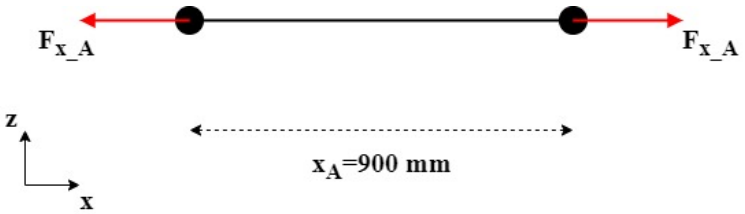

Figure 15 Horizontal arm stick model.

Torque transfer vertical arm

Due to the axial load in the horizontal arm, the vertical arm will be subjected to bending moment in the spline connection as well as a reaction force as seen in *Figure 16*. One of the sides containing a vertical arm is visualized in the figure, whereas the other side will have reaction forces and moments in opposite direction.

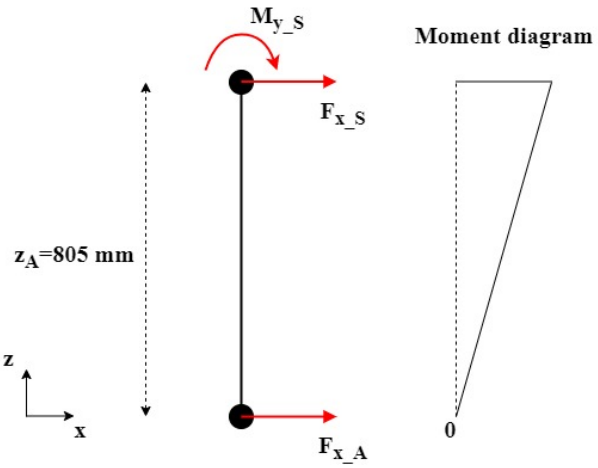

Figure 16 Vertical arm stick model, including moment diagram.

Torque transfer shaft

The shaft will be subjected to both bending and torsional moments, as well as reaction forces as seen in *Figure 17* (dimensions are not to scale). The shaft is seen from above and only bending moments are included.

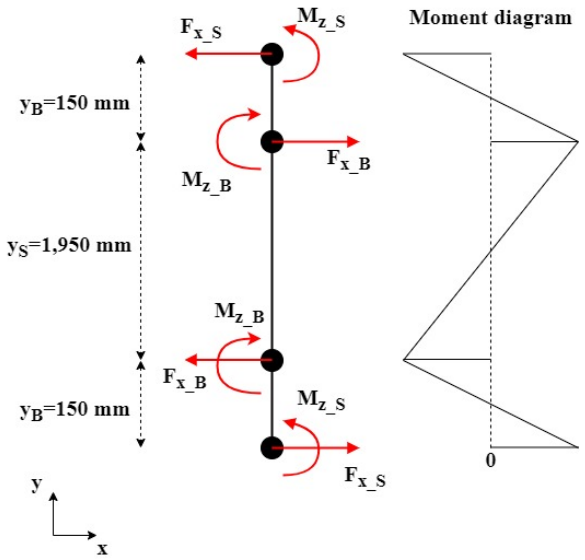

Figure 17 Shaft stick model, including moment diagram.

General terms

Based on the applied torque, the geometry and allowable movement of the active system, the reaction forces and moments will result in the following combined FBD in *Figure 18* (dimensions are not to scale):

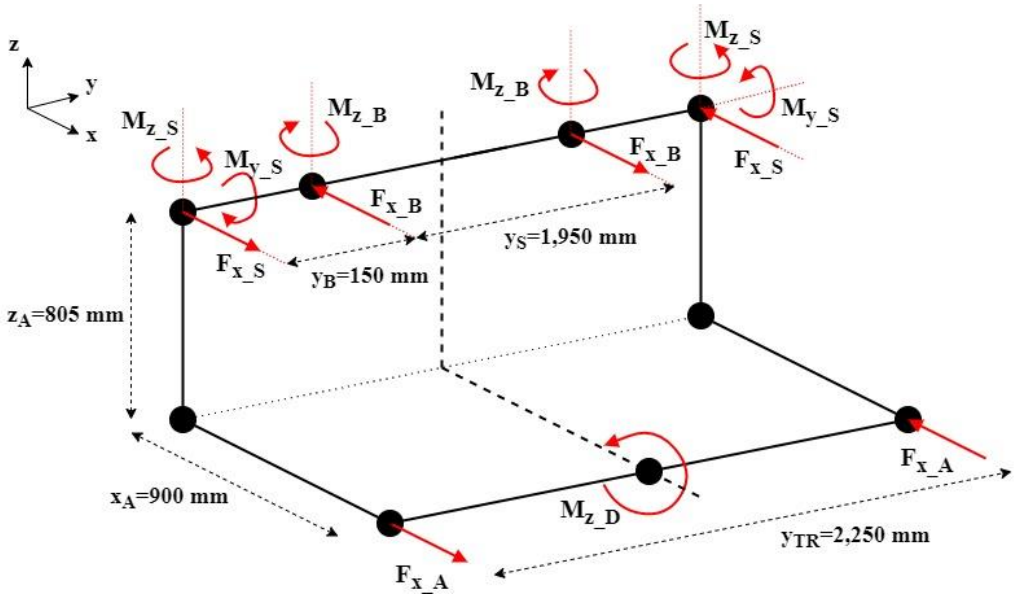

Figure 18 Torque transfer system FBD.

The round bar (spline connection) will experience a resultant force in x-direction, in addition to both moment in y- and z-direction. This will also apply for the vertical arm at the spline connection. The shaft bearing will have a reaction force in x-direction and a moment in z-direction. Moreover, the horizontal arm will have an axial force in the x-direction.

The applied torque will provide reaction forces in x-direction in both the horizontal arm and in the shaft bearings, based on the distance to the force vectors:

$$F_{x\_A} = \frac{M_{z\_D}}{y_{TR}} \quad (3)$$

$$F_{x\_B} = \frac{M_{z\_D}}{y_S} \quad (4)$$

Further, these reaction forces will also provide reaction forces in the round bars (spline connections):

$$F_{x\_S} = F_{x\_B} - F_{x\_A} \quad (5)$$

Lastly, the sum of all reaction forces only has x-components and will become:

$$\Sigma F_x = F_{x\_A} + F_{x\_S} - F_{x\_B} + F_{x\_B} - F_{x\_S} - F_{x\_A} \quad (6)$$

$$\rightarrow \Sigma F_x = 0$$

$$\rightarrow \Sigma F = 0$$

All reaction forces equal zero.

From *Figure 18* it can be observed that the reaction moment in z-direction in the shaft bearings will become:

$$M_{z\_B} = (F_{x\_S} + F_{x\_A}) \bullet y_B \quad (7)$$

Inserting equation (5) into equation (7), leads to:

$$M_{z\_B} = ((F_{x\_B} - F_{x\_A}) + F_{x\_A}) \bullet y_B$$

$$\rightarrow M_{z\_B} = F_{x\_B} \bullet y_B \quad (8)$$

Reaction moment in the round bars (spline connections) will become:

$$M_{z\_S} = F_{x\_B} \bullet y_B \quad (9)$$

Both reaction moments in z-direction in the shaft bearings and the round bars (spline connections) are equal, as seen in equation (8) and equation (9). Summing them will result in zero moment:

$$\Sigma M_z = 2 \bullet M_{z\_S} - 2 \bullet M_{z\_B} \quad (10)$$

$$\rightarrow \Sigma M_z = 0$$

There will also be a reaction moment in y-direction in the round bars (spline connections):

$$M_{y\_S} = F_{x\_A} \bullet z_A \quad (11)$$

Summing the reaction moments in y-direction will result in zero moment:

$$\Sigma M_y = M_{y\_S} - M_{y\_S} \quad (12)$$

$$\rightarrow \Sigma M_y = 0$$

$$\rightarrow \Sigma M = 0$$

Summing reaction moments in all directions also leads to zero moment.

Static equilibrium for the stick model will be fulfilled based on these calculations, and torsional transmission is proved for the torque transfer system.

3.3.1 Specific values

Specific values for the reaction forces and moments are presented for later use in *Chapter 7.1*. *Figure 18* containing the FBD for the combined system should be used for reference to forces, moments and distances. All calculations with input values are also included chronologically in the *Appendix A.2 Mathcad calculations*.

The design torque applied to the system is:

$$M_{z\_D} = 2{,}400\ kNm \quad (13)$$

From equation (3) and (4) the reaction forces at the horizontal arms and shaft bearings becomes:

$$F_{x\_A} = \frac{M_{z\_D}}{y_{TR}} \quad (14)$$

$$\rightarrow F_{x\_A} = \frac{2{,}400\ kNm}{2.250\ m}$$

$$\rightarrow F_{x\_A} = 1{,}066.7\ kN$$

$$F_{x\_B} = \frac{M_{z\_D}}{y_S} \quad (15)$$

$$\rightarrow F_{x\_B} = \frac{2{,}400\ kNm}{1.950\ m}$$

$$\rightarrow F_{x\_B} = 1{,}230.8\ kN$$

Based on equation (5) the resultant forces at the round bars (spline connections) becomes:

$$F_{x\_S} = F_{x\_B} - F_{x_A} \quad (16)$$

$$\rightarrow F_{x\_S} = 1{,}230.8\ kN - 1{,}066.7\ kN$$

$$\rightarrow F_{x\_S} = 164.1\ kN$$

From equation (8) and (9) reaction moment in the shaft bearing and the round bar (spline connection) becomes:

$$M_{z\_B} = M_{z\_S} = F_{x\_B} \bullet y_B \quad (17)$$

$$\rightarrow M_{z\_B} = M_{z\_S} = 1{,}230.8\ kN \bullet 0.150\ m$$

$$\rightarrow M_{z\_B} = M_{z\_S} = 184.6\ kNm$$

From equation (11) the reaction moment in y-direction in the round bar (spline connection) becomes:

$$M_{y\_S} = F_{x\_A} \bullet z_A \quad (18)$$

$$\rightarrow M_{y\_S} = 1{,}066.7\ kN \bullet 0.805\ m$$

$$\rightarrow M_{y\_S} = 858.7\ kNm$$

4 Technical description

In addition to transfer rotational motion from the turret torque tube, all components in the torque transfer system shall allow for tolerances and positional adjustments of the torsion ring in all directions. Since the torque transfer system will be the connected to the turret torque tube it is required to; transfer rotational moment to the geostationary parts, release all other DoF and accommodate all inherent tolerances as described in *Chapter 1.1.2*.

Firstly, rules and regulations applicable to the torque transfer system are undergone and justified. Further, an in-depth description of the main components is conducted. Activation of the system, redundancy system is explained and visualized through figures. Lastly, maintenance and positional adjustments are described.

4.1 Rules and regulation

The torque transfer system shall be designed according to *DNVGL-OS-C101 Offshore Standards, Design of offshore steel structures, general – LRFD method* (DNV GL, 2019). The standard was made available by BW Offshore. The Load and Resistance Factor Design (LRFD) method involves the following two basic variables: loads acting on the structure, and resistance of the structure (or the materials). The target safety level is obtained when design load effect is as closely as possible to design resistance.

The standard defines the limit states applicable to this thesis in *Table 2*, in the following way (DNV GL, 2019, p. 18):

Table 2 Limit states description.

Limit states	Definition
Ultimate limit states (ULS)	Corresponding to the ultimate resistance for carrying loads
Fatigue limit states (FLS)	Related to the possibility of failure due to the effect of cyclic loading
Accidental limit states (ALS)	Corresponding to damage to components due to an accidental event or operational failure

Serviceability Limit State (SLS) will not be considered in these structural analyses.

A structural element is considered to be satisfactory if the design load effect, S_d, is below the design resistance, R_d, (DNV GL, 2019, p. 19):

$$S_d \leq R_d \quad (19)$$

A limit state is defined if; $S_d = R_d$.

The design load effect, S_d, is the result of the most unfavorable design loads, F_d, combined.

Design load, F_d, is defined as follows (DNV GL, 2019, p. 20):

$$F_d = \gamma_f \bullet F_k \quad (20)$$

where γ_f is load factor and F_k is the characteristic load.

The characteristic loads shall apply in both temporary and operational conditions, and determined based on its probability distribution (DNV GL, 2019, p. 24).

The design resistance, R_d, is determined as follows (DNV GL, 2019, p. 20):

$$R_d = \varphi \bullet R_k \quad (21)$$

where R_k is characteristic resistance, and φ is the resistance factor that is defined as follows (DNV GL, 2019, p. 20):

$$\varphi = \frac{1}{\gamma_M} \quad (22)$$

where γ_M is the material factor.

R_k should be determined based on characteristic minimum values set by material standards or determined by testing if the material should have greater resistance. 5th percentile should form the basis for such tests, i.e. probability of 95 % that load values will not be exceed throughout the lifetime.

4.1.1 Ultimate Limit State

For ULS analyses two combinations of loads shall be considered, both temporary and operational. *G* is permanent load, *Q* is variable functional load, *E* is environmental load, and *D* is deformation load. *Table 3* is found in the standard (DNV GL, 2019, p. 21) and shows load factors, γ_f:

Table 3 Load factors for ULS.

Combination of design loads	Load categories			
	G	*Q*	*E*	*D*
Operating	1.3	1.3	0.7	1.0
Temporary	1.0	1.0	1.3	1.0

From the standard, 100-year return period on wave loads is considered for ULS. In other cases, 10,000-year return period is sometimes regarded. The latter requires significantly more design resistance (DNV GL, 2019, p. 21).

The standard also states that structural capacity shall be checked for all components, and that (DNV GL, 2019, p. 45):

> *"The ultimate strength capacity (yield and buckling) of structural elements shall be assessed using a rational, justifiable, engineering approach."*

Additionally, it states that the analyses may be carried out as linear elastic, simplified rigid-plastic, or elastic-plastic. Utilization of both first order or second order analyses can be conducted. Ansys Workbench can utilize all these settings. For this thesis linear elastic second order analyses are chosen, since there is little reason for investigating beyond elastic region or study non-linear behavior.

With respect to ductility, the standard express that all failure modes must be sufficiently ductile so that the anticipated simulation model will replicate the structural behavior. However, no analysis model will capture the true structural behavior. Ductile failure mode will allow the structure to redistribute the applied forces, since the deformation will lead to other areas of the

structure to resist loading. Brittle fractures shall therefore be avoided to ensure structural integrity (DNV GL, 2019, p. 46).

If structural members are susceptible for excessive yielding, they shall be checked accordingly. Design resistance shall be above von Mises equivalent stress for plated structures. However, linear elastic analyses with local peak stresses in areas of geometrical change, may exceed yield stress if it is able to redistribute into the structure's material. Plated structures and tubular members have a material factor γ_M of 1.15 (DNV GL, 2019, pp. 46-47).

4.1.2 Fatigue Limit State

The structure shall be able to resist fatigue loads which may occur during a temporary or an operational phase. Other significant cyclic loads must also be accounted for. Expected load history shall define the representative FLS value. Load factor, γ_f, in FLS will be 1.0 for all loading conditions, but the safety is accounted for by applying a design factor on the design life (DNV GL, 2019, pp. 21-22).

If structures are exposed to cyclic loading, checks shall be conducted to verify that the structure will shake down (damp) without extensive plastic deformations or fracture. However, if linear analysis combined with the resistance formulations are conducted, no further shake down check is required (DNV GL, 2019, p. 45).

SN-curves (also known as Wöhler curves) are normally used for determining fatigue life. The curves describe mean stress level (S) vs. number of cycles (N) to failure. They are based on fatigue tests for a specific material, and the standard specifies that 97.6 % probability of survival shall form the basis for the curves. Further, the structure shall undergo a fatigue assessment for each individual component considered to be exposed to fatigue loading. A detailed fatigue analysis shall support the fatigue assessment in appropriate areas. Any welded joint and attachment of any form or other stress concentrated areas are potentially a source of fatigue fractures and must be evaluated individually. Relevant site specific environmental data for the area the unit will be operated in, shall also be considered (DNV GL, 2019, p. 57).

Further, the structure shall account for Design Fatigue Factor (DFF). The standard defines the torque transfer system to be an (DNV GL, 2019, p. 58):

> *"Internal structure, accessible and not welded directly to the submerged shell plate."*

Therefore, according to the standard the DFF shall be 1.0. However, BW Offshore chose a DFF of 3.0 to assure fatigue safety.

If simplified fatigue investigations result in estimated fatigue life below the acceptable limit, fracture mechanics analysis or more extensive investigations shall be conducted (DNV GL, 2019, p. 59).

4.1.3 Accidental Limit State

All relevant accidental events shall be considered when accessing ALS. "*Low damage probability*" and "*acceptable damage consequences*", shall protect the structure towards accidental damages. If an accidental failure does occur the remaining structure shall be able to withstand a one-year return period environmental condition without loss of floatability, stability

or global structural integrity. BW Offshore have requested that the ALS analyses shall define a maximum accidental load that the torque transfer system is able to withstand, since no realistic design accidental load is defined for the system (DNV GL, 2019, p. 60).

In an accidental event it is required that the torque transfer system shall hold the applied ALS torque until tugboats arrives the FPSO and assists to cease weathervaning. This is to avoid that the piping is teared and twisted off below the Emergency Shutdown (ESD) valves, leading to an oil spill.

Both the load factor, γ_f, and the material factor, γ_M, for accidental loading conditions shall be 1.0. In the strength calculations, both non-linear and dynamic FEA can be applied for all relevant failure modes. Local overloading surpassing yield capacity is acceptable if redundancy in the structure with alternate redistribution of force paths is possible. Sufficient material toughness for actual operation temperature shall also be selected (DNV GL, 2019, p. 60).

Other measures to obtain sufficient ductility of materials and redistribution of forces are (DNV GL, 2019, p. 60):

- Adequate toughness of materials for actual service temperature and member thickness.
- Connection strength shall exceed the strength of the members themselves.
- For non-ductile slender members energy absorption dependency shall be avoided.
- Avoid sudden changes in strength or stiffness, i.e. weak sections.

4.2 Components

An exploded view of the entire torque transfer system is visible in *Figure 19*. According to drawings of the torque transfer system provided by BW Offshore, total weight of the system is 17,621 kg. The assembly drawing are included in the *Appendix A.4 Drawing*. The system has an assembled size of 3,100 mm x 2,490 mm x 1,455 mm (length x width x height), without considering the hydraulic cylinders. None of the locking plate bolts is present in the exploded view or any other view for that matter. For visual purposes, the lower part of the geostationary module tube and the upper part of the turret torque tube are visible in most of the figures. All welds are also considered to be fully penetrated.

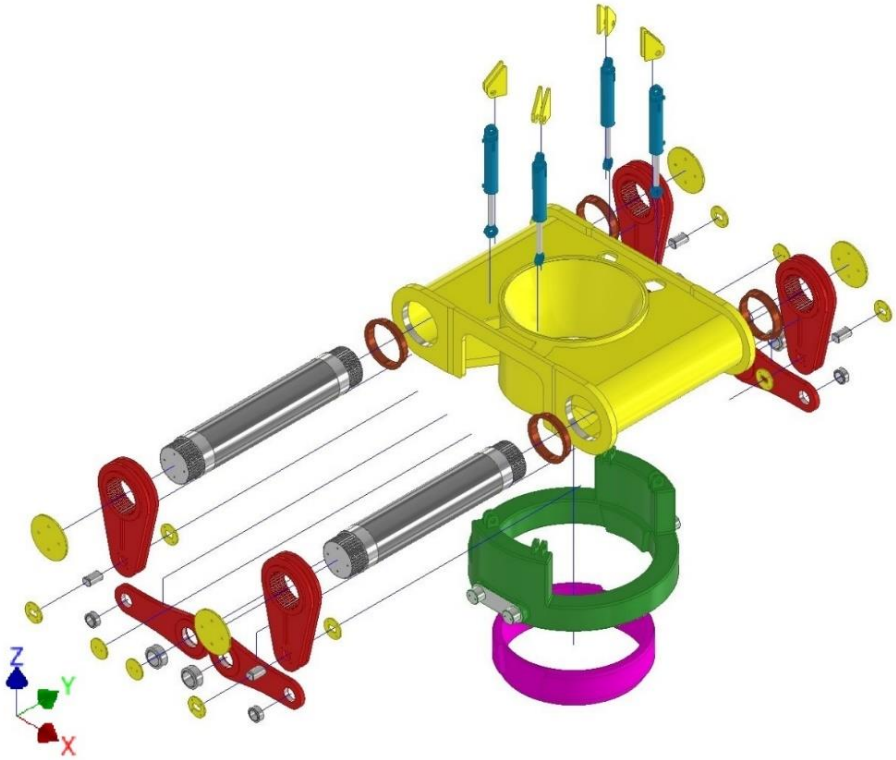

Figure 19 Exploded view of the torque transfer system.

Most of the steel material utilized for the torque transfer system is NVD36, structural equivalent to S355J2G3 from the Norwegian standard steel code. However, NVE36 is used for the horizontal arms, vertical arms and turret torque tube. From the standard (DNV GL, 2019, pp. 40-44), choosing two different material designations are based on thickness of the structural steel for various structural categories and service temperature. NVE36 is structural equivalent to S355J4G3. Only difference from NVD36 is the impact resistance energy test temperature of -40 degrees Celsius. The symbols in the steel code represent the following according to (Norsk Stål AS, 2001):

Table 4 Structural steel code according to European standard.

Symbol	Definition	Note
S	Structural steel	-
355	Minimum yield strength of 355 MPa	-
J2	27 J of impact energy absorbed at test temperature of -20 degrees Celsius	Charpy-V specimen
J4	27 J of impact energy absorbed at test temperature of -40 degrees Celsius	Charpy-V specimen
G3	Normalized heat treatment	Equivalent to “+N” symbol

Transition temperature for brittle/ductile materials, is commonly set to minimum 27 J of absorbed energy for a charpy-V specimen test. Steel with temperature below the transition temperature will be brittle. Whereas steel with temperature above the transition temperature will be ductile. As described in *Chapter 4.1.1*, the standard states that material ductility is demanded for ULS (Lancaster, 2005).

With this in mind, NVE36 have greater toughness than NVD36, since it has the brittle/ductile fracture transition at a lower temperature. Hence, NVE36 will remain ductile until reaching -40 degrees Celsius, while NVD36 will remain ductile until reaching -20 degrees Celsius. Additionally, both materials are considered to have good weldability (Corus Construction & Industrial, 2004), and are defined as shipbuilding steels according to DNV GL (Liberty Steel Dalzell, 2017).

Ultimate tensile stress of 460 MPa are a conservative value for most S355 steels (Waløen, 1989).

4.2.1 Geostationary module tube

The torque transfer system is built around a pipe or tube, that goes through the entire geostationary module in vertical direction as seen in *Figure 20*. This tubular is efficient in transferring torque and is also used to guide the pull-in wire during connection and disconnection of the turret.

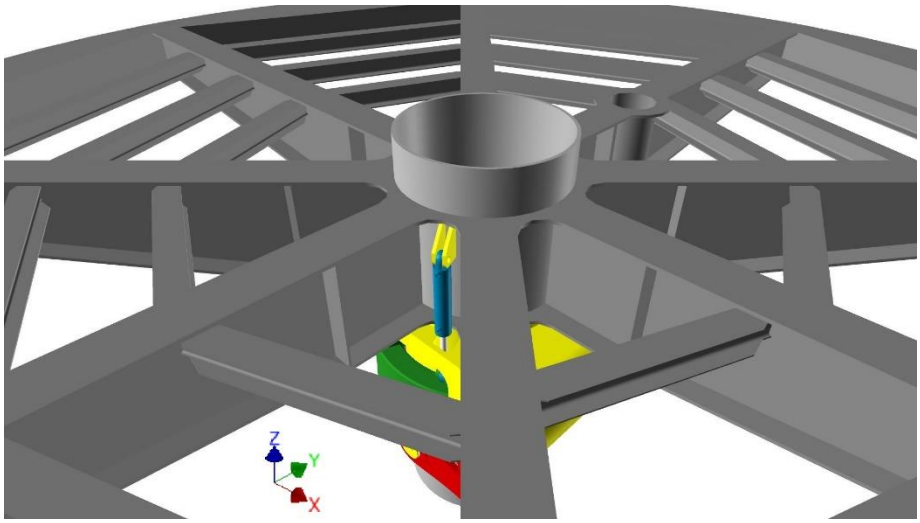

Figure 20 Geostationary module tube.

The geostationary module tube has an external diameter of 1,500 mm and a thickness of 30 mm. In most of the figures of the torque transfer system the geostationary module tube is shown without the entire tube length.

Torque transfer structure

Around the geostationary module tube the torque transfer structure is located as seen in *Figure 21*. It consists of 25 plates, welded around the geostationary module tube. This structure supports all the moving parts to a functional torque transfer system. Total weight of the structure is just below 5,300 kg.

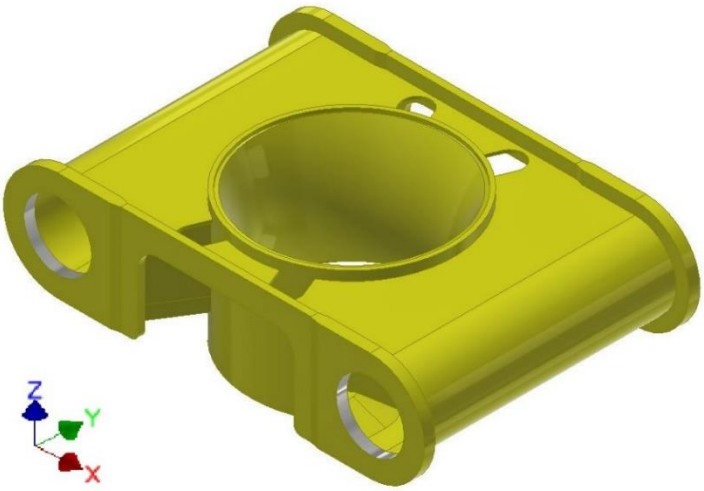

Figure 21 Torque transfer structure assembly.

The curved plate inside the geostationary module tube is simply added to guide the pull-in wire for the buoy/turret and does not provide structural strength to the structure. However, it should give a somewhat different stress distribution in the analyses.

4.2.2 Torque transfer shaft

The torque transfer shaft consists of a two round bars, with spline connection, welded in each end of a central pipe section as seen in *Figure 22*. Choosing a central pipe section as opposed to a central solid section, significantly reduce the weight of the shaft. Consequently, the pipe shall be checked for torsional and bending stress in *Chapter 7.1.7*. The shaft bearing has contact face at the solid cylinder section of the round bar.

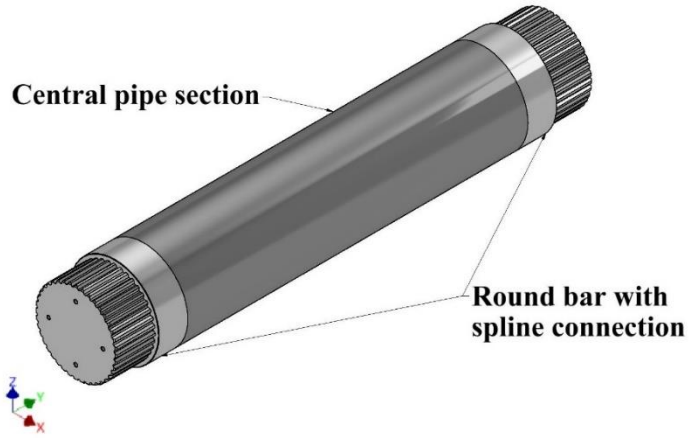

Figure 22 Torque transfer shaft.

Total length of the shaft is 2,450 mm, outer diameter is 455 mm and total weight is 1,411 kg. The finished thickness of the central pipe section is 33.8 mm. Additionally, the round bars have four equally spaced threaded holes to secure the locking plate when the shaft is installed. The locking plate holes will be standard treaded as M20x2.5 - 6H.

A spline connection (male part) is present at the round bars in the shaft as seen in *Figure 23*. The spline is a standard connection defined as; module 10, 40 off teeth and reference diameter of 420 mm, according to the applicable standard DIN 5480-1. Similarly, the vertical arm has a corresponding spline connection (female part).

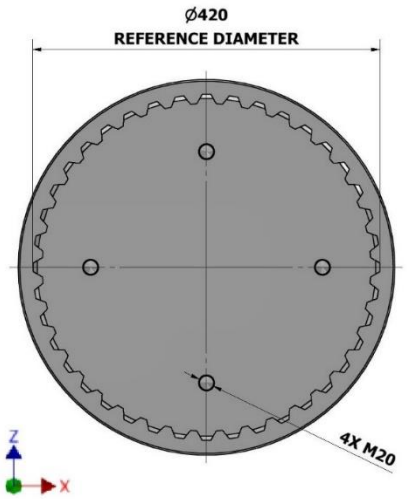

Figure 23 Round bar spline connection (male part) at shaft.

4.2.3 Torque transfer shaft bearing

For the shaft to rotate, two bronze soft tin bearings are inserted into each end of the torque transfer structure. A total of four shaft bearings are needed for the entire system. Additionally, the bearing have a contact face at one end as seen in *Figure* 24, so that the vertical arms can rotate with less friction towards it. The bearings shall be checked for bearing pressure in *Chapter 7.1*.

Figure 24 Torque transfer shaft bearing.

Each bearing weigh 30 kg and have an internal diameter of 455 mm to fit the shaft. It will be inserted 80 mm into the structure. Otherwise, it is important that the bearing is maintenance free and self-lubricated. However, the redundancy measures will allow for replacement of the bearings just in case. Self-lubrication is conducted by solid graphite plugs in the bronze base material (not visible in the figure).

4.2.4 Torque transfer vertical arm

The torque transfer vertical arms are connected to the shaft with a spline connection and allows rotation about the y-axis as seen in *Figure 25*. The vertical arm spline connection will rotate with the shaft and move the rear position, where the rear locking plates and the bolt will connect it to the horizontal arm. As a result, movement of the torsion ring in x-direction can be achieved.

The allowable tolerance movement are constrained by the distance between the torsion ring and torque transfer structure.

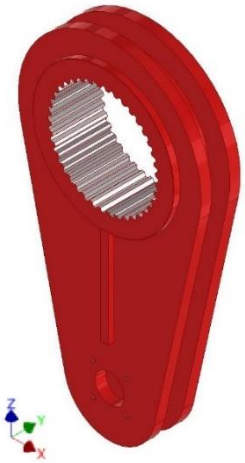

Figure 25 Torque transfer vertical arm.

A vertical arm consists of three plates and a cylinder hub which have the spline connection (female part) inside its internal diameter. The spline hub will be inserted between the two side plates and welded in place. Another plate will be welded vertically downwards from the spline hub, to provide more stiffness to the vertical arm due to the length of the component.

The vertical arm weigh 434 kg. The side plates have 40 mm thickness, while the stiffener plate have 30 mm thickness. Additionally, the lower end bore will have four M16 through holes equally distributed around it, to attach the rear locking plate and secure the axle bolt in place.

4.2.5 Torque transfer horizontal arm

Torque transfer horizontal arm connects the vertical arm to the torsion ring. It allows the torque transfer system to move the torsion ring in y-direction, due to the spherical bearings in the rear and foremost side as seen in *Figure 26*. The horizontal arm consists of a main plate with 55 mm thickness, two different spherical bearings and two round plates to cover the entire thickness of the biggest spherical bearing in the foremost end. Total weight of a horizontal arm will be 207 kg.

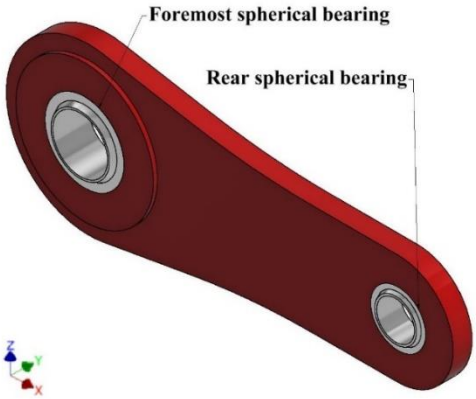

Figure 26 Torque transfer horizontal arm.

According to documentation, both the inner and outer ring in the spherical bearings are stainless steel with a Polytetrafluoroethylene (PTFE) fabric liner and retaining rings. This

bearing type has two plastic seals, it is maintenance free and additional lubrication is not recommenced. Additionally, the bearing shall be protected from dirt and contamination to assure full lifetime (AST® Bearings LLC, 2020).

4.2.6 Locking plates and bolts

Locking plates for three different places is required in the torque transfer system to keep components in place as seen in *Figure 27*. The horizontal arm on the shaft, and both rear and foremost ends of the vertical arm, are all kept in place by the locking plates. Additionally, a bolt of 110 mm in diameter and 180 mm length with two notches in each side, will function as an axle for the rear horizontal arm to the vertical arm. Both the bolt and all locking plates are designed according to applicable standard. Each shaft locking plate have a weight of 31 kg, each rear locking plate weigh 4 kg, each foremost locking plate weigh 5 kg and each rear axle bolt weigh 13 kg.

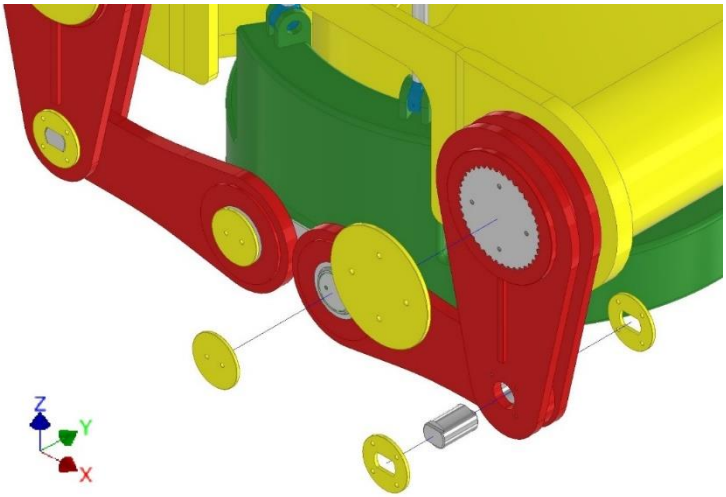

Figure 27 Locking plates including rear axle bolt.

In addition, standard bolts for connecting the locking plates to the desired component is required. For each shaft locking plate four pieces of standard M20x2.5 - 6H bolts are needed. That equals to a total of sixteen M20 bolts for the entire system. Further, four pieces of standard M16 bolts, not longer than 55 mm long, are required for each rear locking plate. Lastly, two pieces of standard M16 bolts are also required for each foremost locking plate. Resulting in twenty-four M16 bolts for the entire system. Four shaft and foremost locking plates, eight rear locking plates and four rear axle bolts are required for the torque transfer system.

4.2.7 Hydraulic cylinder

There are four hydraulic cylinders in the torque transfer system. Their purpose is to activate the system when needed and deactivate it when disconnection is required. The hydraulic cylinders need to carry the self-weight of the components that not directly rest in the torque transfer structure. In *Figure 28* we can observe an activated hydraulic cylinder. The hydraulic cylinders will adjust the position of the torsion ring in z-direction.

Figure 28 Hydraulic cylinder.

From the drawings acquired from BW Offshore, it is found that the cylinders are supplied from the Norwegian company Malm Orstad AS. The assembly drawing are included in the *Appendix A.4 Drawing*. The cylinder is a standard in-stock inventory with spherical bearings in both support ends and 210 bar working pressure (Malm Orstad AS, 2020).

Each of the cylinders have a weight of 51 kg and 350 mm stroke length. The bore diameter is 125 mm and the spherical bearings have an internal diameter of 60 mm. In addition, each spherical bearing has a corresponding lubrication nozzle. There will be a 2.5 mm gap on each side at the connection padeyes in both ends. Hence, they are able to adjust slightly in both x- and y-direction due to the spherical bearings in both ends. Additionally, the cylinders are designed for subsea use and according to applicable standard.

It is somewhat unclear exactly what self-weight the hydraulic cylinders are required to hold. However, the hydraulic cylinders will apply full working force when activating the system, to make the wedge configuration connect the torsion ring and turret torque tube.

Total capacity for the cylinders is checked:

$$1\ bar = 100\ kPa$$

$$\rightarrow P_{HC} = 210\ bar = 21\ MPa \quad (23)$$

Further, the capacity is based on the internal bore diameter of the hydraulic cylinder, $d_{HC} = 125\ mm$, where the stroke arm can operate:

$$A_{HC} = \pi \bullet \left(\frac{d_{HC}}{2}\right)^2 \quad (24)$$

$$\rightarrow A_{HC} = \pi \bullet \left(\frac{125\ mm}{2}\right)^2$$

$$\rightarrow A_{HC} = 12{,}272\ mm^2$$

Total capacity will be all the four hydraulic cylinders combined:

$$F_{g\_HC} = 4 \bullet P_{HC} \bullet A_{HC} \quad (25)$$

$$\rightarrow F_{g\_HC} = 4 \bullet 21\ MPa \bullet 12{,}272\ mm^2$$

$$\rightarrow F_{g\_HC} = 1{,}030.8\ kN \approx 105\ tons$$

The capacity of the four hydraulic cylinders are approximately 105 metric tons. BW Offshore stated that three hydraulic cylinders would be optimal, but geometry limitations require to have four cylinders. To make the torsion ring neatly placed and connected to the turret torque tube, two and two cylinders are connected in series.

4.2.8 Padeye

Two padeyes are placed at the base end of each hydraulic cylinder. The padeyes will be welded to the geostationary module tube. They shall withstand the self-weight of the free air hanging components including the hydraulic cylinders. Likewise, there are two padeyes at the corresponding point at the torsion ring. These two pin connections will allow for some movement of the torsion ring. Each set of padeye will have a weight of 22 kg. In addition, they are designed according to standard, as shown in the drawings. It is currently undecided what kind of axle or pin method that is used to connect the hydraulic cylinder to the padeyes.

4.2.9 Torque transfer torsion ring

The torsion ring will be lowered onto the turret torque tube to initiate torque transfer. It is simply a ring with a wedge on each side of the internal diameter as seen in *Figure 29*. It will guide the torsion ring onto the turret torque tube. In addition, four pairs of padeyes are located at the extruded section of the torsion ring. The extruded section is present for redundancy purposes, that are discussed in *Chapter 4.4*. Two cylinders are extruded from each side of the torsion ring. They are the connection points to the horizontal arm spherical bearings, and is verified for shear stress in *Chapter 7.1.4*.

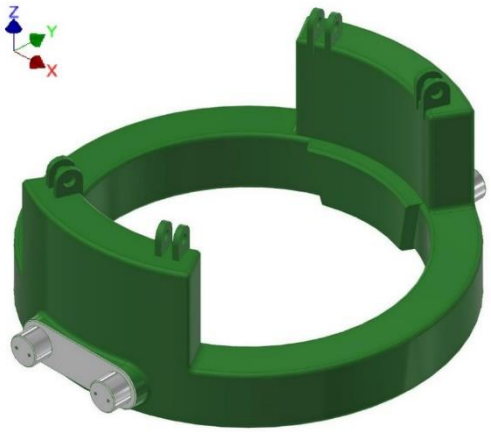

Figure 29 Torque transfer torsion ring.

The torsion ring weigh 5,359 kg. It has an external diameter of 2,100 mm, internal diameter of 1,630 mm and height of 820 mm without the padeyes.

4.2.10 Turret torque tube

In most of the figures, only the upper part interface of the turret torque tube (purple colored) is visualized as seen in *Figure 30*. It is conducted to focus on the torque transfer system itself and

not further into the buoy/turret. The turret torque tube is made as one component to avoid welds in the torque region. A corresponding wedge in the torsion ring will fit the wedge groove in the turret torque tube when connected. The turret torque tube is made from a 100 mm plate.

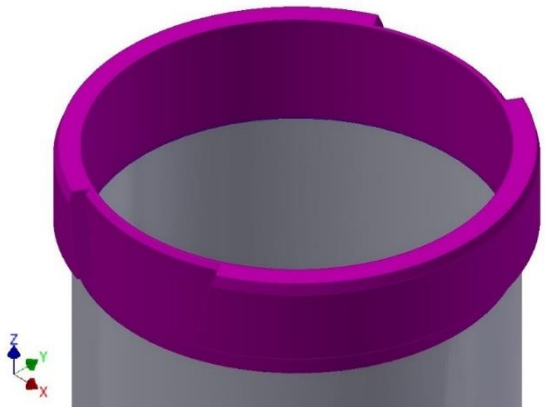

Figure 30 Turret torque tube.

4.3 System activation

When the torque transfer system is installed and integrated into the FPSO at the shipyard, the system will find itself in a deactivated position, as seen in *Figure 31 (a)*. All the hydraulic cylinders will be fully retracted, and the torsion ring will rest in the torque transfer structure. The system will be deactivated during the vessel's sailing to the field and prior to hook up. In addition, whenever the turret needs to be disconnected the torque transfer system will find itself in a deactivated state. Through resting the torsion ring towards a contact face in the torque transfer structure, minimization of vibrations and fatigue are achieved. It is important with respect to FLS condition.

Before activating the torque transfer system the turret torque tube at the buoy/turret, including SURF and mooring lines, needs to be pulled into the ship cone as seen in *Figure 31 (b)*. A pull in wire will be lowered through the geostationary module tube, and further through the center of the torque transfer system and hooked onto the buoy/turret. When pulled completely into the ship cone, the buoy is locked off with a set of locking devices in the ship hull. The buoy will now be connected relative to the FPSO. In locked position, there will be a 50 mm separation between the turret torque tube and the geostationary tube in the torque transfer system. Finally, the geostationary module and swivel needs to be rotated to align the two wedges before activation and lowering of the torsion ring. The alignment is conducted by hydraulic cylinders at the main swivel beam, close to the roller main bearing, that push the geostationary system in activation position.

The four hydraulic cylinders will start to lower the torsion ring towards the turret torque tube lower part as seen in *Figure 31 (c)*. Full stroke length of the hydraulic cylinders is 350 mm. As the lowering starts, the wedge in the torsion ring and the wedge groove in the turret torque tube, will guide the torsion ring into position directly above the turret torque tube. Additionally, the wedge configuration will provide almost no looseness in the contact face. Release of all DoF, except rotation about the z-axis, provides compensation for lateral misalignment due to tolerances in the components. Final stroke length of the hydraulic cylinders somewhat below

the maximum is also quite possible. In *Chapter 7.4*, results from a sensitivity study of 325 mm stoke length is conducted. It will highlight any possible weaknesses of less stroke length and positional adjustment of the torsion ring.

When fully activated the torsion ring be placed neatly directly above at the turret torque tube as seen in *Figure 31 (d)*. Subsequently, the horizontal arms and vertical arms will be positioned perpendicular to each other.

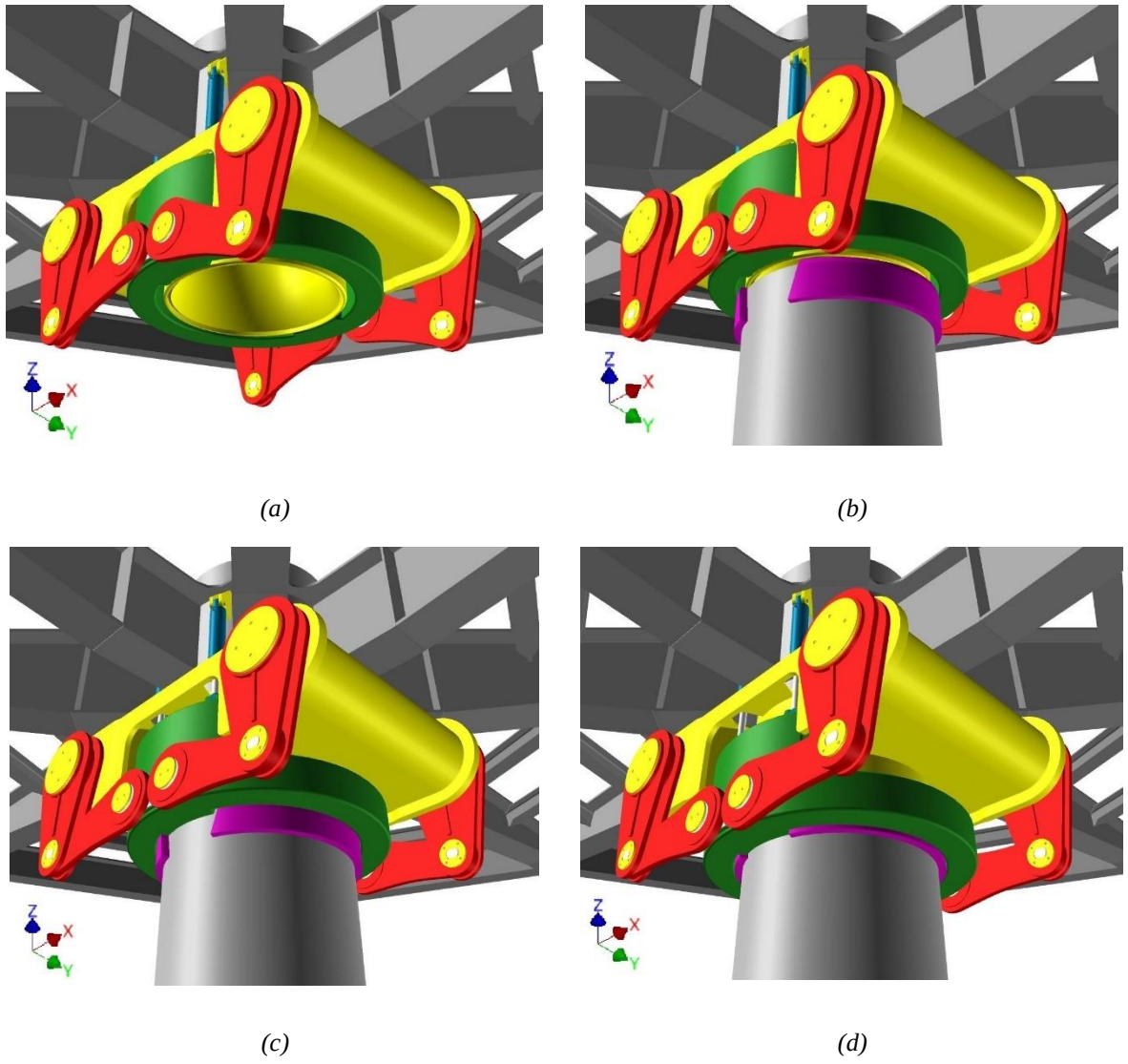

Figure 31 System activation steps: (a) deactivated system, (b) buoy/turret pull in, (c) halfway activated system and (d) fully activated system.

When the torsion ring is connected to the turret torque tube, the piping from the buoy/turret can be connected to the geostationary piping system and production of hydrocarbons can be initiated.

4.4 Redundancy system

Redundancy is the property of doing the required task with more resources than minimally necessary. Maintaining the desired level of functionality will be fulfilled by sufficient redundancy in the system, as it will work around the failures as they occur (Koren and Krishna,

2007). It means that the torque transfer system shall have alternate and “double” systems, to execute the same purpose. In that way, a redundancy system can replace a failed system and conduct its tasks single handedly, even while keeping the torque transfer system in operation.

Full redundancy is required for the torque transfer system in case of total breakdown, to ultimately avoid oil spill. The piping will be connected to the production system after the torque transfer system are activated and operational. In an ALS situation, sufficient redundancy shall avoid that the piping is twisted and teared off. The main redundancy measure, involves that the two sets of independent systems in the torque transfer system, are dimensioned for the entire applied torsional design moment.

Redundancy measures are designed into the structure if an accidental torque is applied to the system. It involves the two vertical extrusions in both sides of the torsion ring. If an unanticipated overload occurs and the torque transfer arms break, the torsion ring itself will be able to lay against the torque transfer structure in both sides as seen in *Figure 32*. In this worst-case situation, only the torsion ring and the torque transfer structure can be considered. There is a 30 mm gap on each side of the torsion ring extrusion towards the structure. Thus, in case of total breakdown the torsion ring will touch the torque transfer structure, and the contact region shall withstand the ALS load.

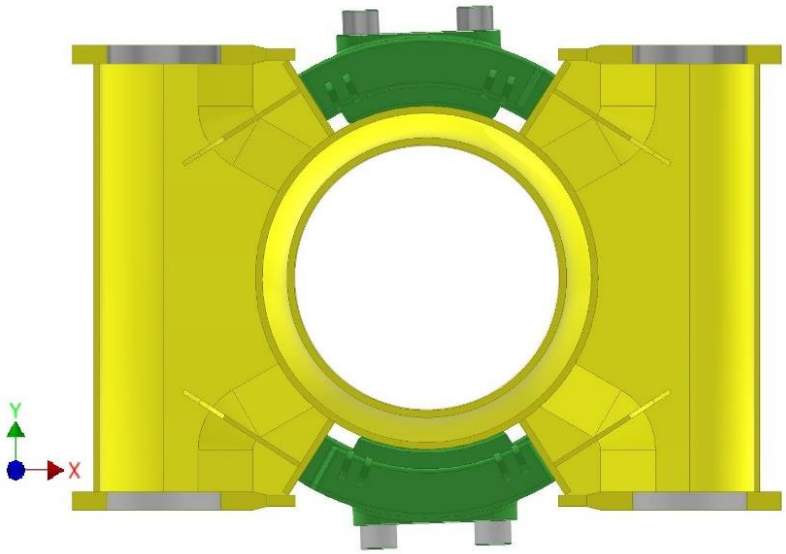

Figure 32 Redundancy in ALS condition, half section top view.

The structure is reinforced for such an accidental case with a stiffener plate perpendicular to the contact face as seen in *Figure 33 (a)*. Additionally, the bottom of the stiffener plate consists of solid reinforcement plate that provides 80 mm of extra thickness in this region as seen in *Figure 33 (b)*. BW Offshore have requested that the analyses shall identify a maximum accidental applied torque that the system will withstand.

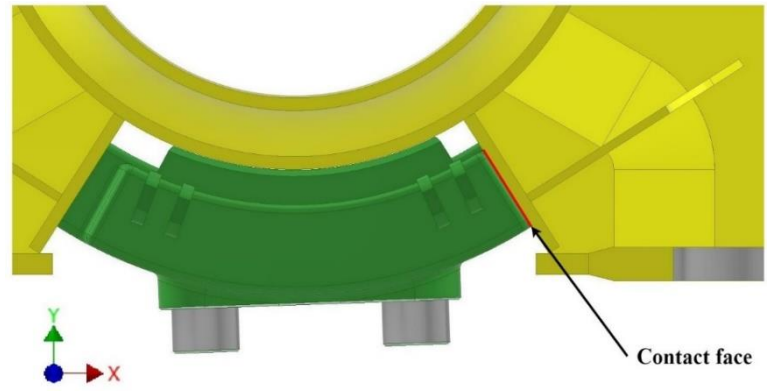

(a)

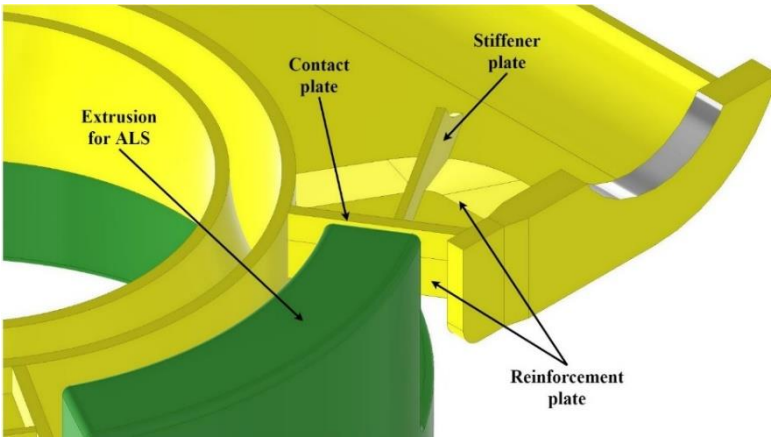

(b)

Figure 33 Redundancy for ALS of (a) zoomed half section top view and (b) oblique section view.

Choosing spline connection for connecting the vertical arms to the shaft is conducted with redundancy in mind. A bolt connection would have required to withstand significantly more load than all the spline teeth. The spline connection in the torque transfer system are designed according to (DIN, 2006).

For load transmitting components splines are similar to stubby gear teeth on the outside of the shaft and inside of the hub. They are generally more expensive than key connections and usually not required for simple torque transmission. However, they are typically utilized for high torque transmission, as for the torque transfer system. Stress concentrations usually peak at the spline ends and where the spline blends into the shaft. Nevertheless, stresses are generally quite moderate. This shaft spline does not have a smooth transition into the shaft. Hence, greater stress concentrations will occur in this region (Budyans and Nisbett, 2015).

Wedge connection do also provide redundancy. Its geometry will accommodate the tolerances in the system and assure smooth connection between the torsion ring and turret torque tube. Additionally, this solution will avoid looseness in the connection, that reduce the chance of unforeseen significant loads.

4.5 Maintenance

It is intended that disconnection of one set of the torque transfer system shall be possible during normal operation to conduct maintenance and replacement of the shaft bearings. Hence, the

FPSO shall continue weathervaning despite of disconnection and maintenance on one of the systems. In such a case, one side of the torque transfer arms are disconnected and slid off the spline connection on the shaft as seen in *Figure 34 (a)*. Further, the other side of torque transfer arms, including the shaft, will be pulled slightly out from the structure as seen in *Figure 34 (b)*. Subsequently, full access to the shaft bearing is available in the disconnected side. Replacement of shaft bearing will be conducted, then the shaft is inserted back in place and lastly the disconnected side will be installed once again.

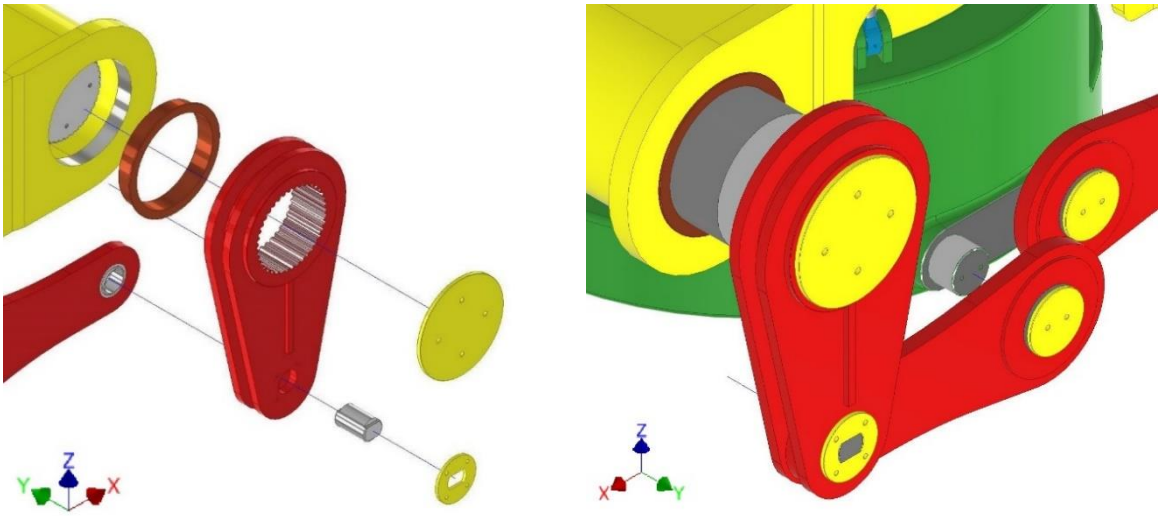

(a) *(b)*

Figure 34 Shaft bearing replacement at (a) disconnected side and (b) connected side.

Having a spline connection at the shaft/vertical arm in contrary to a bolt connection, requires significantly less maintenance and inspection. No maintenance on the torque transfer system is expected. If the system works properly, it shall not move and only remain static. There is some wear on static systems, but significantly more on dynamic systems.

4.6 Positional adjustments

The torque transfer system shall accommodate tolerances in the structure and positional adjustments of the torsion ring in all directions. BW Offshore expect that it is reasonable to assume about 20-25 mm required movement in all directions for the torsion ring. However, the structure geometry will accommodate significantly more.

Spherical plain bearings in the horizontal arms allow rotation in all three directions. Displacement constraints are controlled by the misalignment angle in the bearings and the gap between the side plates in the vertical arm. Misalignment angle is the angle of rotation in all directions in the spherical bearing. Spherical bearings in the horizontal arm leads to that the torsion ring can move in y-direction as seen in *Figure 35*.

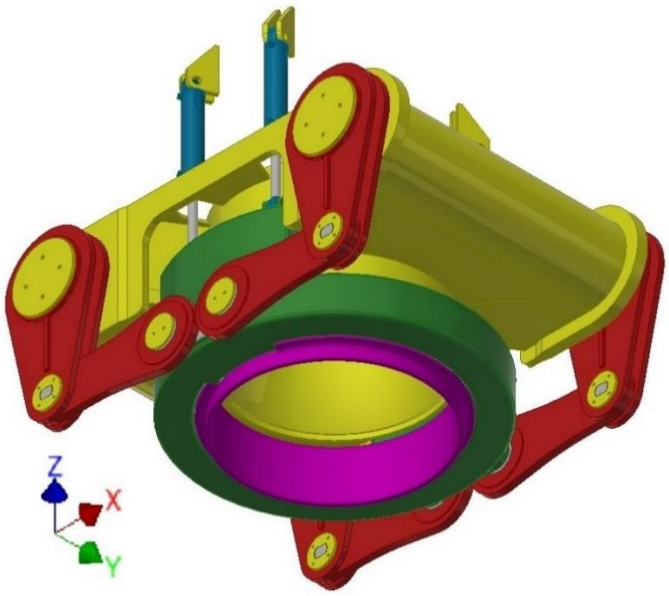

Figure 35 Positional adjustments for the torque transfer system.

From the drawings provided by BW Offshore, the rear spherical bearing (at the vertical arm) is specified as GE110XT/X-2RS and the foremost spherical bearing (at the torsion ring) as GE160XT/X-2RS. The rear spherical bearing can accommodate misalignment angle of 6 degrees[4], and the foremost spherical bearing can have a misalignment angle of 8 degrees (AST® Bearings LLC, 2020).

Movement in x-direction is made possible through the shaft configuration at the vertical arm. Rotation of the shaft leads to movement in x-direction of the lower part of the vertical arm and the entire horizontal arm as seen in *Figure 35*. The hydraulic cylinders allow for movement in the z-direction, but it is expected to be fully extensive when the system is activated.

[4] Courtesy of BW Offshore.

5 Design basis

Design basis for the FEAs and hand calculations are described and justified in this chapter. Equivalent Von Mises stress and mesh quality for FEA are also undertaken and explained.

Input moment for the ULS FEA and sensitivity study is 2,400 kNm. However, it will be applied to the torque transfer system as pressure in the two symmetric contact faces inside the torsion ring. Input moment for FLS FEA are half as for ULS FEA. Regarding ALS FEA a try-and-fail approach will be conducted only having the torque transfer structure and torsion ring present. The sensitivity study utilized the same input moment as for ULS FEA.

Results shall be in accordance with demands from applicable standard (DNV GL, 2019) to be acceptable. Sufficient ductile materials are required so relatively high stresses can be redistributed further into the structure when a structure is deformed. Hence, peak stresses above the material strength are accepted if stress redistribution are fulfilled. Based on the material specifications, both will remain ductile until reaching surrounding temperatures of -20 and -40 degrees Celsius, respectively. Beyond that they will become brittle.

Fatigue analyses are conducted by examine relevant individual components, according to FLS considerations in the standard. It states that fatigue assessments shall be conducted in appropriate areas where there are potential for fatigue fracture. BW Offshore selected DFF of 3.0 to assure fatigue safety. It shall be included in the fatigue analyses (DNV GL, 2019).

For accidental loading cases, local overload surpassing yield capacity is acceptable of stress redistribution paths are available. BW Offshore states that it is desirable for the thesis to define a maximum applied torque the torque transfer system can withstand. For accidental condition it is thought that only the torque transfer structure and torsion ring will remain operational (DNV GL, 2019).

Equivalent Von Mises stress is the comparison metric for the FEAs and hand calculations towards material strength capacity in *Chapter 7.1*. Deformation in FEA and hand calculations shall also be examined and discussed.

For pure uniaxial state of Von Mises stress, σ_{VM}, it becomes (Collins et al., 2010, p. 228):

$$\sigma_{VM} = \sqrt{\sigma_x^2 + 3 \bullet \tau_{xy}^2} \qquad (26)$$

FEA is a powerful tool but it is important to comprehend both the possibilities and limitations of it. Mesh is a term for the network of cells, consisting of elements and nodes that discretize a region. More elements in a given region increases the mesh density, which often improve results in areas of great stress. Improving results is defined as convergence toward the exact solution, and it is generally archived through mesh refinement. However, in regions where increasing mesh density, the transition mesh shall be gradual. A mesh is considered sufficient when minimal change in maximum stress value occur, as it is reasonable to presume that the solution has converged. Ansys estimate the error of the FEA solution through automatic self-adaptive mesh refinement programs. The mesh is automatically revised and reanalyzed before reaching the desired target allowable error. Nevertheless, computational time should be minimized when generating mesh. At some point, finer mesh will not improve results, but

rather give high unrealistic peak stresses or even result in the software being unable to run a solution (Budyans and Nisbett, 2015).

There are several ways to determine quality of generated mesh in Ansys. Element quality, aspect ratio, Jacobian ratio, skewness and orthogonal quality, are some of the mesh metrics for determining quality. This thesis considers skewness and orthogonal quality as mesh metrics, due to their simple indication value and specific quality definition.

According to Ansys documentation and (Fatchurrohman and Chia, 2017), skewness is one of the primary quality mesh metrics. It determines how close to ideal a face or cell is, and ranges between 0 (perfect) and 1 (unacceptable). Whereas mesh quality is important, it is also relevant to minimize computational time and find a suitable combination. One must also investigate regions of low mesh quality in relation to local high stresses in the same regions. *Table 5* lists the range of skewness values and corresponding cell quality definition:

Table 5 Skewness mesh metrics spectrum.

Cell quality	Excellent	Good	Fair	Acceptable	Bad
Level of skewness	0-0.25	0.25-0.50	0.50-0.75	0.75-0.90	0.90-1.00

According to Ansys documentation and (Fatchurrohman and Chia, 2017), orthogonal quality ranges between 0 (unacceptable) and 1 (perfect), i.e. opposite to the skewness scale. Orthogonal quality of a given cell is calculated for each face, based on several quantities that this thesis will not elaborate. *Table 6* lists the range of orthogonal quality values and corresponding cell quality definition:

Table 6 Orthogonal quality mesh metrics spectrum.

Cell quality	Bad	Acceptable	Fair	Good	Excellent
Level of orthogonal quality	0-0.15	0.15-0.20	0.20-0.70	0.70-0.95	0.95-1.00

6 Problem formulation and approach

In ULS FEA the torque will be applied as pressure in the contact faces in the torsion ring of the torque transfer system. FLS FEA will consider critical individual components susceptible for fatigue based on acquired knowledge. ALS FEA will involve a similar approach as the ULS FEA, but rather utilize a try-and-fail approach up to a believed to be maximum allowable stress for the system. For ALS case only the torsion ring and torque transfer structure will be present in the analysis assembly. Sensitivity study also involves the exact similar approach as for ULS FEA. However, the assembly model is changed slightly beforehand to adjust a specified offset for the torsion ring to investigate the structural response of the torque transfer system. Formulation and approach to each of the main FEAs are described in detail in this chapter.

Autodesk Inventor Professional 2020 (Student Version) is used for all Computer Aided Design (CAD) work involved in the thesis. Ansys Workbench R19.2 is used as FEA tool in the analyses of the torque transfer system.

6.1 Ultimate Limit State

ULS FEA are conducted to verify that the torque transfer system does not exceed ULS condition with applied design torque. Simulation setup, geometry, material, connections, mesh and boundary conditions, are all assumptions that forms the basis for the results. Optimization of geometry are also conducted based on identified weak spots.

6.1.1 Setup

It was determined to investigate the torque transfer system as an assembly and not evaluate component by component based on reaction forces and moments. Even though more computational time are required for a larger structure, how the components act in relation to each other will only be obtained through assembly analysis. Only one side of the torque transfer system is considered in the FEAs, since one activated system shall withstand the entire applied torque due to redundancy measures.

6.1.2 Geometry

To limit number of elements/nodes, some parts of the torque transfer system assembly were simplified. All the hydraulic cylinders, including padeyes on both the geostationary module tube and the torsion ring, were removed completely. All bolt holes for the locking plates were also removed. No locking plates were included since they are only present to keep components in place and not withstand significant loads. Since the applied torque are directly defined in the torsion ring, the turret torque tube is not included in the analyses.

All plates in the torque transfer structure are joined by fully penetrated welds. Therefore, six plates had to be slightly changed geometrically to accomplish fully penetrated welds throughout the structure. *Figure 36* shows the six changed plates in the structure to fulfill the continuous plate geometry. If the geometry of the plates were not changed, the software could not mesh the structure due to steep corners and tight angles at the specific plates.

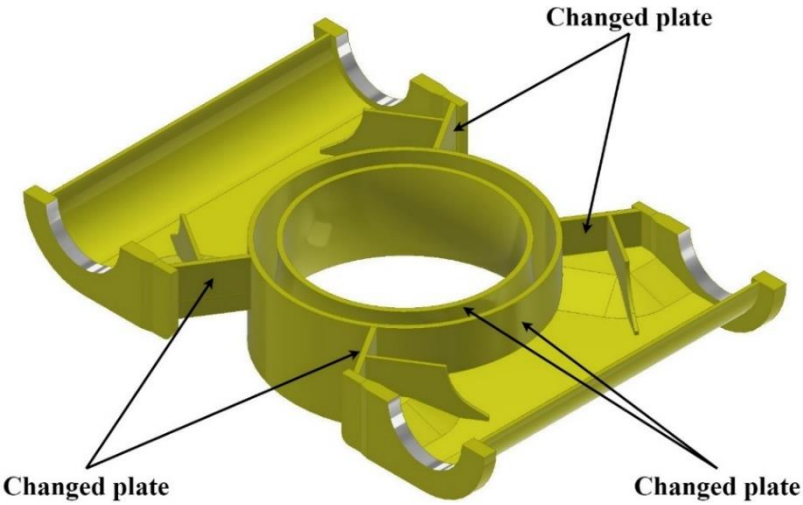

Figure 36 Half section view of torque transfer structure showing changed plates for FEA.

After refining the four contact plates, the geostationary module tube and the curved plate for guiding of pull-in wire, a simplified torque transfer system were assembled as seen in *Figure 37*. The simplified system consists of a torque transfer structure, two shaft bearings, a shaft, two vertical arms, two rear axle bolts, two horizontal arms including four spherical bearings and a torsion ring. Before loading the simplified assembly file into Ansys and choosing the "static structural" analysis solver, the inventor assembly file was converted and exported as a STEP-file.

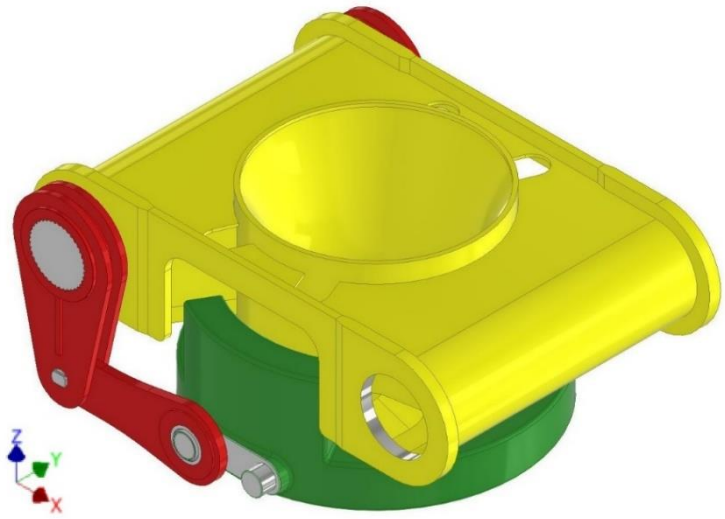

Figure 37 Simplified torque transfer system for ULS FEA.

Ansys automatically defines all contact regions, i.e. surfaces, solids, lines, faces, edges, as "bonded" contacts. According to the documentation, bonded regions involve no sliding or separation between faces and edges. It can be compared to a rigidly glued contact. Changes are made to contacts in the FEA, when defining connection joints at bearings and spline which are described in *Chapter 6.1.4*.

6.1.3 Material

Material assignment are based on a default conventional structural steel in the software, where only yield strength was changed to represent the two materials in the system. In consultation

with UiS supervisor and Ansys support staff, no proper method for defining fracture toughness in Ansys "engineering data" were found. Therefore, all components in the torque transfer system got the same material properties in Ansys. NVD36 was supposed to be applied for all solids except for the vertical and horizontal arms where NVE36 should have been applied. Default surrounding temperature in the analysis is 22 degrees Celsius. Hence, it is believed that lack of proper defined material properties will have no impact on results, since the analysis temperature is well above DBTT for both NVD36 and NVE36, i.e. -20 and -40 degrees Celsius, respectively. Material factor, γ_M, are equal to 1.15 for ULS condition.

6.1.4 Connections

Six joints are defined to represent the bearings in the system. All four spherical bearings are applied as "body-body spherical joints", meaning that the spherical bearings are present between two movable bodies and not grounded. The outer ring is specified as "reference" and the inner ring as "mobile", with the following faces as viewed in *Figure 38 (a)* and *(b)*. The inner ring is "mobile" since it can rotate and move inside the outer ring.

Additionally, the small contact face in the xz-plane at the inner rings of the spherical bearings are defined as "body-body planar joints". The contact face must be able to slide at either the vertical arm side plates or the torsion ring connection face. *Figure 38 (c)* and *(d)* shows how one side of the vertical arm side plates are defined as "reference" and the inner ring as "mobile". In the foremost spherical bearings, the torsion ring contact face will be defined as "reference".

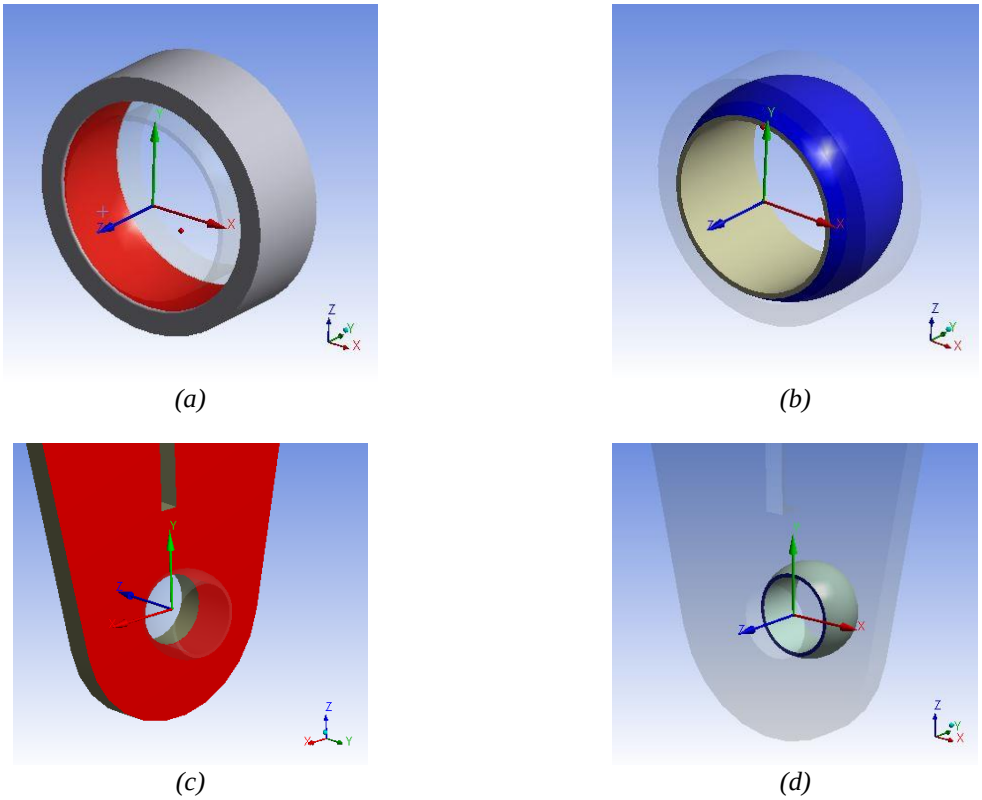

(a) *(b)*

(c) *(d)*

Figure 38 FEA spherical bearings defined as; (a) reference spherical, (b) mobile spherical, (c) reference planar and (d) mobile planar.

Two shaft bearings are defined as "body-body cylindrical joints" where the shaft is placed as viewed in *Figure 39 (a)* and *(b)*. In addition, the flanges of the shaft bearings are defined as

"body-body planar joints", where the hub containing the female spline can move freely towards it, as viewed in *Figure 39 (c)* and *(d)*.

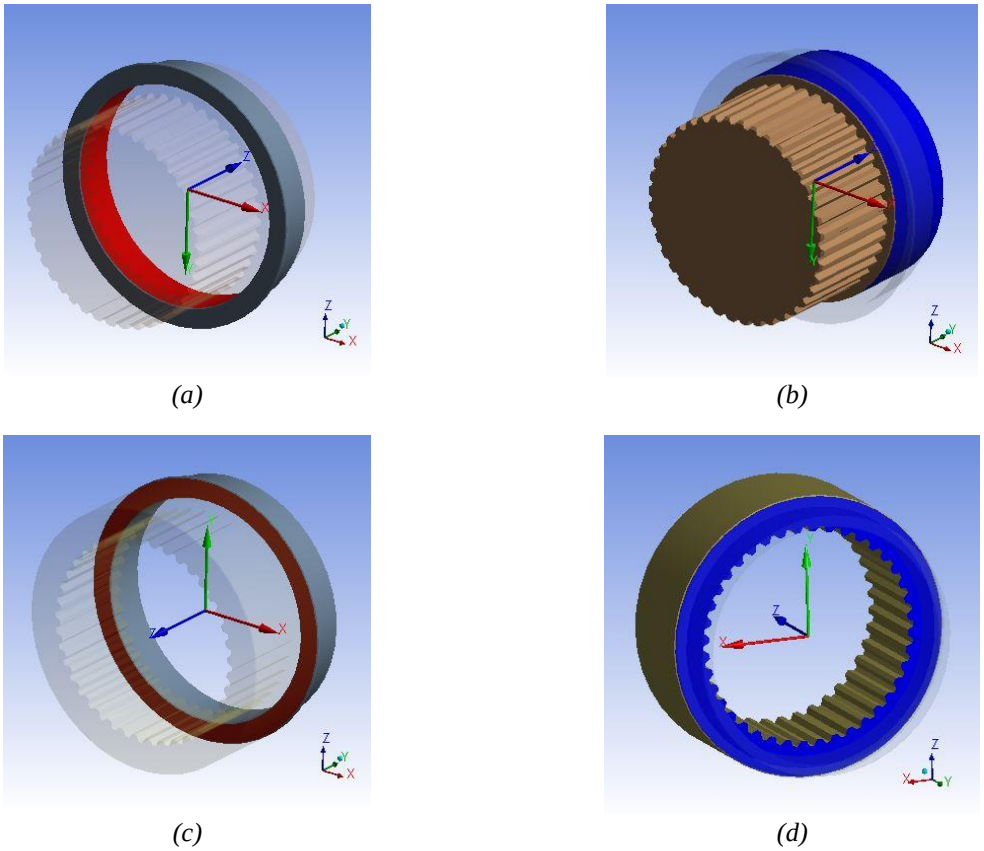

(a) *(b)* *(c)* *(d)*

Figure 39 FEA shaft bearing connection defined as; (a) reference cylindrical, (b) mobile cylindrical, (c) reference planar and (d) mobile planar.

All the shown connection faces are also defined as "frictionless" contact types, meaning that components can slide towards each other frictionless and form gap between faces, according to the documentation. Zero friction coefficient is assumed, thus allowing free sliding. Spline connections between the shaft and vertical arm hubs were also set to "frictionless" contact type. The connection joints between torsion ring and horizontal arm inner ring in the foremost spherical bearing were set to "no separation" for the solution to converge and not be corrupted. "No separation" involve most of the same settings as "frictionless" contact type, without being able to separate as the wording suggests.

6.1.5 Mesh

Initial mesh was generated from the default program-controlled mesh generator. A total of 119,595 nodes and 51,286 elements were generated. Average skewness on the initial automatic generated mesh was 0.576, and based on *Table 5* in *p. 43* it is considered a "fair" mesh. Average orthogonal quality was 0.440, also considered a "fair" mesh based on *Table 6* in *p. 43*.

The program-controlled solver chose quadratic element order, meaning that midside nodes are created at elements in the component solids. Hence, the mesh consists of three different element types: 10-node tetrahedron (Tet10), 20-node hexagonal (Hex20) and 15-node pentagonal/wedge (Wed15).

To improve the mesh quality, some refinements to the mesh properties were made. “Initial size seed” was changed from “assembly” to “part”. That involves the mesh being generated based on the size of each part in the assembly and not the size of the assembly itself, according to the documentation. It means that the mesh is made finer. In addition, the “resolution” of element sizing was upgraded. Mesh “resolution” changes from course (0) to fine (7). It was set from default level of “2” up to “4” for this mesh. With these settings, a total of 449,731 nodes and 193,817 elements were now generated in the final mesh. The generated mesh for ULS FEA are shown in *Figure 40*.

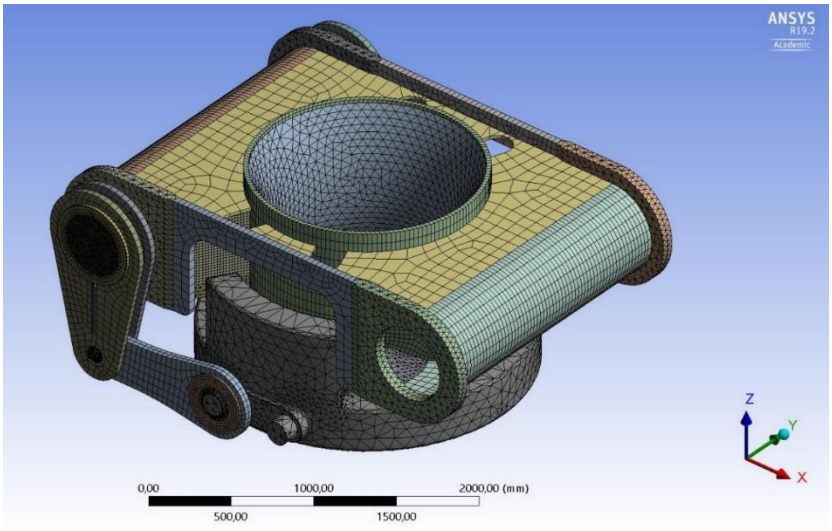

Figure 40 ULS FEA mesh.

Average skewness reached 0.365, and now achieved “good” quality based on *Table 5* in *p. 43*. Average orthogonal quality reached 0.652, an increase from the initial mesh but still in the “fair” quality region based on *Table 6* in *p. 43*. Skewness quality distribution in column chart form is presented in *Figure 41*.

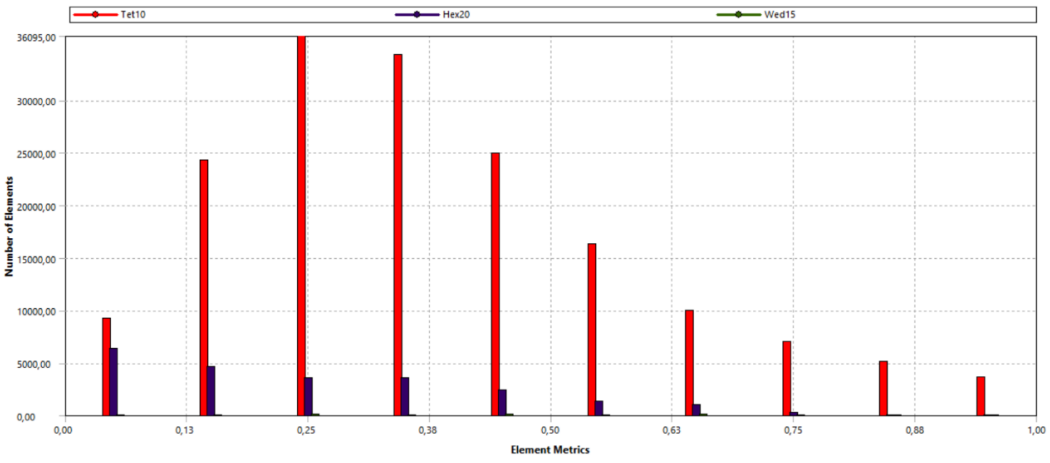

Figure 41 ULS FEA skewness quality distribution.

There are mostly Tet10 elements that are generated in the mesh. Hex20 elements are generated in most of the circular plate components and other plated sections. Only a couple of hundred Wed15 elements are generated, and they are located in circular components to fulfill continuity of the geometrical shapes in the mesh.

When only considering the “bad” regions of skewness quality metric, *Figure 42* shows the elements. The “bad” region of skewness level are present from 0.90-1.00, according to *Table 5* in *p. 43*. Only Tet10 element types where found to have “bad” quality.

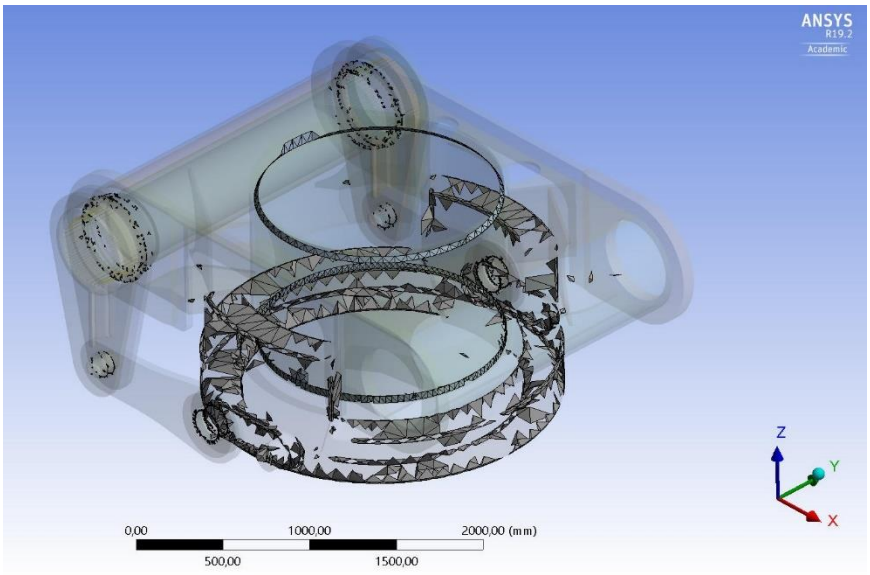

Figure 42 «Bad» quality Tet10 elements based on skewness metric.

“Bad” quality Tet10 elements are mainly present in the regions of the shaft bearings, outer rings of the spherical bearings, upper and lower part of the curved guiding plate, and especially in the torsion ring. That being said, *Figure 43* shows concentrations of “excellent” quality Tet10 elements in most of the same regions containing the “bad” elements. “Excellent” quality is between 0-0.25 level of skewness, according to *Table 5* in *p. 43*. “Bad” quality elements were not present in the contact faces of applied torque in the torsion ring.

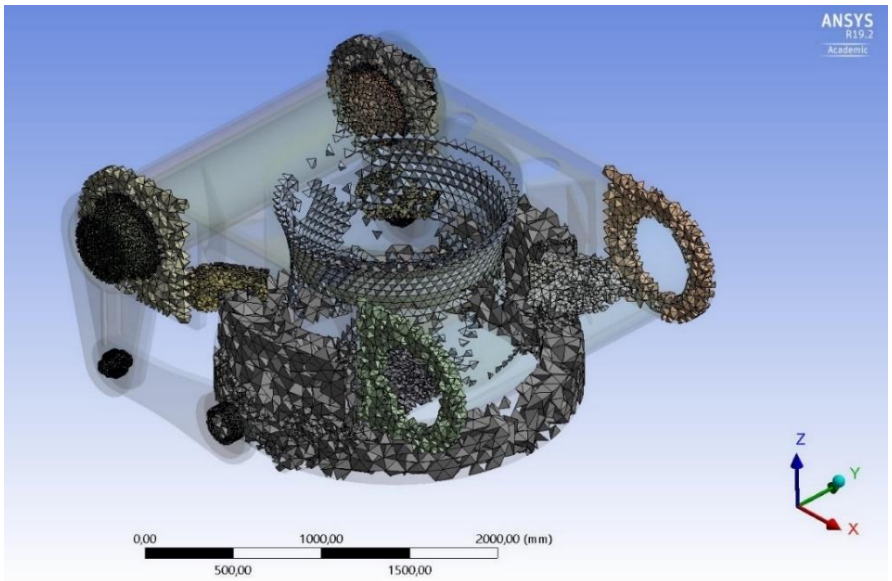

Figure 43 «Excellent» quality Tet10 elements based on skewness metric.

Further mesh refinement, both global and local, only slightly increased the mesh quality. Computational time also increased drastically, and errors corrupted the solution from time to time. If a solution were completed, the results remained quite similar. Higher maximum stresses also occurred, due to smaller size element regions being exposed to most of the

applied forces. Given the geometrical complexity of the components in the torque transfer system, it is believed that the final mesh is acceptably good and provides a realistic stress and deformation distribution result. By including all three element types in the "excellent" quality region, *Figure 44* shows the mesh distribution.

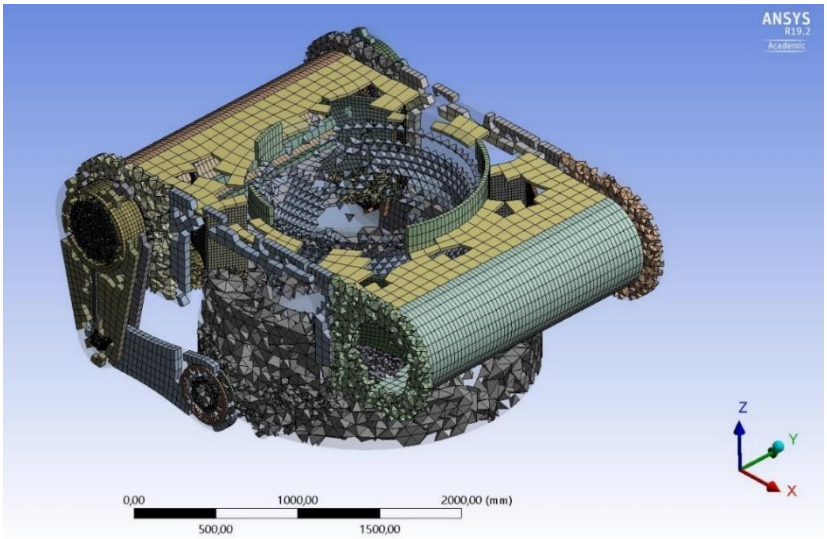

Figure 44 «Excellent» quality mesh elements based on skewness metric.

It is clear that all components have a great amount of "excellent" elements in them, forming a "good" mesh based on level of skewness metric from *Table 5* in *p. 43*. When investigating result values, one shall see it in relation to the "bad" quality mesh regions.

6.1.6 Boundary conditions

A fixed support is applied to the top of the geostationary module tube as viewed in *Figure 45*. The fixed support represents the torque transfer system being fully connected to the geostationary module tube.

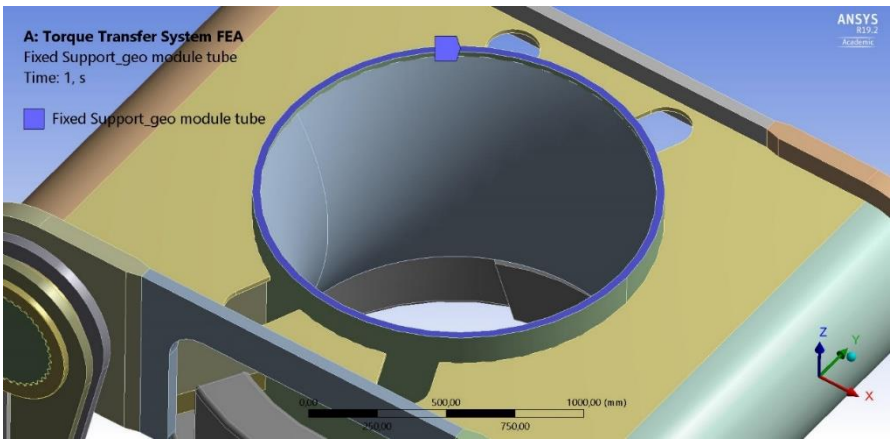

Figure 45 Fixed support at geostationary module tube.

From *Chapter 4.1.1* load factor, γ_f, shall be 1.3 for permanent and variable functional loads during ULS condition. However, it was determined to use load factor of 1.0 since both FLS and ALS have this load factor. It is easier to see the limit states in context of one another when load factor is equal. Load factor is manually added when listing results from hand calculations. Due to linear behavior, deformation and stress distribution will be 30 % larger than shown in ULS and sensitivity study FEAs and shall especially be considered in the most critical regions.

Input moment of 2,400 kNm, M_{z_D}, is applied as pressure load in corresponding contact faces in the torsion ring. The applied load, F_{TR}, is calculated based on the inner diameter of the contact face, $d_{TR} = 1{,}504\ mm$. It is a conservative assumption to take the inner diameter and not the mid diameter at the contact face, to calculate the torsion ring applied load:

$$F_{TR} = \frac{M_{z\_D}}{d_{TR}} \qquad (27)$$

$$\rightarrow F_{TR} = \frac{2{,}400\ kNm}{1{,}504\ mm}$$

$$\rightarrow F_{TR} = 1{,}595.7\ kN$$

The applied load, F_{TR}, is distributed as pressure over the area of the contact face in the torsion ring, A_{CF}. It is 19,708 mm^2, which is found with the "measure tool" in Inventor. The applied pressure, P_{TR}, in the torsion ring becomes the following:

$$P_{TR} = \frac{F_{TR}}{A_{CF}} \qquad (28)$$

$$\rightarrow P_{TR} = \frac{1{,}595.7\ kN}{19{,}708\ mm^2}$$

$$\rightarrow P_{TR} = 81.0\ MPa$$

Pressure, P_{TR}, is applied in the xy-plane directly at the two corresponding contact faces in the torsion ring as seen in *Figure 46*. The applied pressure is not perpendicular applied to the contact face area, as the torsion ring contact face have an angle of 76 degrees relative to the z-axis. However, it is believed that applying pressure in the xy-plane better represents realistic loading conditions then applying it perpendicular to the contact face.

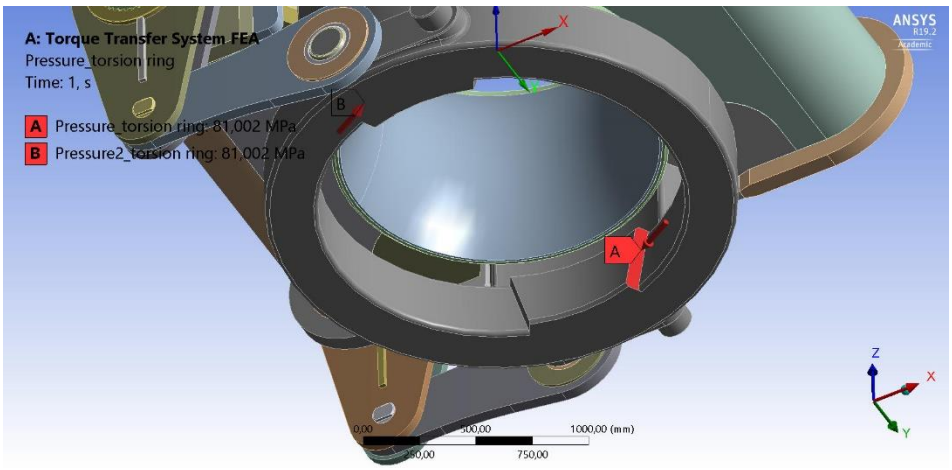

Figure 46 Applied pressure at contact faces in torsion ring.

Input moment are applied in positive z-direction using the right-hand-rule, as viewed in *Figure 46*. There is no gravity applied to the environment in the analysis due to the assumption of static equilibrium.

Before running the analysis, a change in the "solver controls" in the "analysis settings" were conducted. By default, Ansys have turned off so called "large deflection" to save computational

time. By including “large deflection” in the solver, Ansys will account for changes in stiffness due to changes in geometrical shape, according to the documentation. Nonlinear relationship between force and displacement is another way to describe it. Given the relatively complex and varied shapes in the torque transfer system this setting was included. More realistic structural behavior between the assembled components are believed to occur considering the relatively large torque applied to the system. The solver ran for slightly above 44 minutes before completing the solution and obtaining the results. To compare, computational time without including the “large deflection” setting, simulation time would only be about 6 minutes and showing somewhat different results.

6.1.7 Geometry optimization

Based on stress results in *Chapter 7.1.2*, geometry optimization of the torque transfer structure were conducted to strengthen the weakest regions. First, adding fillets to the sharp geometrical changes that experienced stress concentrations were conducted as seen in *Figure 47*. Fillet radius of 20 mm were added to the lower plate, and fillet radius of 5 mm were added to the edges surrounding the hydraulic cylinder holes. Problem formulation and approach were conducted in the same manner as the original ULS FEA. These changes gave a mesh of 458,566 nodes and 198,789 elements, with average skewness quality of 0.374, giving a “good” quality mesh based on *Table 5* in *p. 43*. Elapsed time for the solver were close to 54 minutes.

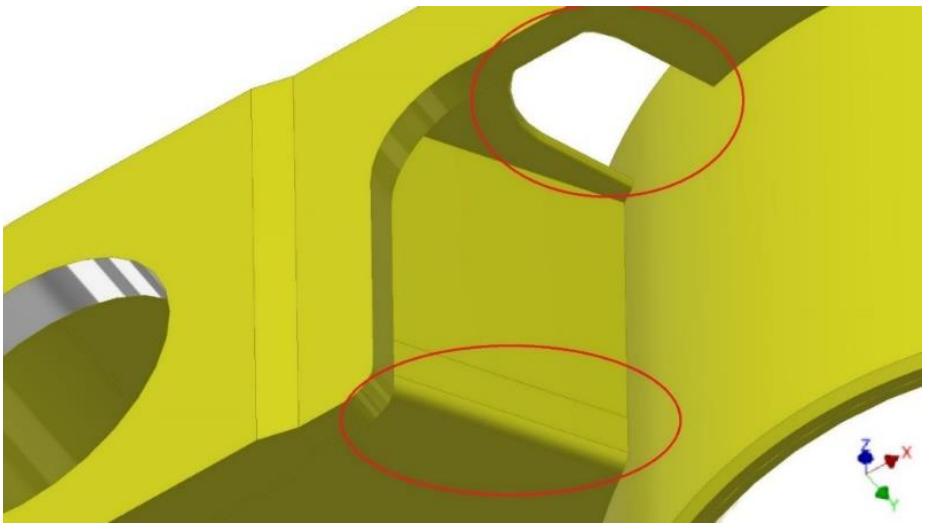

Figure 47 ULS FEA geometry optimization with fillets.

Another optimization method that proved better, were to insert so called sleeves into the hydraulic cylinder holes. Fillet welds were also added to the stress concentration region around the geostationary module tube, contact plate and reinforcement plate, as seen in *Figure 48*.

Figure 48 ULS FEA geometry optimization with sleeves and welds.

Adding sleeves and fillet welds to the torque transfer structure proved to be the best solution and were chosen for further examining. Fillet weld throat thickness of 10 mm were selected. The sleeve was 120 mm long, had 20 mm thickness, outer diameter of 240 mm, giving an inner diameter of 200 mm. The top plate containing the hydraulic cylinder holes also had to be changed. It was made continuous along the geostationary module tube and increasing the hole radius of 20 mm. Problem formulation and approach were conducted in the same manner as the original ULS FEA. These changes gave a mesh of 458,485 nodes and 198,382 elements, with average skewness quality of 0.373, giving a "good" quality mesh based on *Table 5* in *p. 43*. Elapsed time for the solver were close to 1 hour and 5 minutes.

Another possible optimization is to change thickness of the top plate with the hydraulic cylinder holes from 20 mm to 25 mm for instance. However, since the sleeves and the fillet welds mitigated the peak stress regions significantly, increasing plate thickness will only mitigate stress distribution slightly and not be necessary.

6.2 Fatigue Limit State

Even today, fatigue is only partially understood and a highly complicated phenomenon. While many static failures give visible warning, fatigue fractures are sudden and total. Fulfilling FLS condition is the most worrying and uncertain failure state for the torque transfer system. Based on Ansys documentation, resulting "life" distribution in FEA represents the number of cycles until reaching fatigue failure in the component when exposed to constant loading amplitude.

Fatigue shall be investigated component by component in regions probable to be exposed to fatigue loading, as described in (DNV GL, 2019). FLS FEA are setup almost equivalent to the ULS FEA described in *Chapter 6.1*. However, based on findings in *Chapter 7.1*, the optimized torque transfer structure was utilized as geometry. Load and material factor are both equal to 1.0.

BW Offshore expects that half the design torque will be present as loading for FLS condition. Hence, pressure in the torsion ring also becomes half the pressure from ULS FEA:

$$P_{TR\_FLS} = 0.5 \bullet P_{TR} \quad (29)$$

$$\rightarrow P_{TR\_FLS} = 0.5 \bullet 81.0\ MPa$$

$$\rightarrow P_{TR\_FLS} = 40.5\ MPa$$

Endurance limits are commonly determined in well controlled laboratory tests on standard test specimens. It is unlikely that such test results can directly be used to evaluate the fatigue life of any structural component of random size and material under diverse loading conditions. Therefore, there exist several modifying factors, also called Marin factors, when evaluating fatigue for structures in a non-laboratory environment. Fatigue behavior are also affected by matters such as manufacturing method, working environment and design. These modifying factors will reduce the endurance limit of the material and adjust the S-N curve correspondingly. The two most relevant modifying factors are included in FLS FEA, one considering the surface and another considering the geometry size. Loading factor is set to 1.0, since the combined loading is managed using equivalent Von Mises stress (Budyans and Nisbett, 2015).

Conservatively, surface of plates is assumed to be "machined or cold-drawn". Surface modification factor is governed by minimum material ultimate tensile strength, σ_{UTS}, in the following formula (Budyans and Nisbett, 2015, pp. 295-296):

$$k_a = 4.51 \bullet \sigma_{UTS}^{-0.265} \quad (30)$$

$$\rightarrow k_a = 4.51 \bullet (460\ MPa)^{-0.265}$$

$$\rightarrow k_a = 0.888$$

Based on the results under *Chapter 7.1*, the most exposed region to fatigue is located in the torque transfer structure at the reinforcement plate for ALS and have plate thickness of 100 mm. Resulting in a size modification factor, k_b, based on size of the member exposed to fatigue, the formula becomes the following (Budyans and Nisbett, 2015, p. 296):

$$k_b = 1.51 \bullet d^{-0.157} \quad (31)$$

$$\rightarrow k_b = 1.51 \bullet (100\ mm)^{-0.157}$$

$$\rightarrow k_b = 0.733$$

Combined modification factor, k, then becomes:

$$k = k_a \bullet k_b \quad (32)$$

$$\rightarrow k = 0.888 \bullet 0.733$$

$$\rightarrow k = 0.651$$

S-N curves are generated from the so-called stress-life method, where physical test specimens of specific materials are tested. Using semi-log plotting, the S-N curve will have linear decreasing alternating stress for increased number of cycles before failure. S-N curve will at some strength level become constant linear, this is called the endurance limit of the material. It

usually occurs around 1e6 or 1e7 cycles, where fatigue life is considered "infinite" for a greater number of cycles. Fatigue failures are generally classified as low-cycle fatigue up to 1e3 cycles and as high-cycle fatigue for failure at greater than 1e3 cycles. S-N curve will also be approximately linear in both classifications respectively, but with different slopes (Budyans and Nisbett, 2015).

Alternating stress values are simply multiplied by the combined modification factor, $k = 0.651$, to form modified alternating stress. *Table 7* shows experimental data from S355J2+N (S355J2G3/NVD36) tested material specimens that are used to form this thesis S-N curve (Milovanovića et al., 2019). Only the lowest experimental data values are included to get a conservative S-N curve. Since 50,300 is the lowest number of cycles until fatigue failure in the test, extrapolation of the conservative data is conducted to get the entire high-cycle fatigue region, i.e. from more than 1e3 cycles.

Table 7 FLS FEA conservative dataset for S-N curve.

Number of cycles	Alternating stress [MPa]	Modified alternating stress [MPa]
1,000*	352.7*	229.6*
50,300	270.5	176.1
88,300	253.3	164.9
109,600	250.4	163.0
116,000	250.1	162.8
257,700	234.3	152.5
1,117,200	233.0	151.7

*extrapolated value

Based on the number of cycles and modified alternating stress from *Table* 7, the dataset are inserted into "engineering data" in Ansys and the resulting S-N curve are viewed in *Figure 49*. It is important to have a realistic and proper S-N curve based on correct properties and characteristics of the used material.

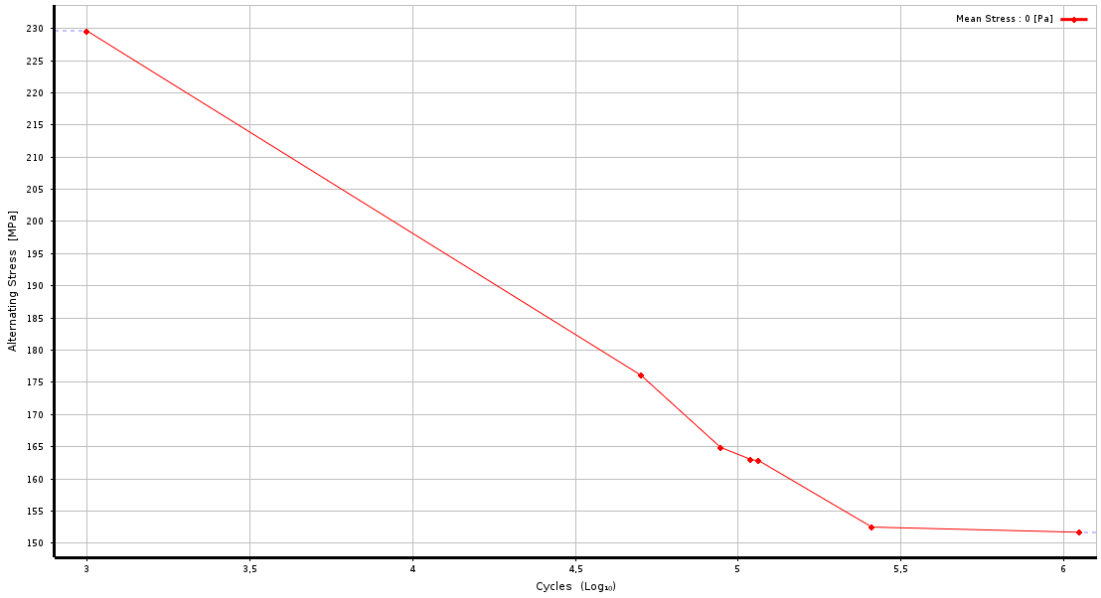

Figure 49 FLS FEA S-N curve Ansys.

Endurance limit occurs at 151.7 MPa of alternating stress and 1.12e6 cycles. Meaning that regions with alternating stress below 151.7 MPa are considered to have "infinite" fatigue life. There exist various S-N curves for S355J2+N steel. Hence, fatigue tests for the specific batch of steel used for the torque transfer system should be acquired, to assure more reliable data.

BW Offshore expects that the torque transfer system will be exposed to approximately 7'500 full loading cycles per year, n_{YR}, equivalent to a little more than 20 cycles per day. It is designed for 20 years of operational service, t_{YR}. Loading are defined as "fully reversed" in Ansys, meaning that the magnitude will change direction one time for each cycle. It will not cycle from zero loading to full loading. In other words, one cycle represents shifting direction of weathervaning two times with full positive and full negative loading magnitude. Fatigue design cycles, n_d, considering DFF of 3.0, for the torque transfer system shall be above:

$$n_d = DFF \bullet n_{YR} \bullet t_{YR} \tag{33}$$

$$\rightarrow n_d = 3.0 \bullet 7{,}500 \ \frac{cycles}{yr} \bullet 20 \ yrs$$

$$\rightarrow n_d = 4.5e5 \ cycles$$

The torque transfer system shall resist 450,000 loading cycles during its lifetime.

FLS FEA ran for 1 hour and 5 minutes before completing a result solution.

6.3 Accidental Limit State

Similarly to *Chapter 6.1* for ULS FEA, ALS FEA have the same formulation and approach. However, only the torque transfer structure and torsion ring are present for ALS condition as previously explained in *Chapter 4.4*. This situation is assumed to be worst-case scenario for the torque transfer system under ALS condition. Torque transfer structure with optimized geometry are also utilized since it proved to be structurally preferable from results found in *Chapter 7.1*. *Figure 50* show the applicable geometry used in the ALS FEA.

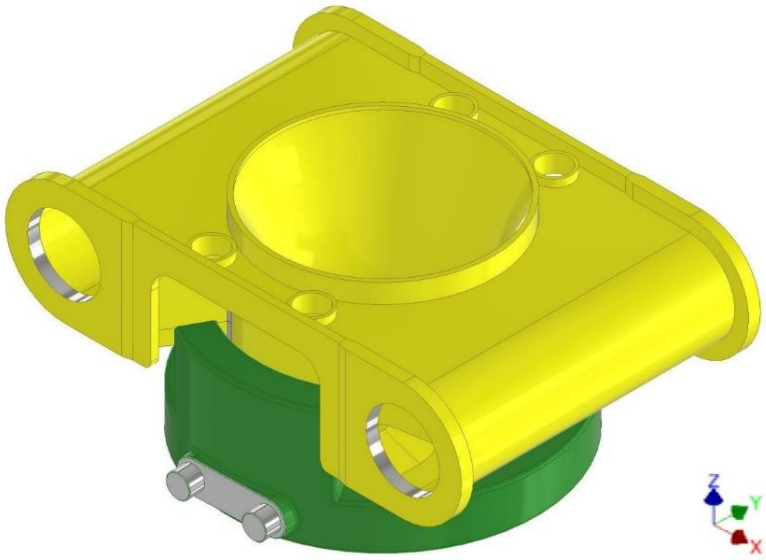

Figure 50 ALS FEA geometry.

Torsion ring extrusion for ALS are defined to make contact at the reinforcement and contact plates in the torque transfer structure. This setup and plates are shown in *Figure 33 (a)* and *(b)* under *Chapter 4.4* for redundancy system.

Generating mesh with similar settings as for ULS in *Chapter 6.1.5* resulted in 168,165 nodes and 61,351 elements, with an average level of skewness of 0.384. From *Table 5* in *p. 43* the mesh are considered to have "good" quality.

Several different magnitudes of applied load were tested, to verify the maximum that the torque transfer system can withstand for ALS condition. An initial test with design torque of 2,400 kNm similar to ULS condition, are conducted to observe structural behavior under ALS condition. Consequently, try-and-fail approach for increasing applied torque are conducted. At some point, the applied torque is considered to maximize structural strength capacity and a believed to be ALS maximum value are found. *Table 8* show different applied torques resulting is similar increase in magnitude of applied pressure in torsion ring.

Table 8 ALS FEA loading magnitude test cases.

Loading magnitude factor	Applied torque [kNm]	Applied pressure [MPa]
1.0	2,400	81. 0
1.5	3,600	121.5
2.0	4,800	162.0
3.0	7,200	243.0

Loading and material factor are considered to be 1.0 under ALS condition as described in (DNV GL, 2019). *Figure 51* shows the applied pressure for a loading magnitude factor of 2.0, for the torque transfer system under ALS condition. As observed, the torsion ring make contact to the torque transfer structure in the applied torque direction.

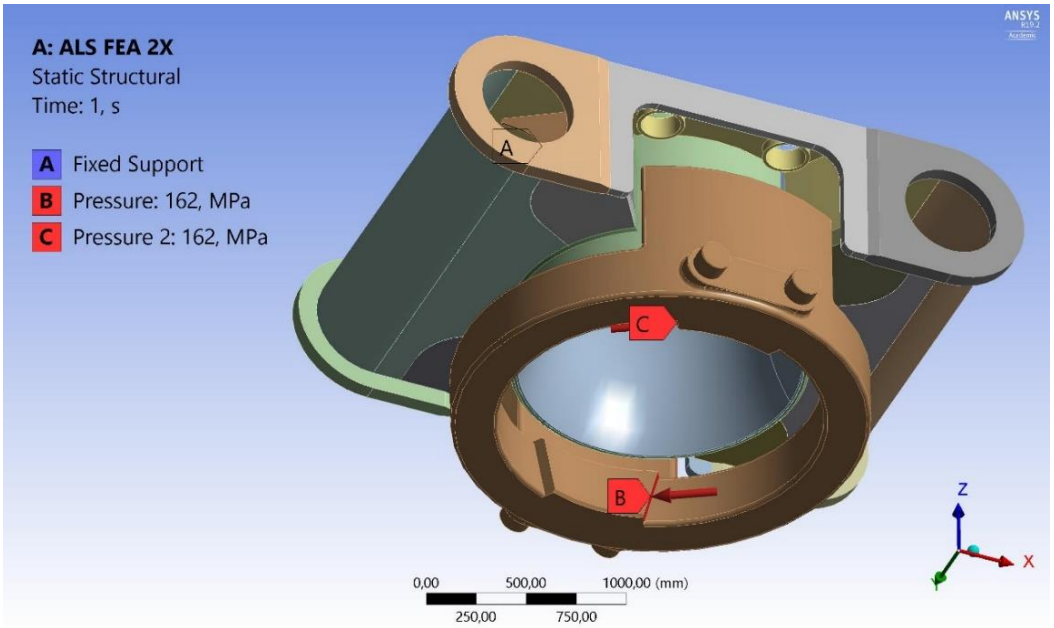

Figure 51 ALS FEA applied pressure.

Solving time were under 3 minutes for all loading cases in ALS FEAs.

6.4 Sensitivity study

Since the torque transfer system are designed to accommodate positional adjustments, it is relevant to conduct a sensitivity study to examine how the structure respond to non-symmetrical loading. The sensitivity study have exact similar problem formulation and approach as for ULS FEA in *Chapter 6.1*. However, the torsion ring have a positional offset in all directions as viewed in *Figure 52 (a)* and *(b)*. Positional movement also correspondingly relates to the horizontal arms, vertical arms, spherical bearings, axle and shaft.

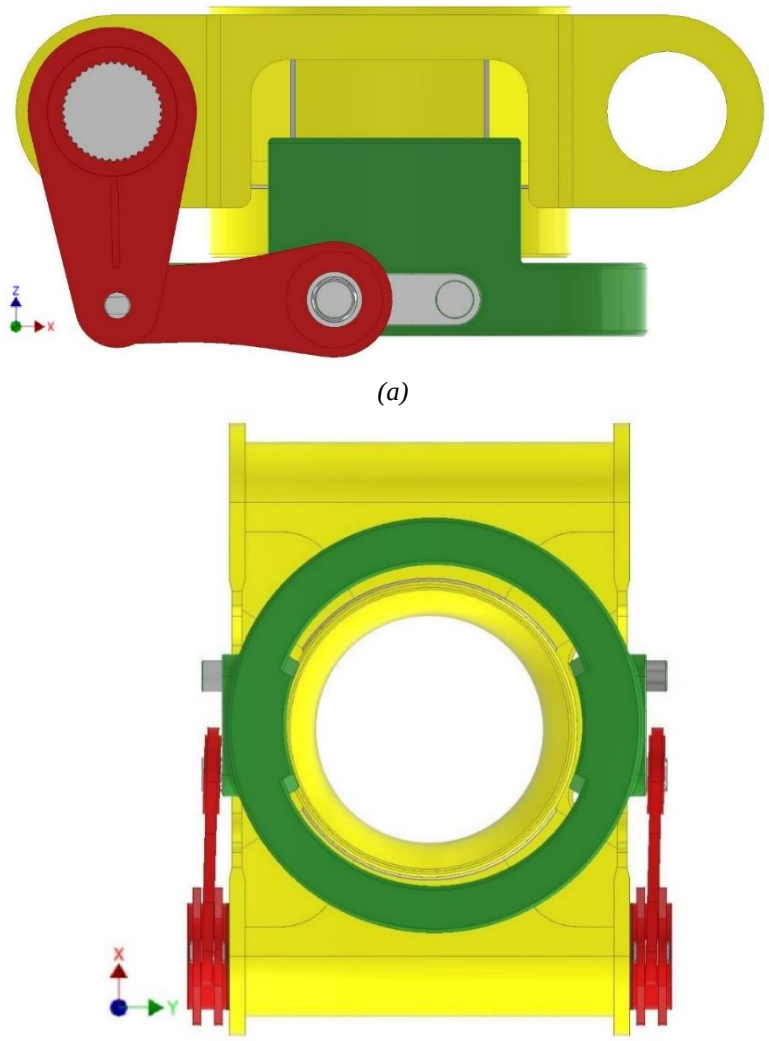

(a)

(b)

Figure 52 Sensitivity study with unsymmetrical loading shown in (a) x-z plane and (b) x-y plane.

The torsion ring has adjusted positional movement of +20 mm in x-direction, +23.5 mm in y-direction and + 25 mm in z-direction. It relates to 1.5 degrees of misalignment angle in the spherical bearings and 325 mm of stroke length in the hydraulic cylinders, i.e. 25 mm less than fully activated hydraulic cylinders.

Optimized torque transfer structure geometry is utilized in the sensitivity study. 2,400 kNm of torque are applied to system, corresponding to 81.0 MPa of pressure in the torsion ring. Like the ULS condition, material factor of 1.15 are also applicable to the sensitivity study. Load factor of 1.3 must also be accounted for in the deformation and stress distributions figures.

7 Results and discussion

Results are presented and discussed through extensive use of figures from the various limit state condition FEAs. Deformation is examined by visualize structural behavior and check for excessive deformation in key regions. Equivalent stress forms the basis for verifying structural integrity of components when comparing to material capacity. Hand calculations will be performed consecutively in relevant sections to validate results from ULS FEAs. *Chapter 7.1* on ULS is divided into several subchapters with the main components, as a great amount of information are presented.

"Contour bands" and "no wireframe" were selected in Ansys to better view the resulting stress and deformation distribution in the components. "True scale" of the structure was also selected, if not otherwise stated, to get the most realistic representation of the resulting structural behavior.

7.1 Ultimate Limit State

Deformation of the structure will first be examined. Afterwards, equivalent Von Mises stress are reviewed and discussed. Based on maximum results in certain regions that occur, optimization proposals will be presented and tested. Other key components will also be examined individually and have hand calculations performed, even if stress is well below material strength capacity. This are conducted both to assure validity of the FEAs and highlight weakest parts of each main component. Finally, a conclusion is drawn regarding the ULS condition FEAs.

For ULS condition and sensitivity study, material strength capacity with material factor, $\gamma_M = 1.15$, are specified in (DNV GL, 2019). Material capacity in both equivalent stress and shear stress are based on material yield strength. Material yield strength of NVD36 and NVE36 is $\sigma_{YS} = 355\ MPa$, and material factor, $\gamma_M = 1.15$, are defined for plated structures and tubular members. This gives material equivalent stress capacity, σ_{cap}, and shear stress capacity based on Von Mises criterion, τ_{cap}, of the following:

$$\sigma_{cap} = \frac{\sigma_{YS}}{\gamma_M} \tag{34}$$

$$\rightarrow \sigma_{cap} = \frac{355\ MPa}{1.15}$$

$$\rightarrow \sigma_{cap} = 308.7\ MPa$$

$$\tau_{cap} = \frac{\sigma_{YS}}{\gamma_M \bullet \sqrt{3}} \tag{35}$$

$$\rightarrow \tau_{cap} = \frac{355\ MPa}{1.15 \bullet \sqrt{3}}$$

$$\rightarrow \tau_{cap} = 178.2\ MPa$$

Load factor, $\gamma_f = 1.3$, is added manually to the hand calculations and FEA results for ULS condition. Meaning that the deformation and stress distributions will become 30 % larger than

shown in the FEA figures. It is most important to be aware of the loading factor when considering the most critical regions.

7.1.1 Deformation

The largest deformations occurs in the torsion ring as seen in *Figure 53*. Maximum deformation of 5.3 mm (with loading factor) occurs at the tip of the torsion ring facing the non-activated system side. Deformation appears to act symmetric in the torque transfer system. It is intuitive given the boundary conditions applied to the system.

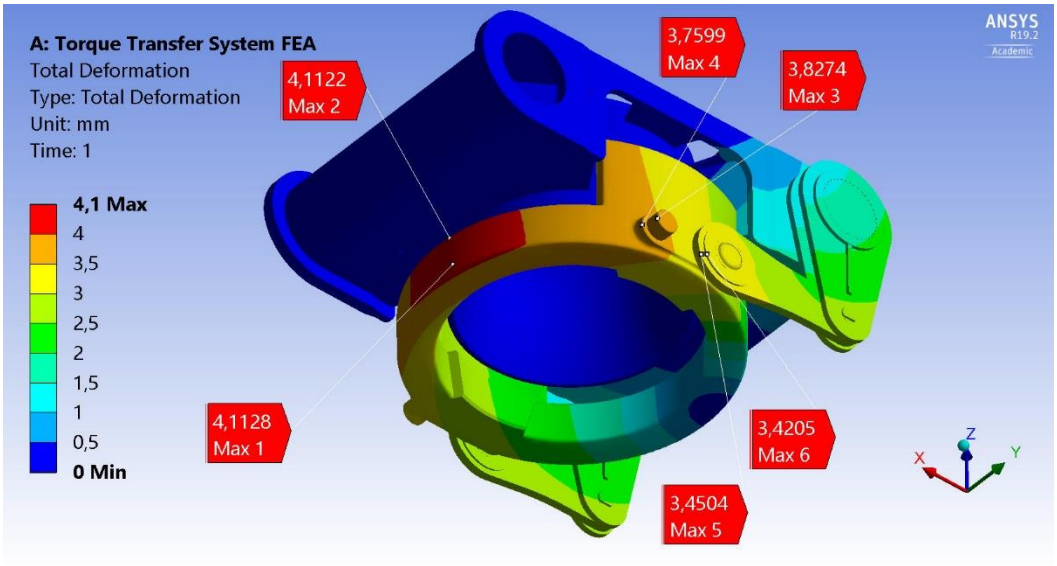

Figure 53 ULS FEA total deformation including maximum points.

To examine the structural behavior, directional deformation in x-direction is shown in *Figure 54 (a)*. From the figure it is observed that the torsion ring sides, and the two horizontal arms will move in opposite direction, naturally explained from the direction of the applied torque. Directional deformation in z-direction is viewed in *Figure 54 (b)*. The two sides of the torque transfer system will move in opposite vertical direction, also explained by the direction of the applied torque. These two directional deformations show almost equally opposite values of deformation. This also confirms the quality of the analysis as it shows intuitive deformation results.

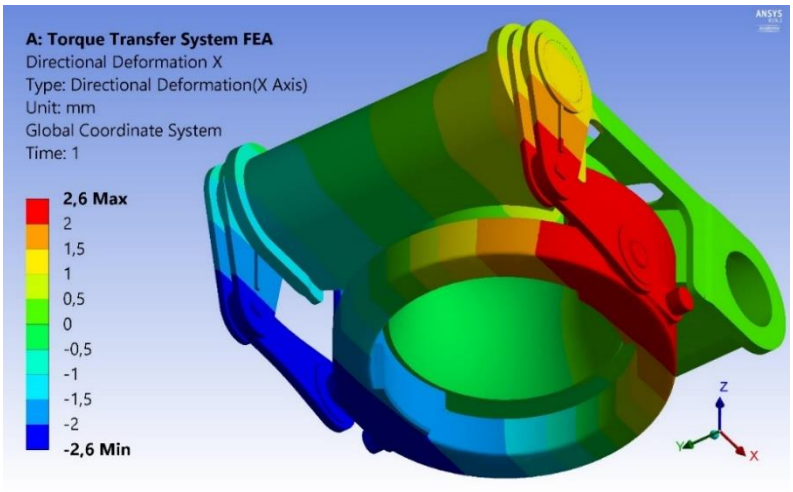

(a)

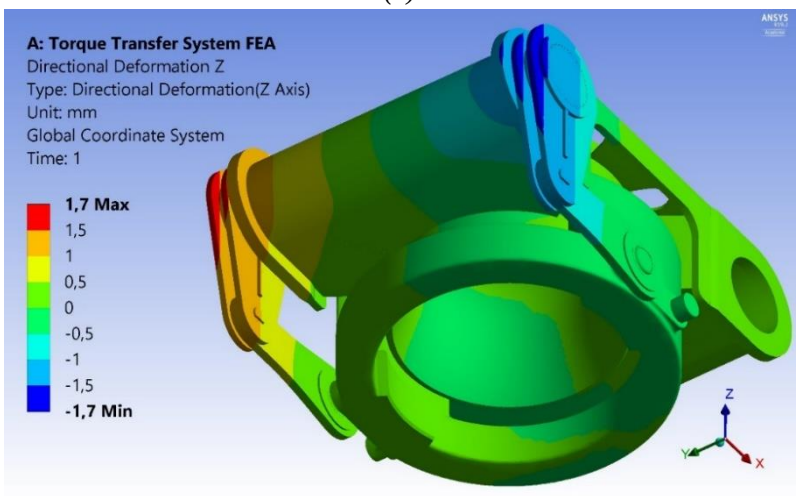

(b)

Figure 54 ULS FEA directional deformation in (a) x-direction and (b) z-direction.

Hundred times the deformation scale is added to *Figure 55* in order to observe the structural behavior of the vertical arms more clearly. However, only about 2.5-4.0 mm deformation (with loading factor) will occur in the vertical arms. It is intuitive that the vertical arms will move in opposite direction and create a twisting motion of the shaft. Changing the direction of the applied torque naturally changes the deformation direction of the vertical arms and twisting motion.

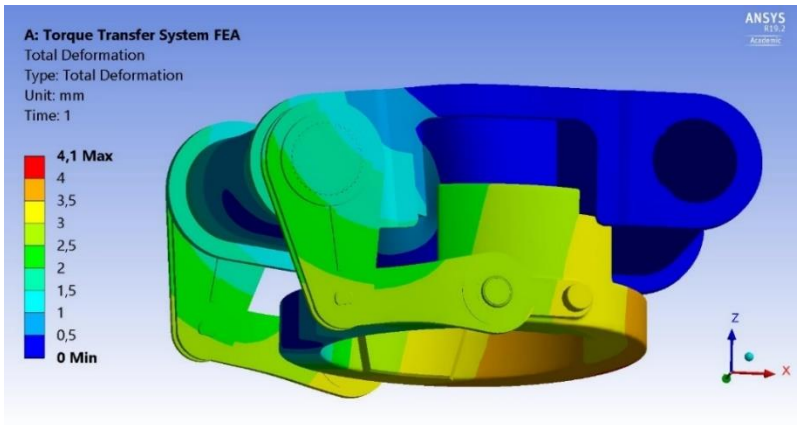

Figure 55 ULS FEA total deformation, 100x scale.

The deformation of the shaft is viewed in *Figure 56*. The outer ends will experience maximum total deformation of 2.6 mm (with loading factor), and deformation will decline towards the center of the shaft.

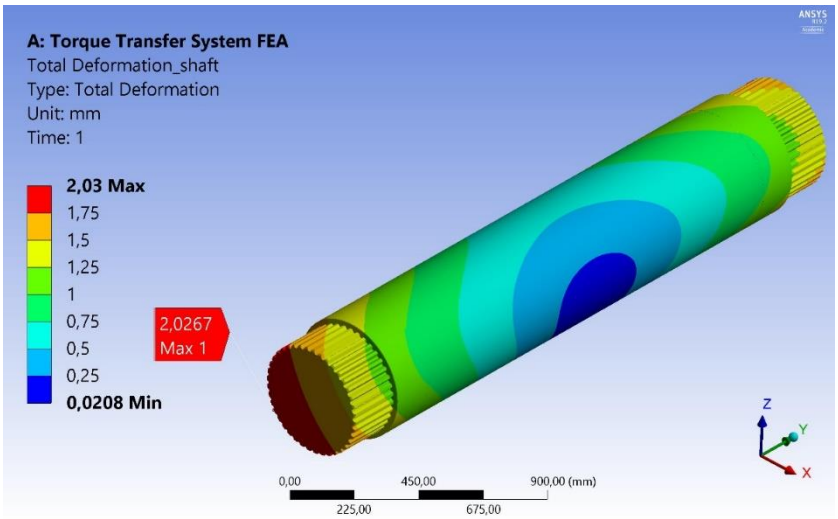

Figure 56 ULS FEA total deformation of shaft.

The shaft is exposed to both bending and twisting moments. *Figure 57* shows the angle of twist in the shaft, assuming the entire section to be hollow.

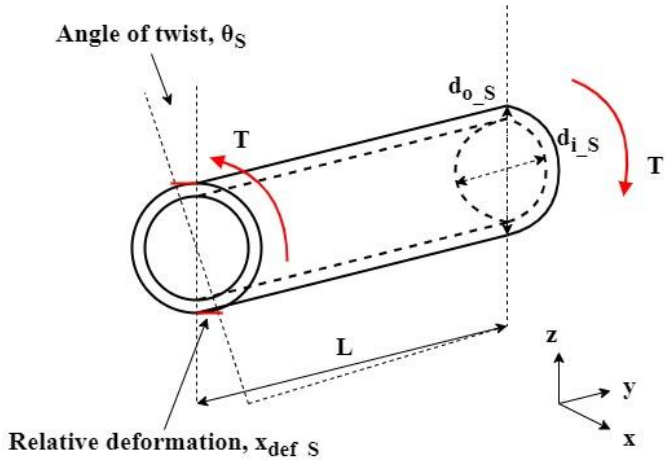

Figure 57 Deformation of shaft based on angle of twist.

Hand calculation on relative deformation at shaft outer ends based on angle of twist, θ_S, are performed (Budyans and Nisbett, 2015, pp. 115-116):

$$\theta_S = \gamma_f \bullet \frac{T \bullet L}{G \bullet J} \qquad (36)$$

Where γ_f is load factor, T is applied torque/torsion or in this case reaction y-moment at round bars (spline connection), $M_{y\_S} = 858.7\ kNm$. L is length of shaft exposed to the torque/torsion, $L = 2 \bullet y_B + y_S = 2{,}250\ mm$. G is shear modulus or modulus of rigidity, which are based on Young's modulus or modulus of elasticity of $E = 200\ GPa$ and Poisson's ratio of $\nu = 0.3$:

$$G = \frac{E}{2 \bullet (1 + \nu)} \tag{37}$$

$$\rightarrow G = \frac{200\ GPa}{2 \bullet (1 + 0.3)}$$

$$\rightarrow G = 76.9\ GPa$$

Lastly, J is polar second moment of area, where only the hollow section is considered. It is a conservative assumption as the real shaft have the two solid spline connections at each end. Outer diameter of central pipe section of shaft is $d_o = 455\ mm$, and inner diameter of central pipe section of shaft is $d_i = 387.4\ mm$.

$$J = \frac{\pi}{32} \bullet (d_o^4 - d_i^4) \tag{38}$$

$$\rightarrow J = \frac{\pi}{32} \bullet ((455\ mm)^4 - (387.4\ mm)^4)$$

$$\rightarrow J = 2e9\ mm^4$$

Inserting (37) and (38) values into (36) gives an angle of twist, θ_S, in the shaft of:

$$\rightarrow \theta_S = 1.3 \bullet \frac{858.7\ kNm \bullet 2{,}250\ mm}{76.9\ GPa \bullet 2e9\ mm^4}$$

$$\rightarrow \theta_S = 0.937\ deg$$

Using the angle of twist, relative deformation in the shaft become the following:

$$x_{\text{def\_}S} = \frac{d_o}{2} \bullet \sin(\theta_S) \tag{39}$$

$$\rightarrow x_{\text{def\_}S} = \frac{455\ mm}{2} \bullet \sin(0.937\ deg)$$

$$\rightarrow x_{\text{def\_}S} = 3.7\ mm$$

Compared to FEA deformation results of about 2.6 mm in *Figure 56*, the calculated value of 3.7 mm is a little higher. It is also intuitive for what to expect given the fact that the FEA shaft have solid spline connections in both ends that provide stiffness to the shaft. Hence, less deformation is present in the FEA. All specific hand calculations are also included chronologically in *Appendix A.2 Mathcad calculations*.

To summarize, local maximum deformation in each main component are listed in *Table 9*. The hand calculation is also included.

Table 9 ULS FEA: local max. deformation values at symmetric locations.

Local max. deformation at symmetric locations [mm]	Component	Placement, figure reference
5.3	Torsion ring	Figure 53
4.6	Horizontal arms	Figure 53
3.8	Vertical arms	Figure 53
2.6	Torque transfer structure	Figure 53
2.6	Shaft	Figure 56
3.7*		Figure 57

*hand calculation

Deformation in the torque transfer system is not of concern based on these results. Given the size of approximately 3.1 m x 2.5 m x 1.5 m for the entire system and the huge amount of forces applied, some millimeter deformation is inevitable. Deformation will be reduced approximately 50 %, when two torque transfer systems are activated.

7.1.2 Stress

Figure 58 show the equivalent Von Mises stress distribution in the torque transfer system. At first glance, the main regions of the torque transfer system seem to be exposed to minor stress values around 100-200 MPa (with loading factor). Stress values also appears to act symmetric in the torque transfer system, similar to the deformation distribution. It is intuitive that the stress values are approximately similar at symmetric locations given the boundary conditions.

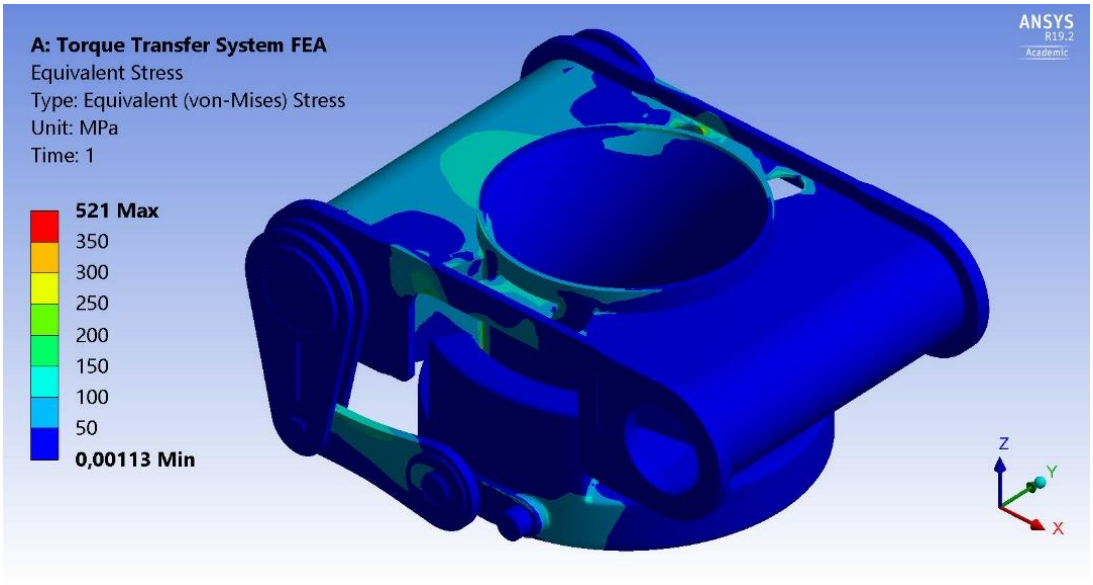

Figure 58 ULS FEA equivalent stress distribution.

All six maximum local stress values occur in the torque transfer structure as seen in *Figure 59 (a)*. They will occur at symmetric locations in the torque transfer system with approximately the same values. *Figure 59 (b)* shows maximum stress values in the reinforcement plate lower corner next to the geostationary module tube in the torque transfer structure. Equivalent stress of 677 MPa (with loading factor) is the maximum value that appears. *Figure 59 (c)* focuses on the maximum stress value of 450 MPa (with loading factor) found at the edge in the holes for the hydraulic cylinders.

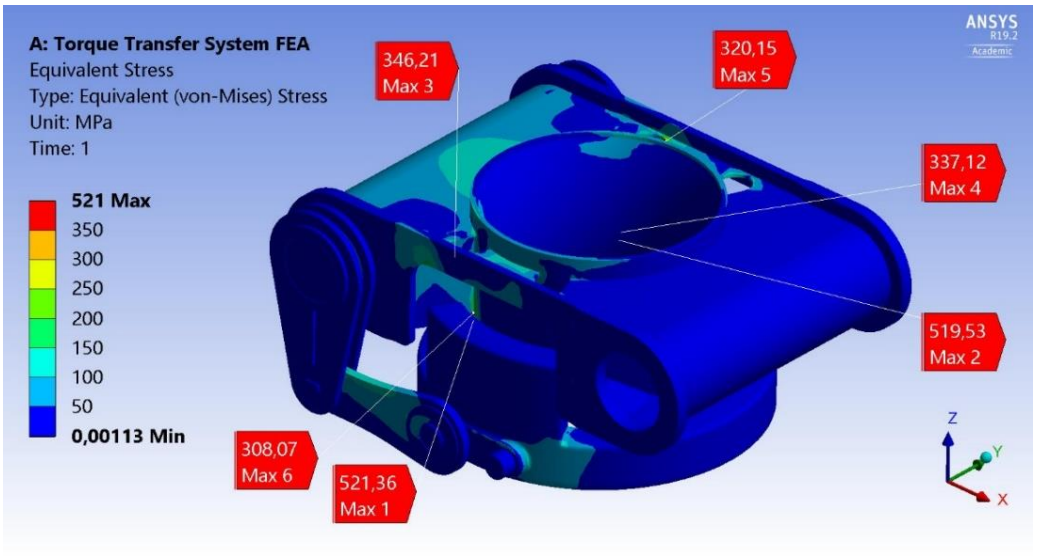

(a)

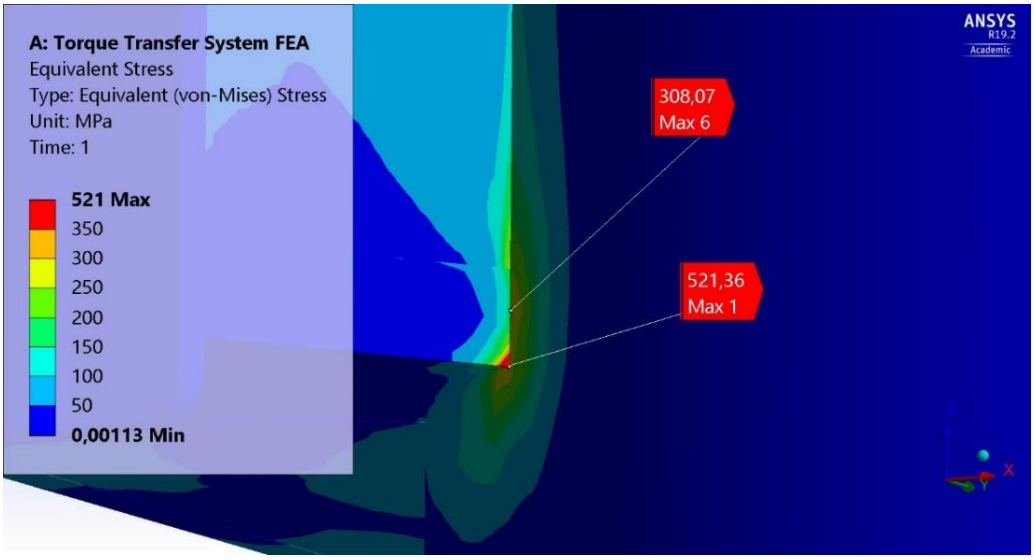

(b)

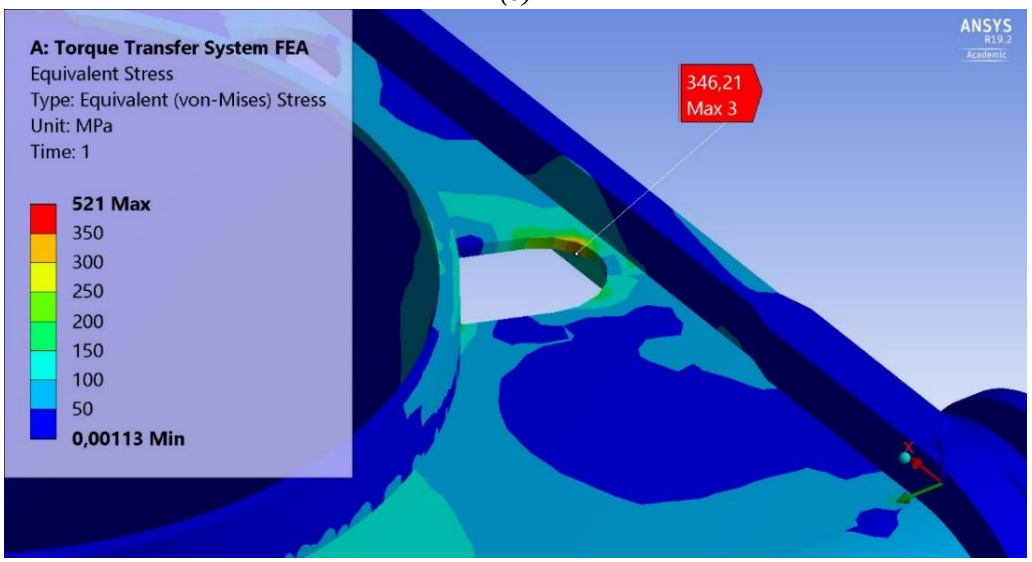

(c)

Figure 59 ULS FEA max. equivalent stress in (a) torque transfer system, (b) reinforcement plate and (c) hydraulic cylinder hole.

Sharp geometrical change is present in the maximum stress region viewed in *Figure 59 (b)*. Especially at the tip corner of geometrical change shows maximum stress value. This result is negligible, as the applicable standard specifies that local peak stresses in areas of geometrical change may exceed material strength capacity if it is able to redistribute into the structure's material (DNV GL, 2019). Little stress in the area around also supports the decision to neglect it, as the stresses are able to redistribute into the surrounding structure. The reinforcement plates exposed to peak stress have thickness of 100 mm for redundancy purposes as portrayed and discussed under *Chapter 4.4*. Mesh quality is well within acceptable limits with respect to level of skewness and cannot be blamed for unrealistic results. Based on the reasoning above, stress concentrations of around 300 MPa (with loading factor) will be present in the region, but not exceed material strength capacity of 308.7 MPa. The software considers elastic and not plastic behavior. Some small yielding in these regions may not affect functionality and operational capacity of the system, even though it shall be avoided as described in the standard.

Stress concentrations around the hydraulic cylinder holes occurs in real loading conditions. However, 450 MPa (with loading factor) of stress occurs in sharp geometrical change region and are negligible. Around 300 MPa (with loading factor) appear in this region and are therefore slightly below material strength capacity of 308.7 MPa. One can also argue that some local peak stresses are able to redistribute further into the structure. "Bad" mesh quality is not source of concern when considering the maximum stress values in these regions. Hence, even though the two described regions are believed to be sufficient, it is the weakest spots in the torque transfer system and mitigation measures are recommended.

Figure 60 shows region around the hydraulic cylinder holes of approximately 300 MPa (with loading factor) from below, including the maximum value of 450 MPa (with loading factor).

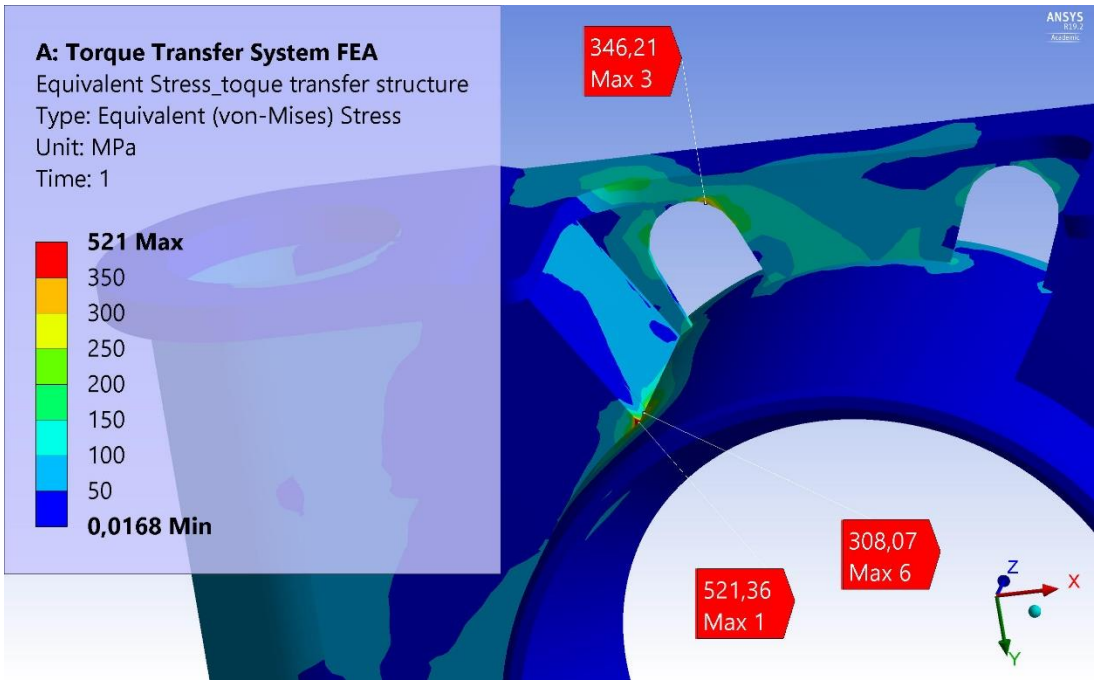

Figure 60 ULS FEA stress concentration region around hydraulic cylinder holes.

To summarize, *Table 10* provides a description of the symmetric maximum local peak stress locations. Only the maximum stress value out of the two symmetric locations are included in the table, as the maximum is governing. The table also suggest what maximum stress values that are negligible, based on the previous discussed matters.

Table 10 ULS FEA: local max. stress values.

Local max. stress [MPa]	Component	Placement, figure reference	Applicable	Surrounding stress region [MPa]
677	Torque transfer structure	Figure 59 (b)	Negligible	100-300
450	Torque transfer structure	Figure 59 (c)	Negligible	100-300
438	Torque transfer structure	Figure 59 (b)	Negligible	100-300

Given the findings the current structure shall fulfill ULS condition and equivalent stress are below material strength capacity of 308.7 MPa. However, geometry optimization is implemented to improve stress distribution further, when also considering improving results for FLS, ALS and sensitivity study condition.

7.1.3 Stress with geometry optimization

Based on the findings, some geometry optimization measures were implemented to the torque transfer structure to mitigate peak stress regions. Fillet radius of 20 mm were added to the edge of the plate with peak stress of 677 MPa (with loading factor), and fillet radius of 5 mm were added to the edges surrounding the hydraulic cylinder holes that had peak stress of 450 MPa (with loading factor). FEA with the same setup as the original ULS FEA were conducted. *Figure 61 (a)* and *(b)* shows stress distribution in peak stress regions with added fillets.

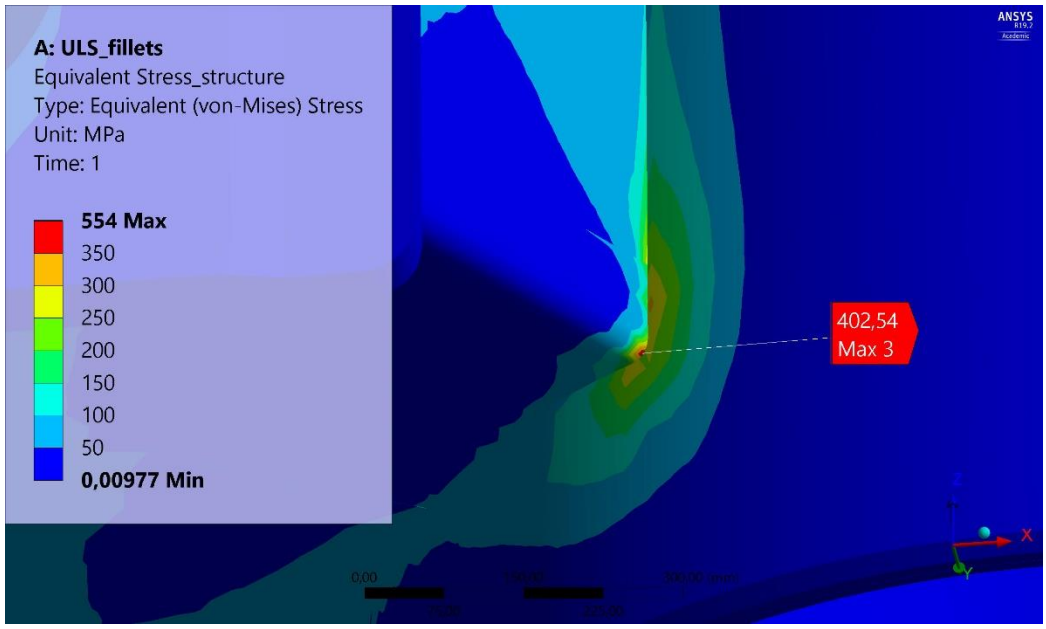

(a)

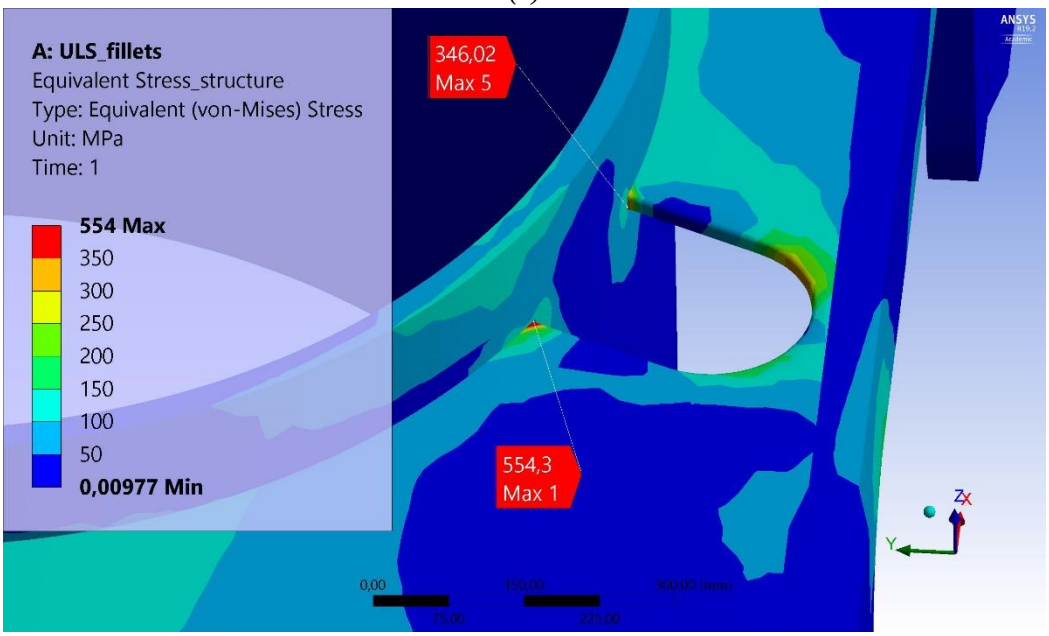

(b)

Figure 61 ULS FEA stress with fillets as geometrical optimization in (a) reinforcement plate for ALS and (b) hydraulic cylinder holes.

Somewhat lower peak stress value occur in the now fillet corner of the reinforcement plate as seen in *Figure 61 (a)*. For the hydraulic cylinder hole, the peak stress values have now changed close to the geostationary module tube. One of them are higher and the other similar to prior values. Adding fillets to the stress concentrated regions simply shifted position of some of the local peak stress spots and had little effect on decreasing the stress distribution.

Another ULS FEA with corrective actions and similar setup as the original one were conducted as described in *Chapter 6.1.7*. Sleeves for the hydraulic cylinders were inserted, as well as adding fillet welds with 10 mm throat thickness to the stress concentration regions surrounding

the reinforcement plate and contact plate next to the geostationary module tube. *Figure 62 (a)* and *(b)* shows the resulting stress distribution after the geometry optimization in the peak stress regions. Even though ULS condition is expected to be fulfilled by the original design, this corrective action is also relevant for fulfilling the FLS condition by reducing surrounding stress concentrations.

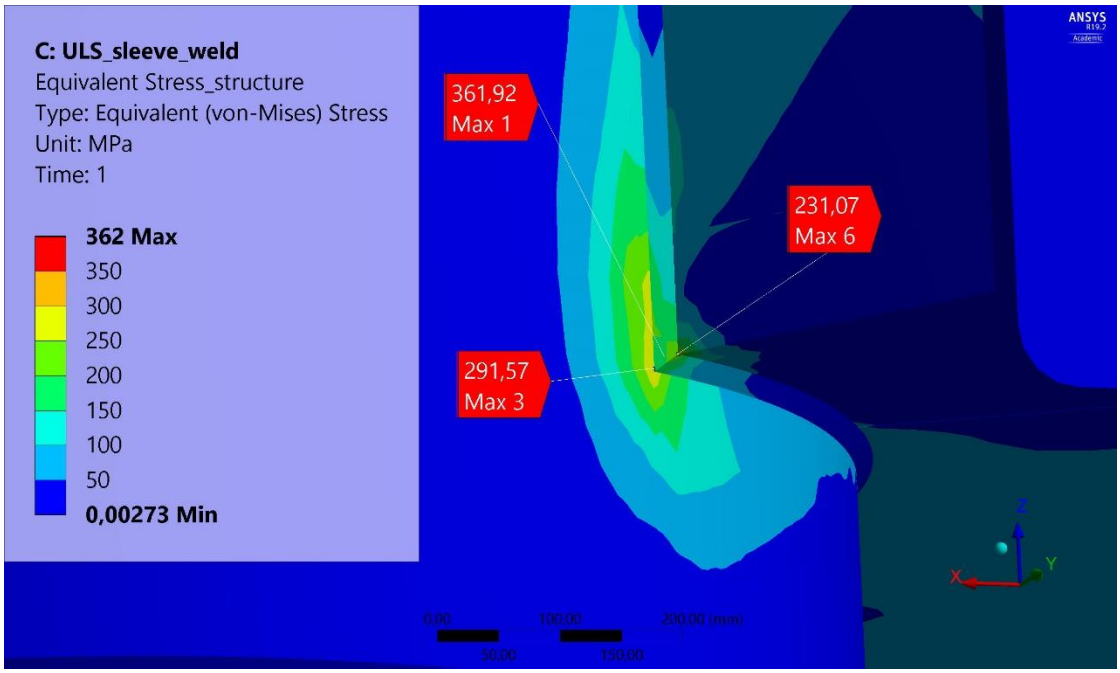

(a)

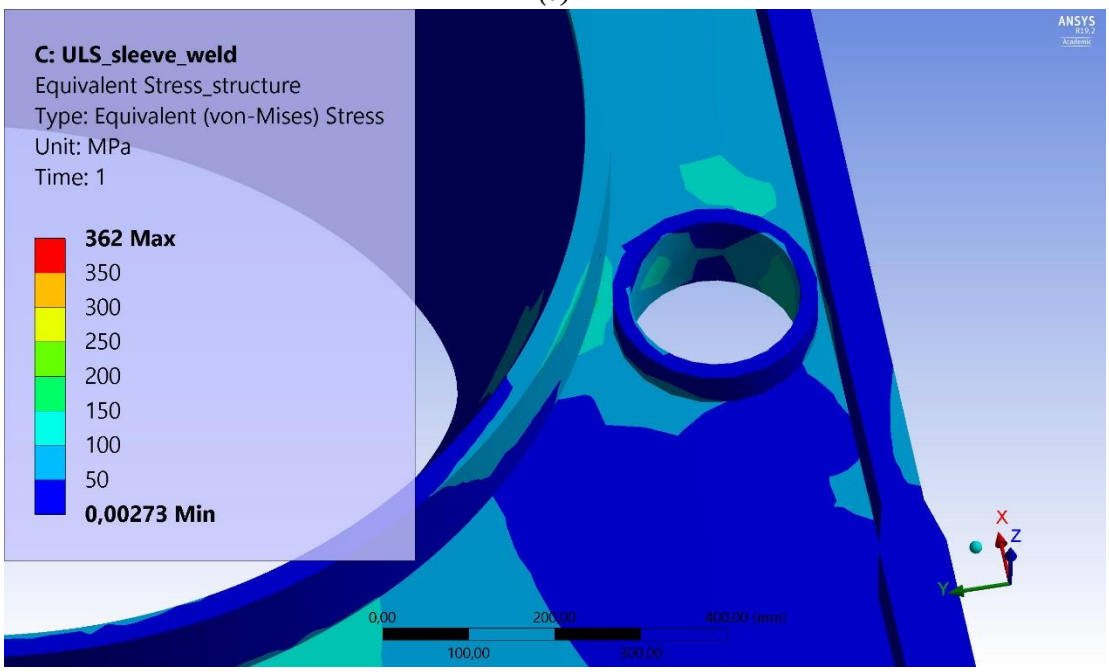

(b)

Figure 62 ULS FEA stress with geometrical optimization showed at (a) fillet welds and (b) sleeve.

Local peak stress of 677 MPa got reduced to 471 MPa (both with load factor) from the applied fillet weld. This value is still believed to be considered negligible based on the previous

discussed matters. Likewise, the other peak stress value got reduced from 438 MPa to 380 MPa (both with load factor) from adding welds but is also still negligible.

When only examining the reinforcement plate and contact plate alongside the geostationary module tube from *Figure 62 (a)*, it is observed that the stress are able to redistribute even further into the reinforcement plate as seen in *Figure 63*.

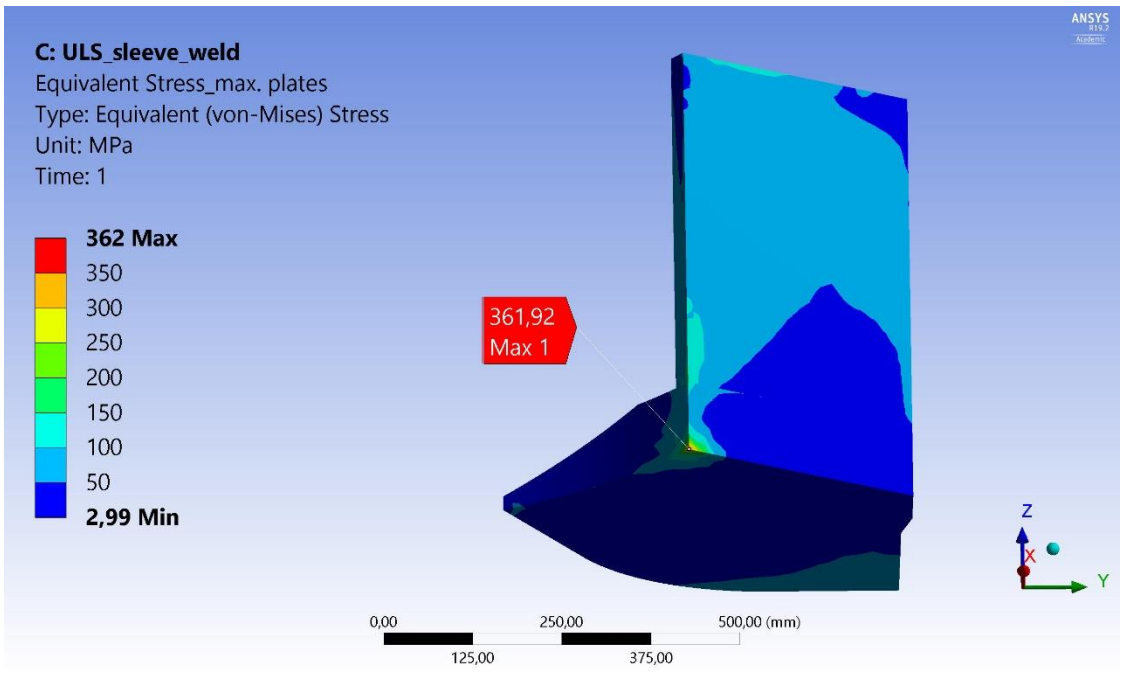

Figure 63 ULS FEA max. stress region with geometrical optimization in reinforcement and contact plates.

The region surrounding the hole for the hydraulic cylinders, got reduced stress concentration from 450 MPa to 246 MPa (with load factor). Thus, a significant reduction of stress due to the implemented geometry optimization. Stress distribution comparison between the original design towards the optimized top plate of the torque transfer structure are visualized in *Figure 64 (a)* and *(b)*.

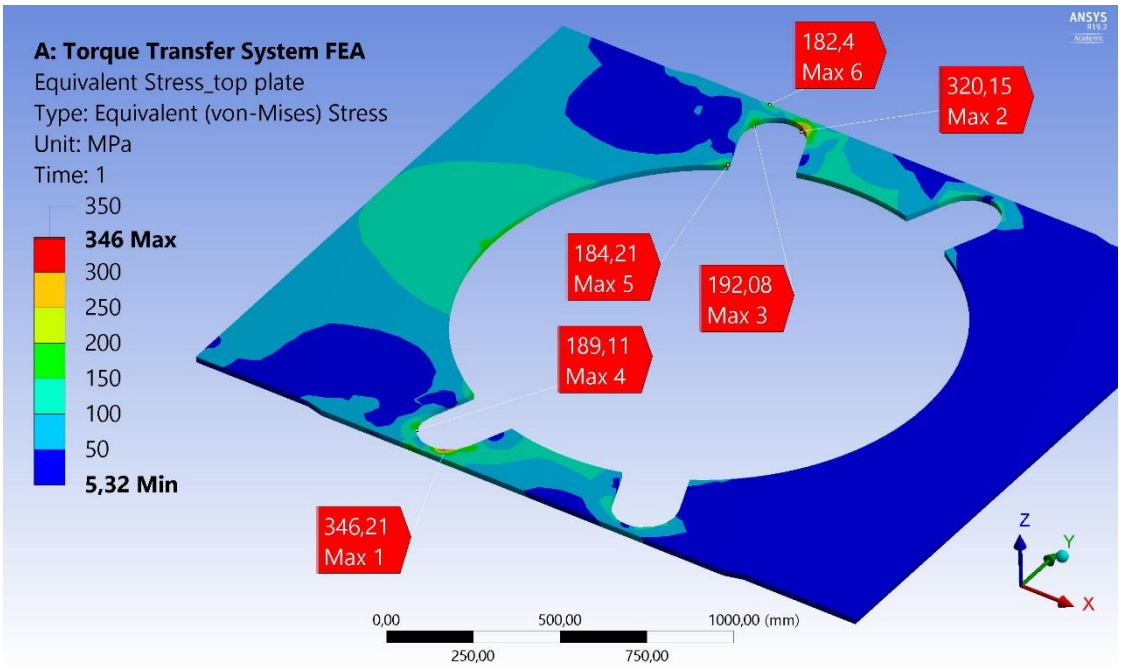

(a)

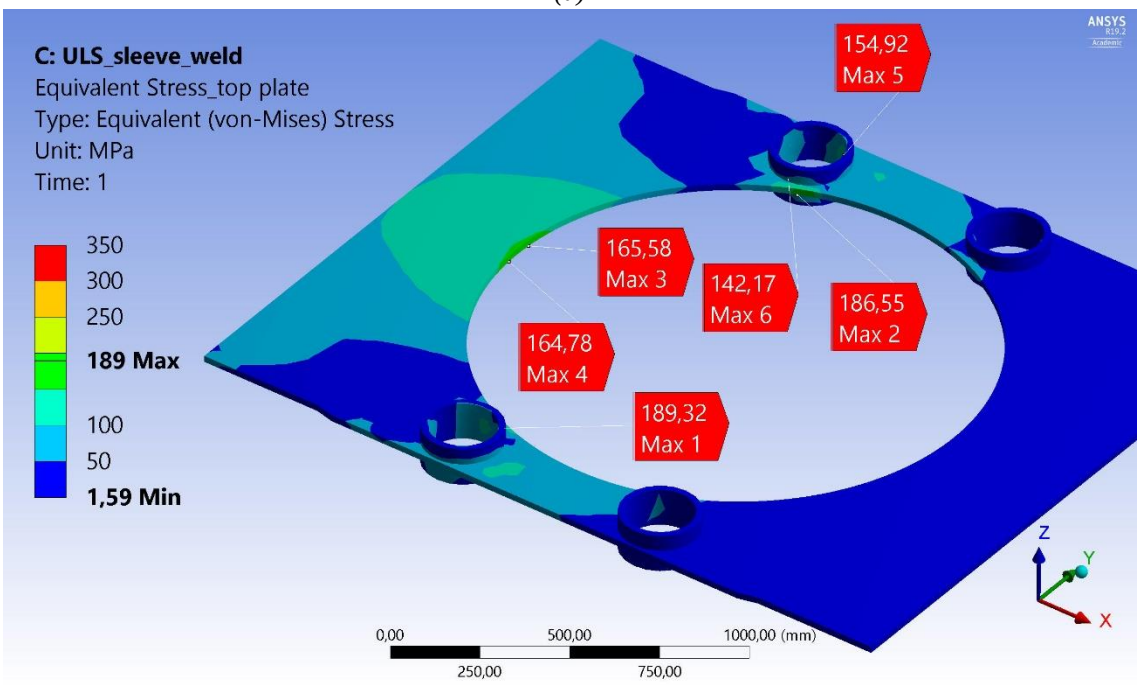

(b)

Figure 64 ULS FEA comparison of top plate from (a) original design vs. (b) geometry optimization.

Stress concentration region around the hydraulic cylinder holes are significantly reduced from around 300 MPa to 150 MPa (both with load factor). The sleeves provide greater stiffness and strength to the region. Maximum stress value now appears in the opposite side of the hydraulic cylinder holes, close to the geostationary module tube. Geometrical optimization by adding sleeves and fillet welds will also be utilized in the FLS, ALS and sensitivity FEAs.

Table 11 provides a comparison of the symmetric maximum local peak stress locations in the torque transfer structure, between the original design and the optimized geometry. It is structured in the same manner as *Table 10, p. 67*.

Table 11 ULS FEA: local max. stress comparison in torque transfer structure with geometry optimization.

Local max. stress [MPa]		Placement, figure reference	Applicable	Surrounding stress region [MPa]	
Original	Optimization			Original	Optimization
677	471	Figure 62 (a)	Negligible	100-300	100-250
450	246	Figure 64 (b)	Negligible	100-300	80-150
438	380	Figure 62 (a)	Negligible	100-300	100-250

Examining the other main components for themselves are conducted to identify maximum stress regions for each main component. It is important to identify the weakest regions of the components, even though they are well below material strength capacity and fulfill ULS condition.

7.1.4 Stress in torsion ring

Maximum stress values in the torsion ring are seen in *Figure 65*. Maximum stress of 190 MPa (with load factor) occurs at the outer corner of the extruded section for ALS. Stress concentration also occurs at the extrusion for the horizontal arm connection joints.

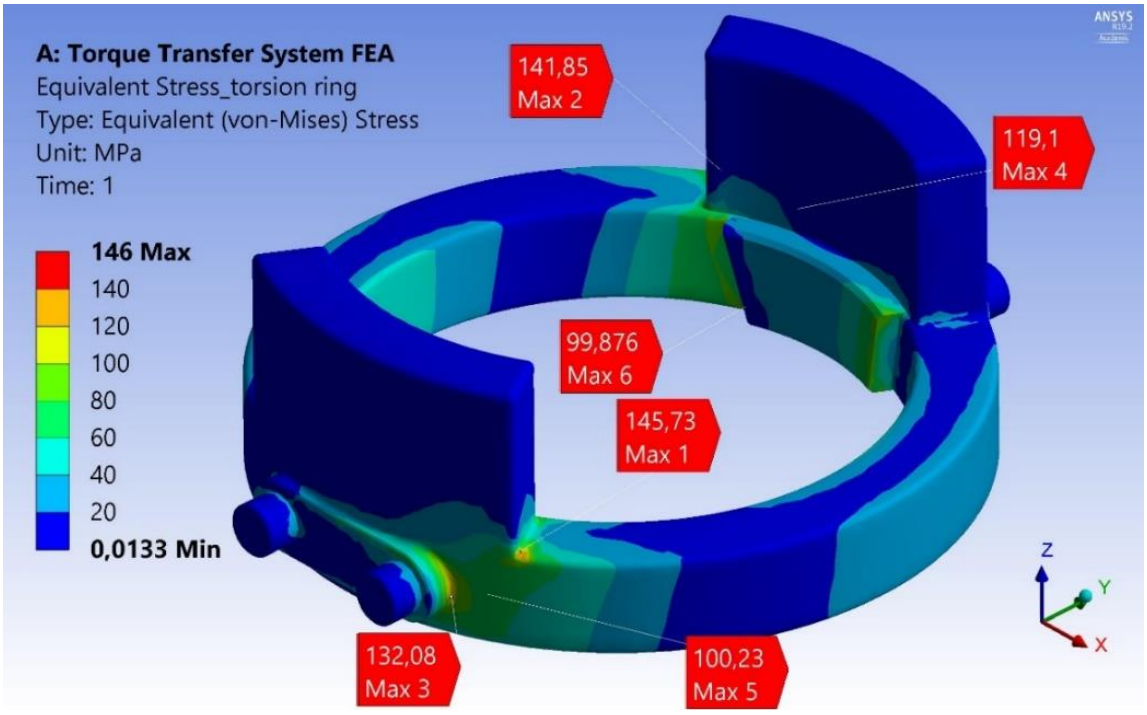

Figure 65 ULS FEA maximum stresses in torsion ring.

Figure 66 (a) shows close up view of the maximum stress concentration regions and *Figure 66 (b)* shows its level of skewness distribution from *Table 5* in *p. 43*.

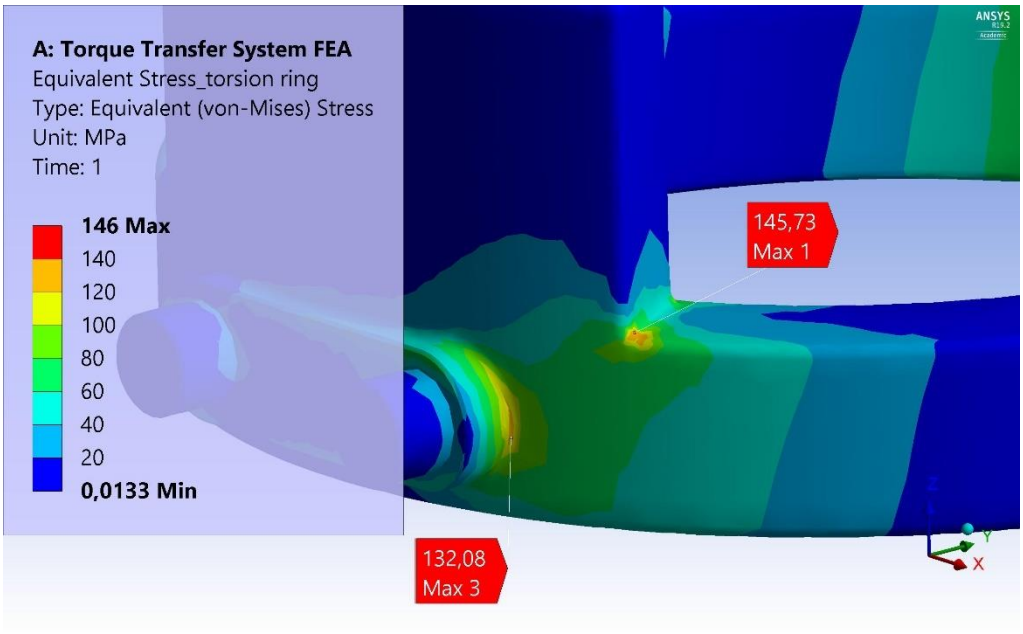

(a)

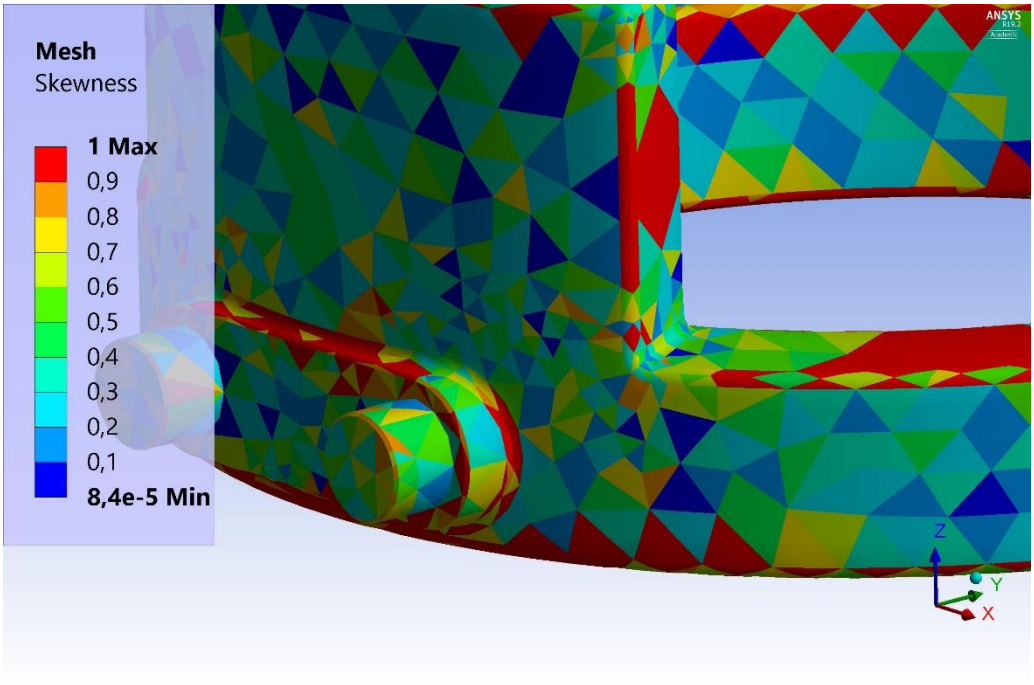

(b)

Figure 66 ULS FEA maximum stress in torsion ring at (a) extrusion region and (b) its level of skewness.

Maximum value of 146 MPa occurs in a region of somewhat sharp geometrical change and with "good" quality mesh based on level of skewness from *Table 5* in *p. 43*. However, the geometrical change is not that sharp as in the torque transfer structure since there is 20 mm radius fillet along the transition edge and the region have similar stress distribution. Some of the surrounding mesh is "bad" quality. However, it is not of significant concern given the discussed matters. Maximum value of 172 MPa (with load factor) have "bad" mesh quality in its region. Even though, it is believed that the extrusion for horizontal arm will reach the shown stresses, as it is suggested by similar values in the surrounding region. 20 mm radius fillet is also present around the horizontal arm extrusion, so sharp geometrical change is limited.

When examining the opposite side of the contact face for applied pressure, 130 MPa (with load factor) appears at a local point of significant geometrical change as viewed in *Figure 67*. Most of the mesh quality around the stress concentration are sufficient. It is intuitive that this region will experience stress concentrations from the applied pressure at the opposite side of the contact face extrusion.

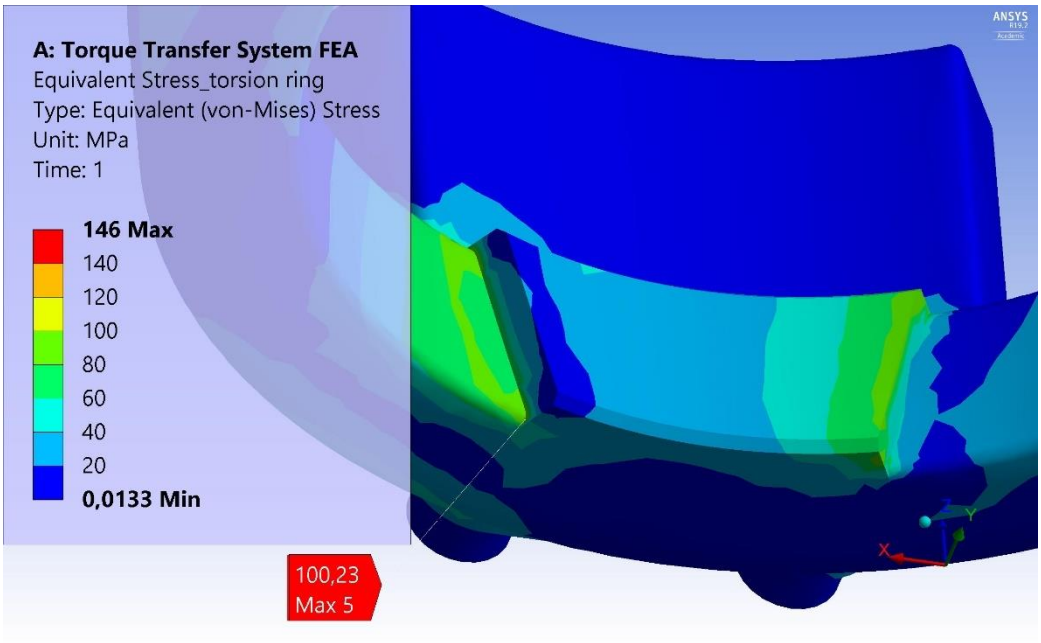

Figure 67 ULS FEA maximum stress in torsion ring at contact face extrusion.

The contact face for applied pressure also experience stresses of close to 130 MPa (with load factor) as seen in *Figure 67*. Stresses also seems to be able to redistribute further into the contact face extrusion if required.

It is identified that the horizontal arm connection joints are weak spots in the torsion ring when considering pure shear. *Figure 68* shows how pure shear is considered from the applied torque.

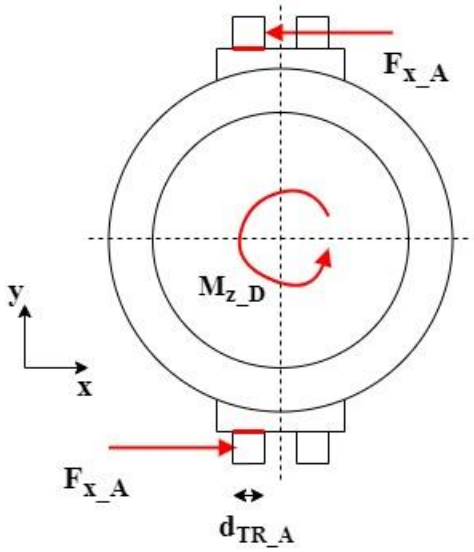

Figure 68 Torsion ring hand calculation.

Diameter of torsion ring connection joint to horizontal arms, $d_{TR\_A} = 160\ mm$, forms the basis for shear area. The solid cylinder gives a cross sectional area, A_{TR_A}, of:

$$A_{TR\_A} = \pi \bullet \left(\frac{d_{TR\_A}}{2}\right)^2 \quad (40)$$

$$\rightarrow A_{TR\_A} = \pi \bullet \left(\frac{160\ mm}{2}\right)^2$$

$$\rightarrow A_{TR\_A} = 20{,}106\ mm^2$$

Shear stress in torsion ring with loading factor then becomes:

$$\tau_{TR\_A} = \gamma_f \bullet \frac{F_{x\_A}}{A_{TR\_A}} \quad (41)$$

$$\rightarrow \tau_{TR\_A} = 1.3 \bullet \frac{1{,}066.7\ kN}{20{,}106\ mm^2}$$

$$\rightarrow \tau_{TR\_A} = 69.0\ MPa$$

Shear stress capacity gives utilization for torsion ring:

$$u_{TR\_A} = \frac{\tau_{TR\_A}}{\tau_{cap}} \quad (42)$$

$$\rightarrow u_{TR\_A} = \frac{69.0\ MPa}{178.2\ MPa}$$

$$\rightarrow u_{TR\_A} = 0.39$$

When comparing to maximum shear stress in the connection joint to the horizontal arm exposed to compression, the values are around 43 MPa (with load factor) as seen in *Figure 69*. Hand calculation assumes pure shear, while some bending stress will be present in real loading conditions. These stress values are neither maximum or critical in the torsion ring and is not of concern.

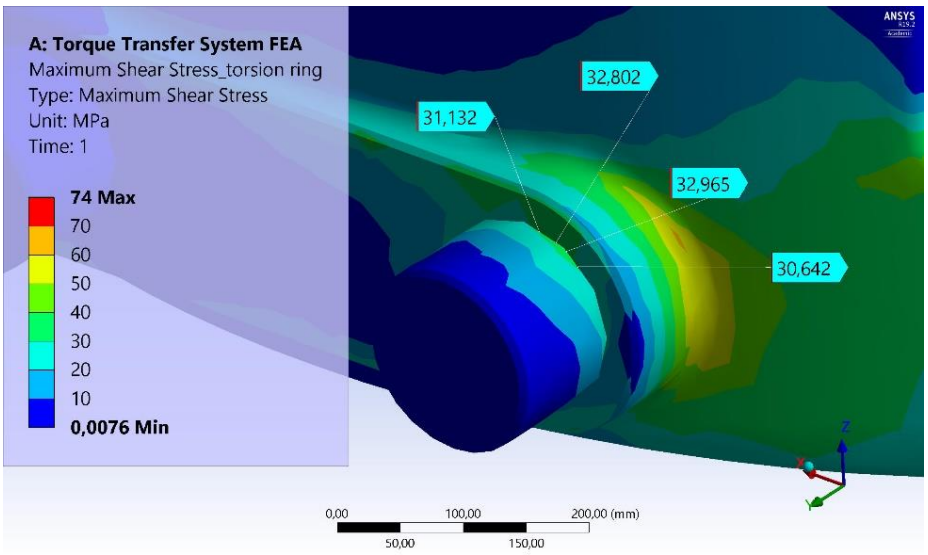

Figure 69 ULS FEA torsion ring max. shear stress hand calculation comparison.

Table 12 provides a description of the symmetric maximum local peak stress locations in the torsion ring. It is structured in the same manner as *Table 10, p. 67*.

Table 12 ULS FEA: local max. stress in torsion ring.

Local max. stress [MPa]	Torsion ring placement, figure reference	Applicable	Surrounding stress region [MPa]
190	Figure 66 (a)	Yes	80-190
172	Figure 66 (a)	Yes	80-172
130	Figure 67	Yes	80-130

7.1.5 Stress in horizontal arms

All initial maximum stress regions in the horizontal arms appear in the small contact face at the foremost inner rings of the spherical bearings as viewed in *Figure* 70. The foremost spherical bearings are connected to the torsion ring. These stresses are unrealistic values as most of the reaction forces are applied to a relatively small contact face. Width of only 5 mm are present at the contact face at the inner ring. In addition, sharp geometrical change with no fillet or chamfer at the transition edge leads to unrealistic peak stresses.

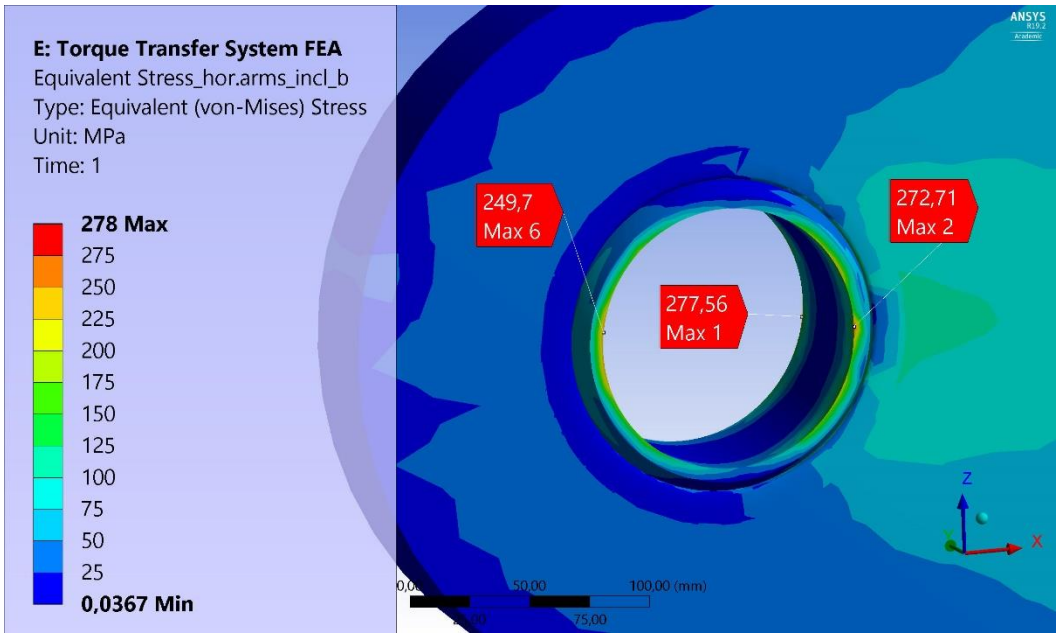

Figure 70 ULS FEA maximum stress in horizontal arms at spherical bearings.

One can also argue that spherical bearings normally are standard parts that do not require structural analysis themselves. The purpose of these FEAs are to validate the torque transfer system components. The spherical bearings are simply added to reflect structural behavior of the assembly. All four spherical bearings will now be negligible, to investigate the stress distribution in the horizontal arms themselves.

Figure 71 shows stress distribution of the horizontal arms without showing the four spherical bearings. Maximum stress of 164 MPa (with load factor) occurs inside the rear spherical bearing hole.

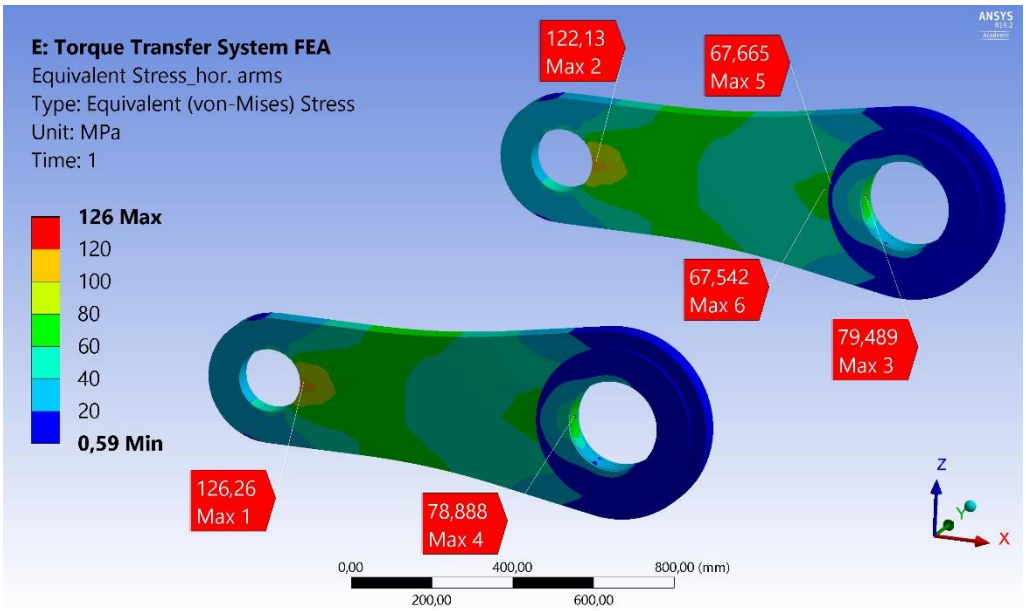

Figure 71 ULS FEA maximum stress in horizontal arms shown without spherical bearings.

Furthermore, stresses of about 103 MPa (with load factor) appears inside the foremost spherical bearing hole. As seen in *Figure 71* the stress distribution in the two horizontal arms appear symmetrical and approximately equal, intuitive for what to expect from the boundary conditions. The horizontal arms are proved to be pure tension/compression members.

It is also clear that the rear hole experience more stress than in the foremost hole. The rear hole is now checked for tear-out shear stress and axial tension stress as seen in *Figure 72*.

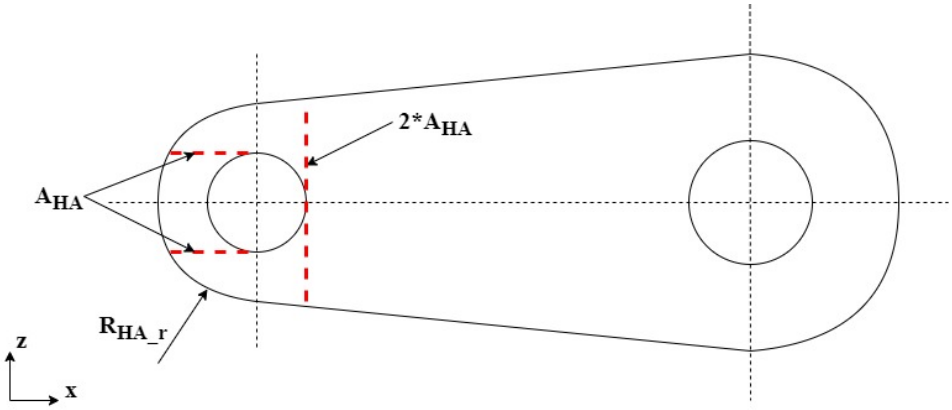

Figure 72 ULS hand calculation of tear-out in horizontal arms.

$R_{HA\_r} = 160\ mm$ is outer radius of the rear horizontal arms and $t_{HA} = 55\ mm$ is thickness of the horizontal arms. These forms the basis for the tear-out and axial area from the rear hole, which is equivalent:

$$A_{HA} = t_{HA} \bullet R_{HA_r} \qquad (43)$$

$$\rightarrow A_{HA} = 55\ mm \bullet 160\ mm$$

$$\rightarrow A_{HA} = 8{,}800\ mm^2$$

Tear-out shear stress of horizontal arms with loading factor become:

$$\tau_{HA} = \gamma_f \bullet \frac{F_{x\_A}}{2 \bullet A_{HA}} \quad (44)$$

$$\rightarrow \tau_{HA} = 1.3 \bullet \frac{1{,}066.7\ kN}{2 \bullet 8{,}800\ mm^2}$$

$$\rightarrow \tau_{HA} = 78.8\ MPa$$

Shear stress capacity gives utilization of horizontal arms:

$$u_{HA} = \frac{\tau_{HA}}{\tau_{cap}} \quad (45)$$

$$\rightarrow u_{HA} = \frac{78.8\ MPa}{178.2\ MPa}$$

$$\rightarrow u_{HA} = 0.44$$

Utilization of shear stress capacity are 0.44 and is not of concern. When comparing to FEA somewhat lower maximum shear stress values of around 65 MPa (with load factor) are present.

Axial stress of horizontal arms with loading factor become equivalent to tear-out shear stress:

$$\sigma_{HA} = \gamma_f \bullet \frac{F_{x\_A}}{2 \bullet A_{HA}} \quad (46)$$

$$\rightarrow \sigma_{HA} = 1.3 \bullet \frac{1{,}066.7\ kN}{2 \bullet 8{,}800\ mm^2}$$

$$\rightarrow \sigma_{HA} = 78.8\ MPa$$

Shear stress capacity gives utilization of horizontal arms:

$$u_{HA\_a} = \frac{\sigma_{HA}}{\sigma_{cap}} \quad (47)$$

$$\rightarrow u_{HA\_a} = \frac{78.8\ MPa}{308.7\ MPa}$$

$$\rightarrow u_{HA\_a} = 0.26$$

Utilization of stress capacity are 0.26 and is not of concern. *Figure 73* shows stress in the horizontal arm seen from the rear side. Stress are equally distributed into the horizontal arm and axial stress in the region of about 70 MPa (with load factor) are present.

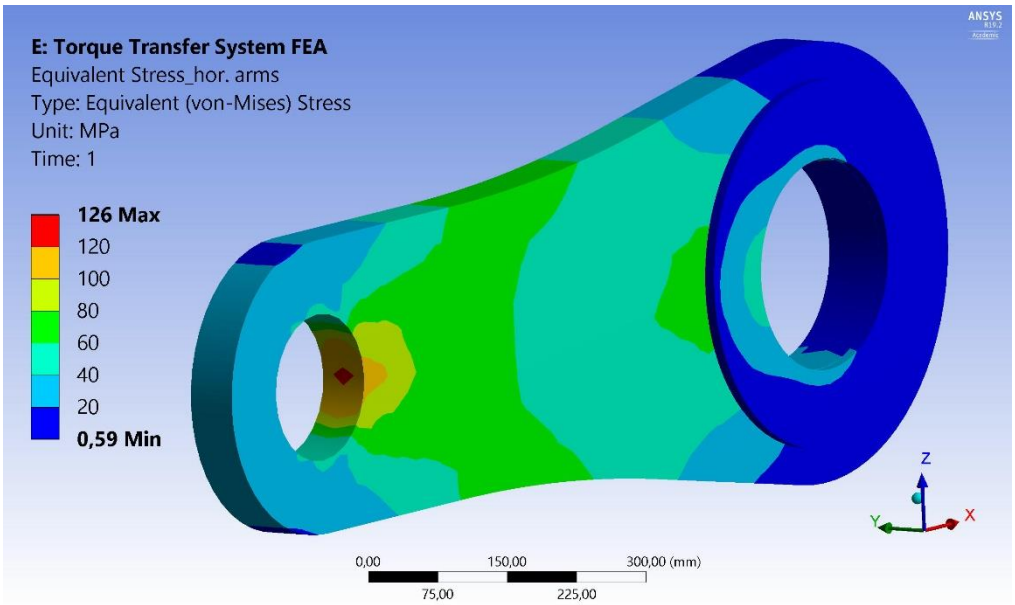

Figure 73 ULS FEA maximum stress in horizontal arms without spherical bearings from other side.

Stress at symmetric locations in the horizontal arms are presented in *Table 13*. It is structured in the same manner as *Table 10, p. 67*.

Table 13 ULS FEA: local max. stress in horizontal arms.

Local max. stress [MPa]	Horizontal arms placement, figure reference	Applicable	Surrounding stress region [MPa]
164	Figure 70	Yes	80-164
103	Figure 71	Yes	60-103
88	Figure 71	Yes	40-88

7.1.6 Stress in vertical arms

Maximum stress of 558 MPa (with load factor) in the vertical arms occurs in the lower part of the spline hub as viewed in *Figure 74 (a)* and *(b)*.

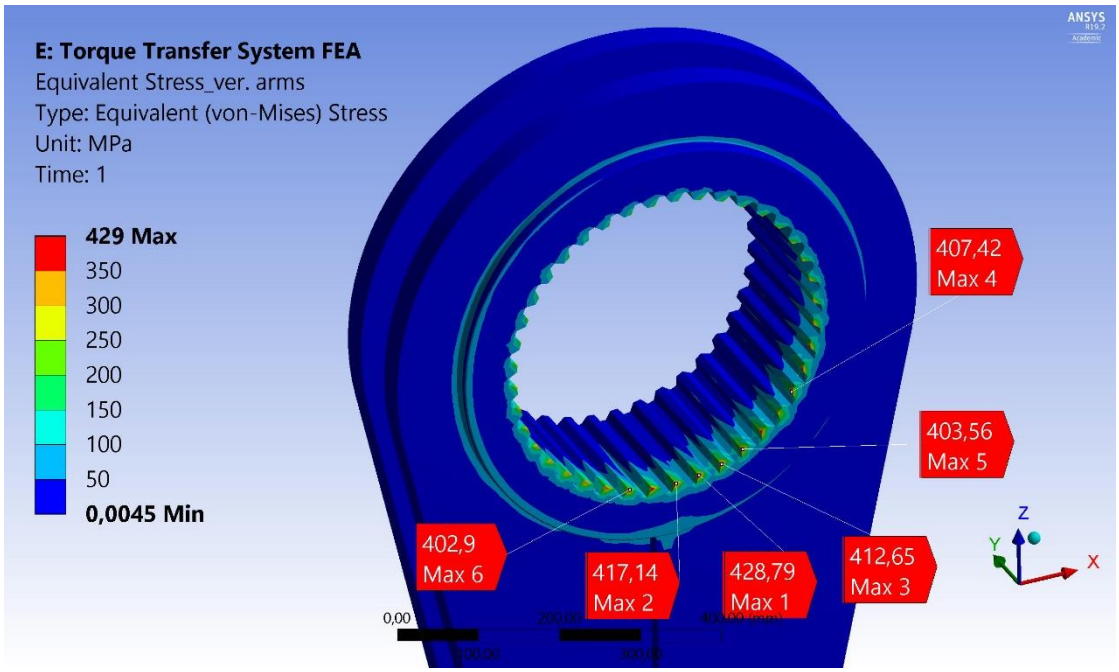

(a)

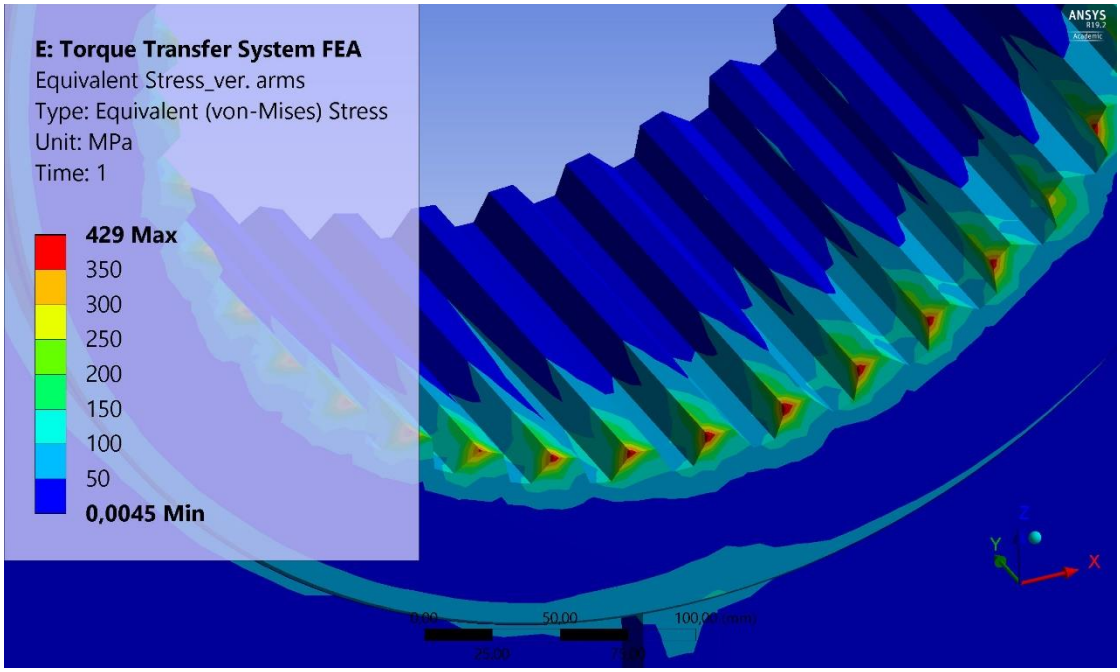

(b)

Figure 74 ULS FEA maximum stress in (a) vertical arms and (b) magnified stress region.

The mesh quality in the region is "fair" based on level of skewness from *Table 5* in *p. 43*. There are sharp geometrical changes that explains the stress concentrations. They occur at the tip corner of the spline teeth and are considered negligible. However, the spline region will see stress distribution of around 150 MPa (with load factor).

Hand calculations for equivalent stress in the spline hub are conducted to compare towards FEA. Resulting moments and force from *3.3.1 Specific values* are used for determining stress as seen in *Figure 75*. (Budyans and Nisbett, 2015, pp. 104, 115-116) and (Lemu, 2016, pp. 14-15, 24) are used for the hand calculations. The spline hub is considered as a pipe section. This is quite conservative as the shaft will be inserted into the hub and form a solid section in real loading condition.

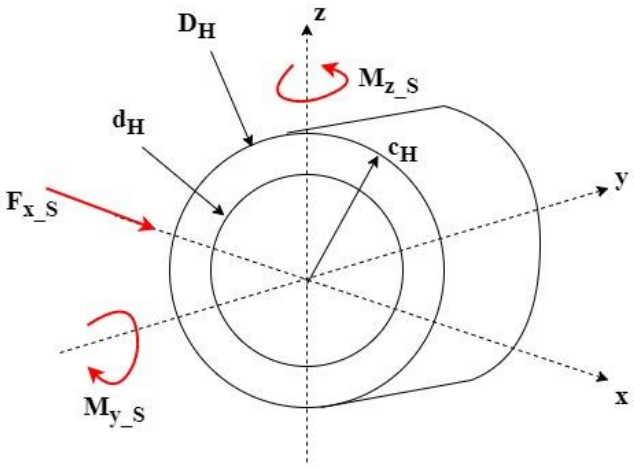

Figure 75 Maximum equivalent stress in hub of vertical arms.

Outer diameter of $D_H = 540\ mm$ and inner diameter of $d_H = 420\ mm$ are present for the hub. Inner diameter is reference diameter for the spline connection. These forms cross-sectional area of hub, A_H, second-area moment of hub, I_H, and hub polar second moment of area, J_H:

$$A_H = \pi \bullet \left(\left(\frac{540\ mm}{2}\right)^2 - \left(\frac{d_H}{2}\right)^2\right) \quad (48)$$

$$\rightarrow A_H = \pi \bullet \left(\left(\frac{540\ mm}{2}\right)^2 - \left(\frac{420\ mm}{2}\right)^2\right)$$

$$\rightarrow A_H = 90{,}478\ mm^2$$

$$I_H = \frac{\pi}{64} \bullet (D_H^4 - d_H^4) \quad (49)$$

$$\rightarrow I_H = \frac{\pi}{64} \bullet ((540\ mm)^4 - (420\ mm)^4)$$

$$\rightarrow I_H = 2.6e9\ mm^4$$

$$J_H = \frac{\pi}{32} \bullet (D_H^4 - d_H^4) \quad (50)$$

$$\rightarrow J_H = \frac{\pi}{32} \bullet ((540\ mm)^4 - (420\ mm)^4)$$

$$\rightarrow J_H = 5.3e9\ mm^4$$

From *Chapter 3.3.1*, shear force of $F_{x\_S} = 164.2\ kNm$, bending moment of $M_{z\_S} = 184.6\ kNm$ and torsion of $M_{y\_S} = 858.7\ kNm$ are applied to the hub. Maximum distance to

the outer surface is $c_H = \frac{D_H}{2} = 270\ mm$. Shear stress from shear force, τ_H, maximum shear stress from torsion in hub, $\tau_{\max\_H}$, and maximum bending stress, $\sigma_{\max\_H}$, then becomes:

$$\tau_H = \frac{F_{x\_S}}{A_H} \quad (51)$$

$$\rightarrow \tau_H = \frac{164.2\ kNm}{90{,}478\ mm^2}$$

$$\rightarrow \tau_H = 1.8\ MPa$$

$$\tau_{\max\_H} = \frac{M_{y\_S} \bullet c_H}{J_H} \quad (52)$$

$$\rightarrow \tau_{\max\_H} = \frac{858.7\ kNm \bullet 270\ mm}{5.3e9\ mm^4}$$

$$\rightarrow \tau_{\max\_H} = 43.8\ MPa$$

$$\sigma_{\max\_H} = \frac{M_{z\_S} \bullet c_H}{I_H} \quad (53)$$

$$\rightarrow \sigma_{\max\_H} = \frac{184.6\ kNm \bullet 270\ mm}{2.6e9\ mm^4}$$

$$\rightarrow \sigma_{\max\_H} = 18.8\ MPa$$

Maximum equivalent Von Mises stress in the female spline hub, σ_{VM_H}, and utilization of equivalent stress capacity, u_H, with loading factor then becomes:

$$\sigma_{\mathrm{VM}\_H} = \gamma_f \bullet \sqrt{\sigma^2_{\max\_H} + 3 \bullet \left(\tau_H + \tau_{\max\_H}\right)^2} \quad (54)$$

$$\rightarrow \sigma_{\mathrm{VM}\_H} = 1.3 \bullet \sqrt{(18.8\ MPa)^2 + 3 \bullet (1.8\ MPa + 43.8\ MPa)^2}$$

$$\rightarrow \sigma_{\mathrm{VM}\_H} = 105.6\ MPa$$

$$u_H = \frac{\sigma_{\mathrm{VM}\_H}}{\sigma_{cap}} \quad (55)$$

$$\rightarrow u_H = \frac{105.6\ MPa}{308.7\ MPa}$$

$$\rightarrow u_H = 0.34$$

Utilization of equivalent stress capacity is 0.34 and is not of concern. Comparing to equivalent stress around the hub show similar values around 90 MPa (with load factor) at several locations as seen in *Figure 76*.

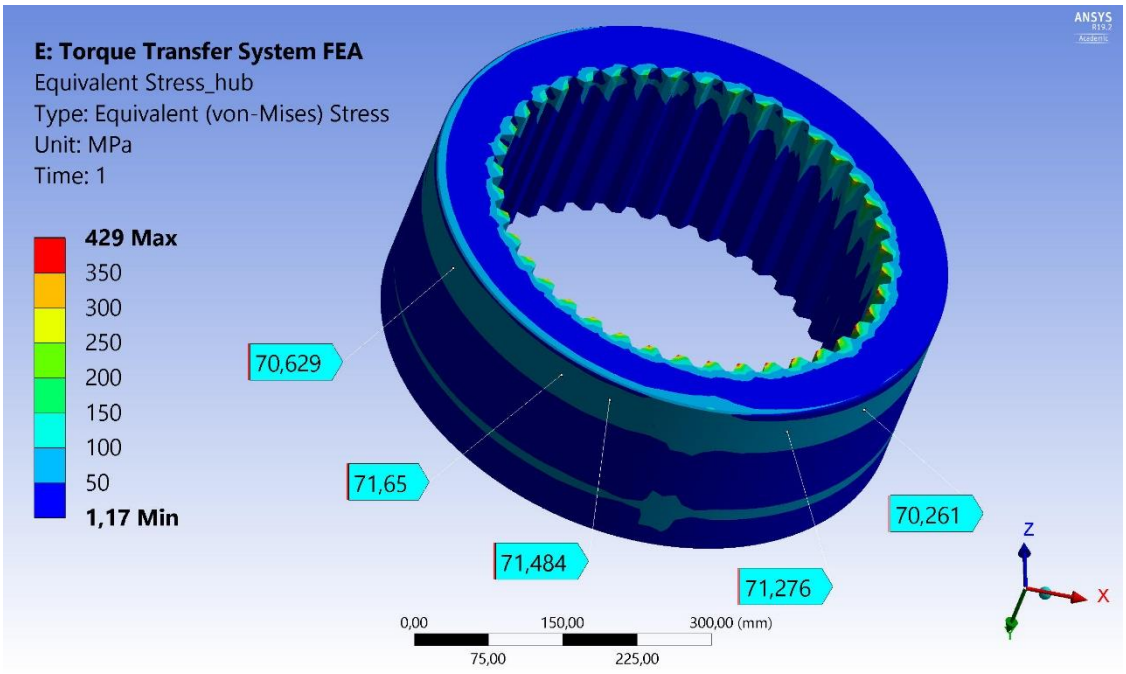

Figure 76 ULS FEA equivalent stress comparison in hub of vertical arms.

Another hand calculation are conducted on the cross-section just below the hub of the vertical arms as shown in *Figure 77*.

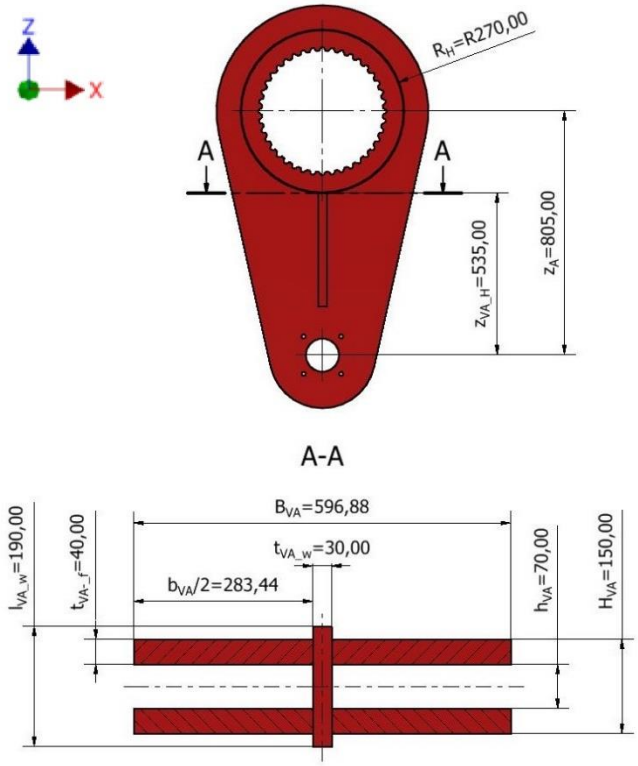

Figure 77 ULS FEA hand calculation for stress in vertical arms below hub.

The cross-section is simplified to an I-beam, where section modulus is calculated to find bending stress just below the hub. Shear stress are also combined to equivalent Von Mises stress in the region. Cross-sectional area are found by length, $l_{VA\_w} = 190\,mm$, and thickness,

$t_{VA\_w} = 30\ mm$, of the web. Flange width, $\frac{b_{VA}}{2} = 283\ mm$, and thickness, $t_{VA\_f} = 40\ mm$, are also used to find the area:

$$A_{VA} = t_{VA\_w} \bullet l_{VA_w} + 4 \bullet \left(t_{VA\_f} \bullet \frac{b_{VA}}{2}\right) \quad (56)$$

$$\rightarrow A_{VA} = 30\ mm \bullet 190\ mm + 4 \bullet (40\ mm \bullet 283\ mm)$$

$$\rightarrow A_{VA} = 50{,}980\ mm^2$$

Based on applied loading, section modulus of the I-beam about the y-axis are found, as it is considered neutral axis. Width of the cross-section, $B_{VA} = 596\ mm$, and combined flange width with no web, $b_{VA} = 566\ mm$. Height of the cross-section becomes, $H_{VA} = 150\ mm$, and height between flanges, $h_{VA} = 70\ mm$.

$$w_{y\_VA} = \frac{B_{VA}^2 \bullet (H_{VA} - h_{VA})}{6} + \frac{(B_{VA} - b_{VA})^3 \bullet h_{VA}}{6 \bullet B_{VA}} \quad (57)$$

$$\rightarrow w_{y\_VA} = \frac{(596\ mm)^2 \bullet (150\ mm - 70\ mm)}{6} + \frac{(596\ mm - 566\ mm)^3 \bullet 70\ mm}{6 \bullet 596\ mm}$$

$$\rightarrow w_{y\_VA} = 4.74e6\ mm^3$$

Reaction force in x-direction at the vertical arms, $F_{x\_A} = 1{,}066.7\ kN$, from *Chapter 3.3.1* are used as both shear force and bending moment force. Distance from applied reaction force to maximum equivalent stress location are based on length of vertical arm, $z_A = 805\ mm$, and hub radius, $R_H = 270\ mm$. Distance becomes; $z_{VA} = z_A - R_H = 535\ mm$.

$$\tau_{VA} = \frac{F_{x\_A}}{A_{VA}} \quad (58)$$

$$\rightarrow \tau_H = \frac{1{,}066.7\ kNm}{50{,}980\ mm^2}$$

$$\rightarrow \tau_H = 20.9\ MPa$$

$$\sigma_{VA} = \frac{F_{x\_A} \bullet z_{VA\_H}}{w_{y\_VA}} \quad (59)$$

$$\rightarrow \sigma_{VA} = \frac{1{,}066.7\ kNm \bullet 535\ mm}{4.74e6\ mm^3}$$

$$\rightarrow \sigma_{VA} = 120.5\ MPa$$

Maximum equivalent Von Mises stress in the vertical arms below the hub, $\sigma_{\mathrm{VM}\ \_VA}$, and utilization of equivalent stress capacity, u_{VA}, with loading factor finally becomes:

$$\sigma_{\mathrm{VM}\ \_VA} = \gamma_f \bullet \sqrt{\sigma_{VA}^2 + 3 \bullet {\tau_{VA}}^2} \qquad (60)$$

$$\rightarrow \sigma_{\mathrm{VM}\ \_VA} = 1.3 \bullet \sqrt{(120.5\ MPa)^2 + 3 \bullet (20.9\ MPa)^2}$$

$$\rightarrow \sigma_{\mathrm{VM}\ \_VA} = 163.6\ MPa$$

$$u_{VA} = \frac{\sigma_{\mathrm{VM}\ \_VA}}{\sigma_{cap}} \qquad (61)$$

$$\rightarrow u_{VA} = \frac{163.6\ MPa}{308.7\ MPa}$$

$$\rightarrow u_{VA} = 0.53$$

Utilization of equivalent stress capacity is 0.53 and is not of concern. Comparing to equivalent stress at the cross-section similar values around 140 MPa (with load factor) are present in FEA as seen in *Figure 78*.

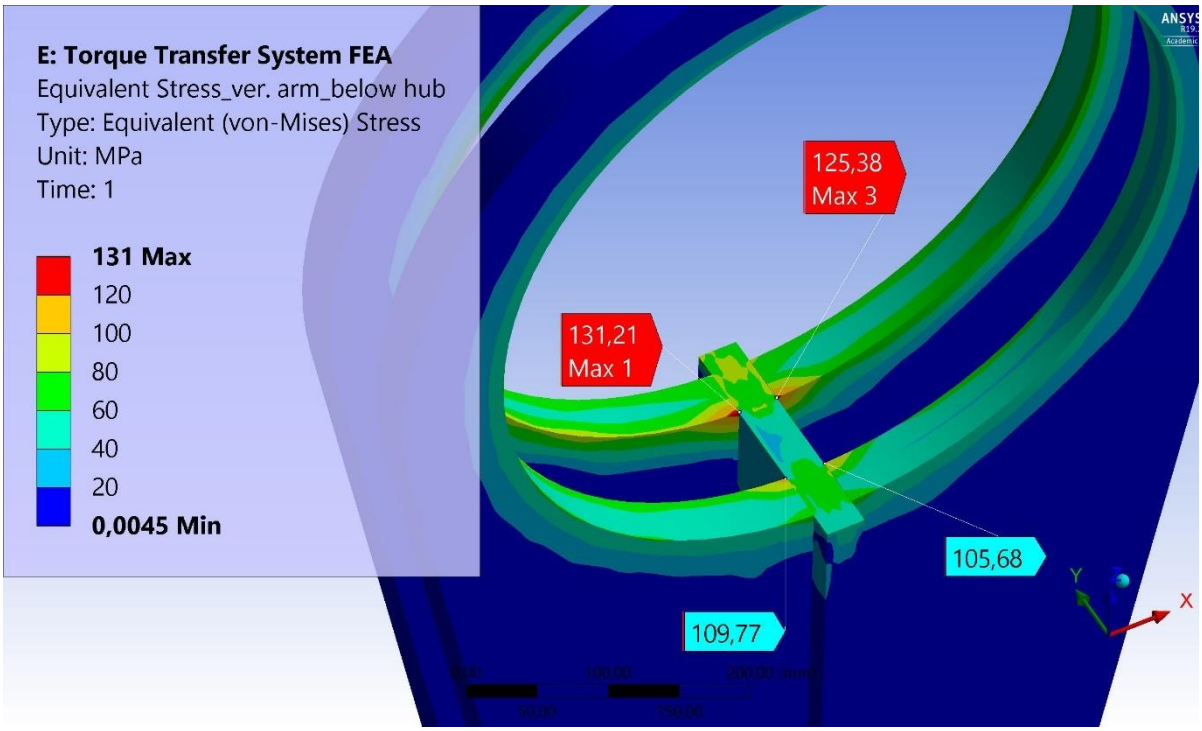

Figure 78 ULS FEA hand calculation comparison of cross-section in vertical arm below hub.

Axle hole in the lower part of the vertical arm sees stress around 100 MPa (with load factor). However, the axle experience maximum stress of 342 MPa (with load factor) as seen in *Figure 79*. It occurs in the transition region from the spherical bearing inner ring in the horizontal arm to the axle hole in the vertical arm.

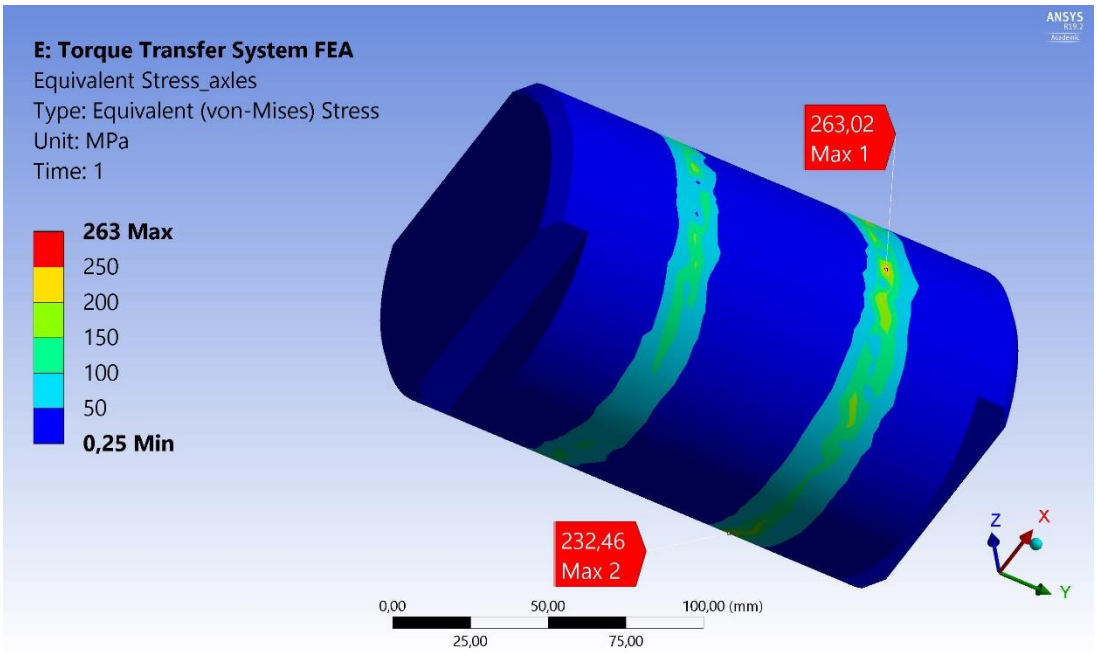

Figure 79 ULS FEA maximum stress in axle.

In real loading conditions, stress will also be more redistributed into the rest of the axle. The spherical bearings in the horizontal arms are negligible due to unrealistic peak stresses. It also leads to unrealistic peak stresses at the corresponding locations in the axle as discussed in *Chapter 7.1.5*. Mesh quality is "good" based on skewness metric from *Table 5* in *p. 43*. Hence, the peak stress regions are negligible whereas the surrounding stress regions of 150 MPa (with load factor) occur.

Hand calculations of pure shear in the axle are conducted to verify stress distribution. Diameter of axle is $d_A = 110\ mm$, giving a cross-sectional area of sectional area, A_A, of:

$$A_A = \pi \bullet \left(\frac{d_A}{2}\right)^2 \tag{62}$$

$$\rightarrow A_A = \pi \bullet \left(\frac{110\ mm}{2}\right)^2$$

$$\rightarrow A_A = 9{,}503\ mm^2$$

Tear-off shear stress in axle with loading factor then becomes:

$$\tau_A = \gamma_f \bullet \frac{F_{x\_A}}{2 \bullet A_A} \tag{63}$$

$$\rightarrow \tau_A = 1.3 \bullet \frac{1{,}066.7\ kN}{2 \bullet 9{,}503\ mm^2}$$

$$\rightarrow \tau_A = 73.0\ MPa$$

Utilization of shear stress capacity in axle is:

$$u_A = \frac{\tau_A}{\tau_{cap}} \quad (64)$$

$$\rightarrow u_A = \frac{73.0\ MPa}{178.2\ MPa}$$

$$\rightarrow u_A = 0.41$$

Utilization of 0.41 is not of concern. Similar shear stress values around 60 MPa (with load factor) are present in *Figure 80*. Shear values will become lower than the local peak values and the surrounding stress region will be governing.

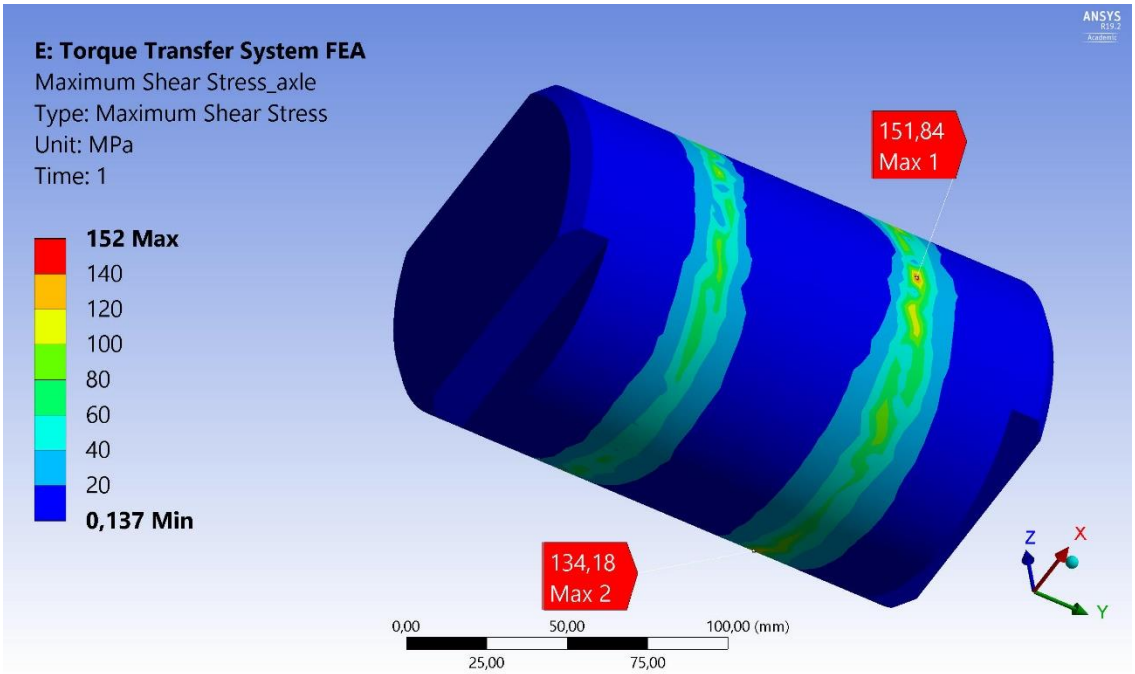

Figure 80 ULS FEA comparison maximum shear stress in axle.

Stress at symmetric locations in the vertical arms are presented in *Table 14*. It is structured in the same manner as *Table 10, p. 67*.

Table 14 ULS FEA: local max. stress in vertical arms and axle.

Local max. stress [MPa]	Vertical arms placement, figure reference	Applicable	Surrounding stress region [MPa]
558	Figure 74 (a) and (b)	Negligible	50-150
342	Figure 79	Negligible	50-150

7.1.7 Stress in shaft

Maximum stress of 655 MPa (with load factor) in the shaft occurs at the transition from round bar spline connection to central pipe shaft as viewed in *Figure 81*. All other maximum stresses also appear in the same region.

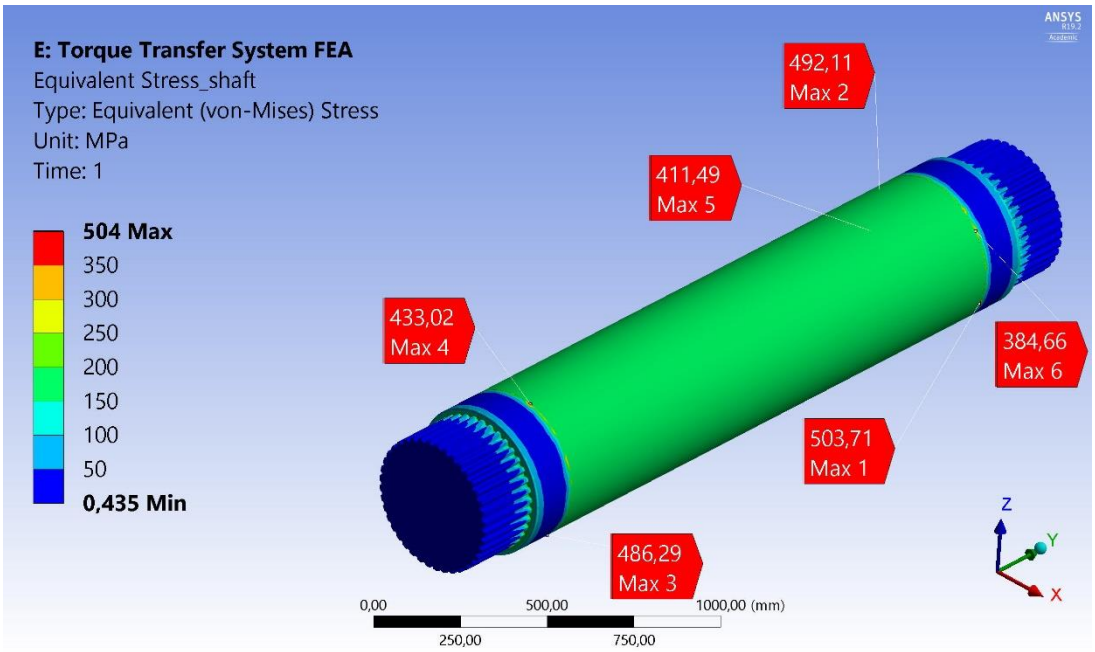

Figure 81 ULS FEA maximum stress in shaft.

Sharp geometrical change occurs in the transition and peak stresses occur at concentrated spots. Hence, maximum stress concentrations are neglected. Equivalent to the spline hub in the vertical arms, around 150 MPa (with load factor) appear in the corresponding region at the male spline connection. The middle pipe section experience stresses of around 220 MPa (with load factor) throughout.

Dimensions and moments applied to the shaft are viewed in *Figure 82*. The shaft is not exposed to shear stress, as this will occur at the shaft bearing and not the central pipe section.

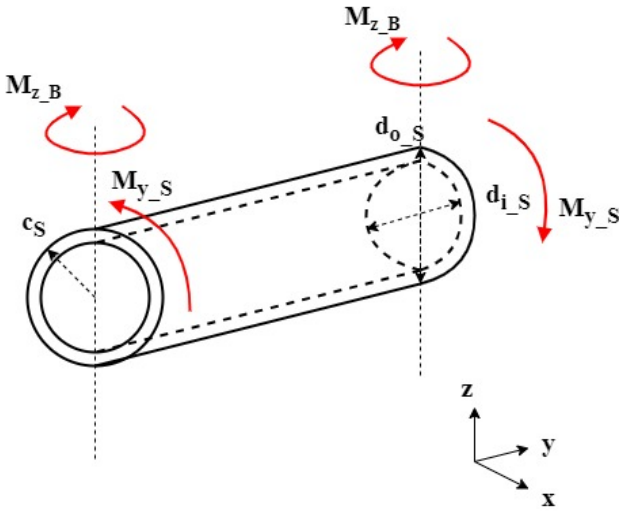

Figure 82 Hand calculation of central pipe section in shaft.

Outer diameter of $D_S = 455\ mm$ and inner diameter of $d_S = 387.4\ mm$ are dimensions for the shaft. These forms second-area moment of shaft, I_S, and shaft polar second moment of area, J_S:

$$I_S = \frac{\pi}{64} \bullet (D_S^4 - d_S^4) \quad (65)$$

$$\rightarrow I_S = \frac{\pi}{64} \bullet ((455\ mm)^4 - (387.4\ mm)^4)$$

$$\rightarrow I_S = 1.0e9\ mm^4$$

$$J_S = \frac{\pi}{32} \bullet (D_S^4 - d_S^4) \quad (66)$$

$$\rightarrow J_S = \frac{\pi}{32} \bullet ((455\ mm)^4 - (387.4\ mm)^4)$$

$$\rightarrow J_S = 2.0e9\ mm^4$$

From *Chapter 3.3.1*, bending moment of $M_{z\_S} = 184.6\ kNm$ and torsion of $M_{y\_S} = 858.7\ kNm$, are applied to the shaft. Maximum distance to the outer surface is $c_S = \frac{D_S}{2} = 227.5\ mm$. Maximum bending stress, $\sigma_{\max\ \_S}$, and maximum shear stress from torsion in shaft, $\tau_{\max\ \_S}$, then becomes:

$$\tau_{\max\ \_S} = \frac{M_{y\_S} \bullet c_S}{J_S} \quad (67)$$

$$\rightarrow \tau_{\max\ \_S} = \frac{858.7\ kNm \bullet 227.5\ mm}{2.0e9\ mm^4}$$

$$\rightarrow \tau_{\max\ \_S} = 97.8\ MPa$$

$$\sigma_{\max\ \_S} = \frac{M_{z\_S} \bullet c_S}{I_S} \quad (68)$$

$$\rightarrow \sigma_{\max\ \_S} = \frac{184.6\ kNm \bullet 227.5\ mm}{1.0e9\ mm^4}$$

$$\rightarrow \sigma_{\max\ \_S} = 42.1\ MPa$$

Maximum equivalent Von Mises stress in the shaft, $\sigma_{\mathrm{VM}\ \_S}$, and utilization of equivalent stress capacity, u_S, with loading factor then becomes:

$$\sigma_{\text{VM }\_S} = \gamma_f \bullet \sqrt{\sigma_{\max\ \_S}^2 + 3 \bullet \tau_{\max\ \_S}{}^2} \quad (69)$$

$$\rightarrow \sigma_{\text{VM }\_S} = 1.3 \bullet \sqrt{(42.1\ MPa)^2 + 3 \bullet (97.8\ MPa)^2}$$

$$\rightarrow \sigma_{\text{VM }\_S} = 227.0\ MPa$$

$$u_S = \frac{\sigma_{\text{VM }\_S}}{\sigma_{cap}} \quad (70)$$

$$\rightarrow u_S = \frac{227.0\ MPa}{308.7\ MPa}$$

$$\rightarrow u_S = 0.74$$

Utilization of equivalent stress capacity is 0.74 and is not of concern. When comparing to equivalent stress in the shaft, ULS FEA show significantly stress values around 220 MPa (with load factor) as seen in *Figure 83*.

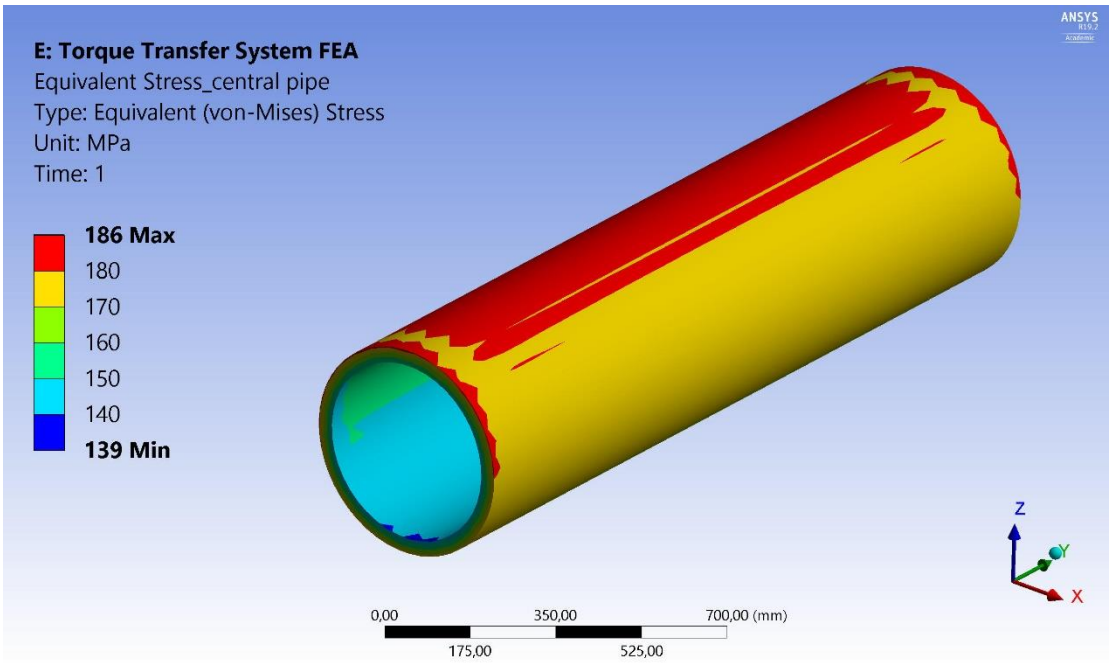

Figure 83 Comparison of ULS FEA and hand calculation in shaft.

The shaft bearings experience peak stresses in the transition region as viewed in *Figure 84 (a)*. These are negligible due to "bad" level of skewness and sharp geometrical change as shown in *Figure 84 (b)*.

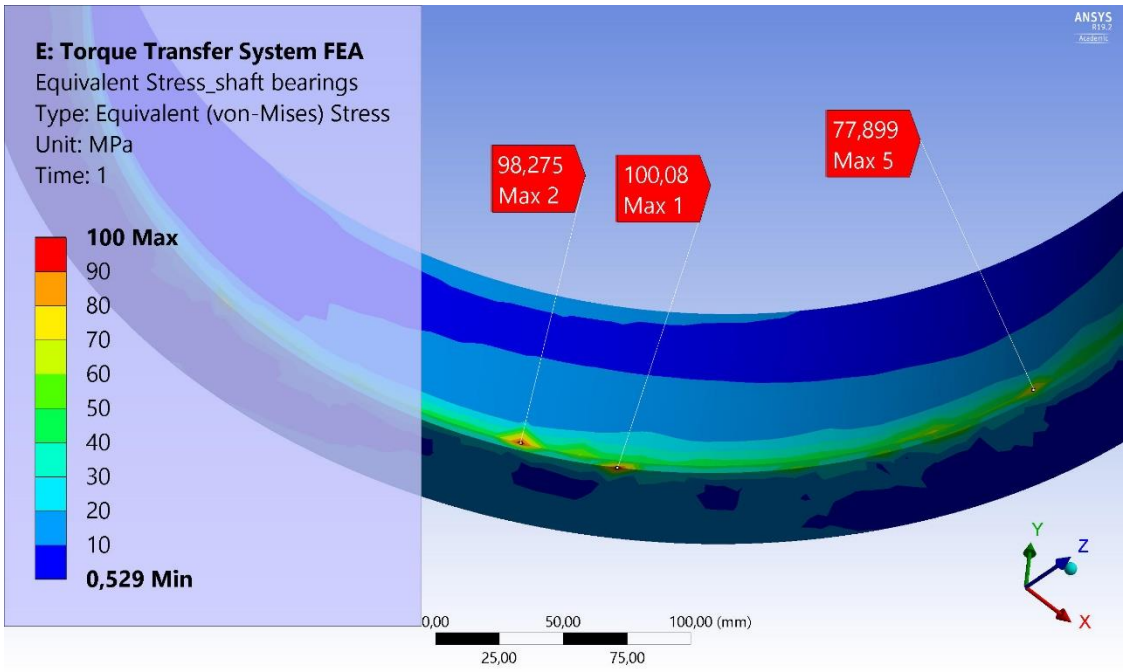

(a)

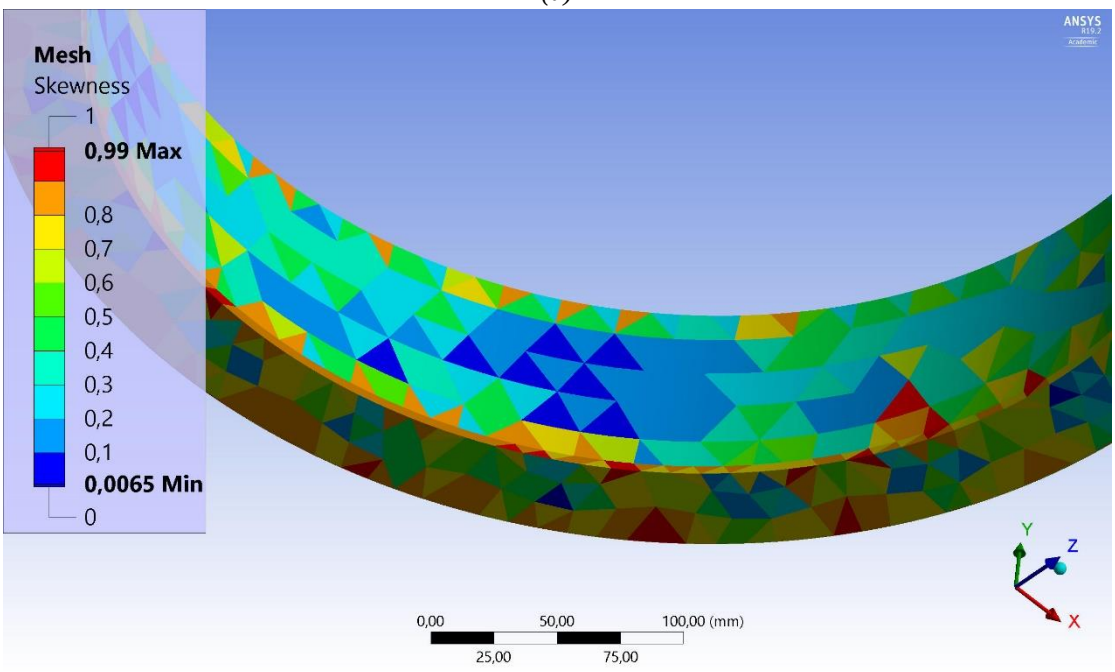

(b)

Figure 84 ULS FEA shaft bearings showing (a) maximum stress and (b) level of skewness.

The planar flange will be exposed to stress of 20 MPa (with load factor) from contact with the vertical arm hub. Closer towards the edge stresses of about 130 MPa (with load factor) occur. Internal bearing pressure stress of 35 MPa (with load factor) appears in the lower half of the shaft bearing.

A quick hand calculation on bearing pressure are conducted to confirm FEA stresses. $l_B = 90\ mm$ is length of shaft bearing, $d_B = 455\ mm$ is inner diameter of shaft bearing and $F_{x\_B} = 1{,}230.8\ kN$ is bearing force. Exact pressure distribution acting in the bearing is unclear, but

typical distribution area are simply assumed to be length times inner diameter of bearing including loading factor (Budyans and Nisbett, 2015, p. 444).

$$\sigma_B = \gamma_f \bullet \frac{F_{x\_B}}{l_B \bullet d_B} \quad (71)$$

$$\rightarrow \sigma_B = 1.3 \bullet \frac{1{,}230.8\ kN}{90\ mm \bullet 455\ mm}$$

$$\rightarrow \sigma_B = 39.1\ MPa$$

Bearing pressure are quite low and compared to *Figure 84 (a)*, it appears similar as shown in FEA.

Stress at symmetric locations in the shaft are presented in *Table 15*. It is structured in the same manner as *Table 10, p. 67*.

Table 15 ULS FEA: local max. stress in shaft and shaft bearings.

Local max. stress [MPa]	Shaft placement, figure reference	Applicable	Surrounding stress region [MPa]
655	Figure 81	Negligible	220
130	Figure 81 (b)	Negligible	35

7.1.8 Ultimate Limit State conclusion

To summarize the ULS FEA, two weak spots in the torque transfer structure were identified and proposals for optimization implementation were presented. Weakest regions in each of the main components were also highlighted. Hand calculations of similar result also supported the FEA basis.

Maximum deformation of 5.3 mm occurred in the non-activated side of the torsion ring. The other main components have less deformation. Given the size of the torque transfer system a few millimeters of deformation are inevitable and is considered ok.

Reinforcement plate and contact plate in the torque transfer structure reaches stress slightly below material strength capacity of 308.7 MPa. Similar stress distribution appears in the surrounding region of the hydraulic cylinder holes in the torque transfer structure. These regions are believed to be the weak spots in the entire torque transfer system, as stress distribution close to material strength capacity are observed to appear. Otherwise, some regions experience unrealistic amounts of stress values in the FEAs due to “bad” mesh and/or sharp changes in geometry. Two optimization cases were conducted whereas one of them significantly improved results by inserting sleeves into the hydraulic cylinder holes and adding fillet welds around the contact plate and reinforcement plate. Geometry optimization reduced maximum stress concentration from about 300 MPa to 250 MPa around the reinforcement plate and contact plate. Stress concentration region around the hydraulic cylinder holes got reduced from about 300 MPa to 150 MPa.

The torsion ring experience maximum stress of 190 MPa at the outer corner of the extrusion for ALS condition. Horizontal arms see about 164 MPa of stress inside the rear spherical bearing holes. The horizontal arms proved to be pure tension/compression members. Vertical arms

appear to reach stress of about 150 MPa inside the spline hub. Whereas the axle will also reach stress of 150 MPa. Shaft bearings are exposed to bearing pressure of 35 MPa and the shaft themselves around 220 MPa appear in the central pipe section.

Based in the problem formulation and approach for the FEAs, no components are expected to reach material strength capacity. If proposed geometry optimization are implemented, stress distribution will be improved even further. Hence, ULS condition for the torque transfer system are fulfilled.

Local maximum stress that occur based on discussed matters in *Chapter 7.1* are presented in *Table 16*. Figures are also referenced to ease finding location for the presented stresses. Loading factor are included in the values in the table and in-text description. However, loading factor is not included in the stress distribution figures.

Table 16 ULS FEA: local max. stress in main components.

Local max. stress [MPa]	**Component**	**Stress location, figure reference**
300	Torque transfer structure (reinforcement plate region)	Figure 59 (b)
250	Torque transfer structure (reinforcement plate region), optimized	Figure 62 (a)
300	Torque transfer structure (hydraulic cylinder holes)	Figure 59 (c)
150	Torque transfer structure (hydraulic cylinder holes), optimized	Figure 64 (b)
190	Torsion ring	Figure 66 (a)
164	Horizontal arm	Figure 71
150	Vertical arm	Figure 74 (b)
150	Axle	Figure 79
220	Shaft	Figure 81

Table 17 shows an overview of result comparison between ULS FEA and hand calculations.

Table 17 Comparison of ULS FEA results and hand calculations.

Component	Type [MPa]	ULS FEA, approximate	Hand calculation
Shaft	Angle of twist [mm]	2.6	3.7
Torsion ring	Shear stress	43	69.0
Horizontal arm	Shear stress, tear-out	65	78.8
	Axial stress	70	78.8
Vertical arm	Equivalent Von Mises stress in hub	90	105.6
	Equivalent Von Mises stress below hub	140	163.6
Axle	Shear stress, tear-off	60	73.0
Shaft	Equivalent Von Mises stress	220	227.0
Shaft bearing	Bearing pressure (equivalent stress)	35	39.1

Hand calculations are quite similar to what found in the FEAs, and thus supporting one another.

7.2 Fatigue Limit State

Fatigue life is examined when determining if the torque transfer system fulfills FLS condition. Fatigue life is number of cycles until reaching fatigue failure when exposed to constant loading amplitude. To support fatigue life observations, equivalent Von Mises stress and safety factor with respect to fatigue life, are also examined in relevant regions. *Figure 85 (a)* shows equivalent Von Mises stress and *Figure 85 (b)* shows fatigue life.

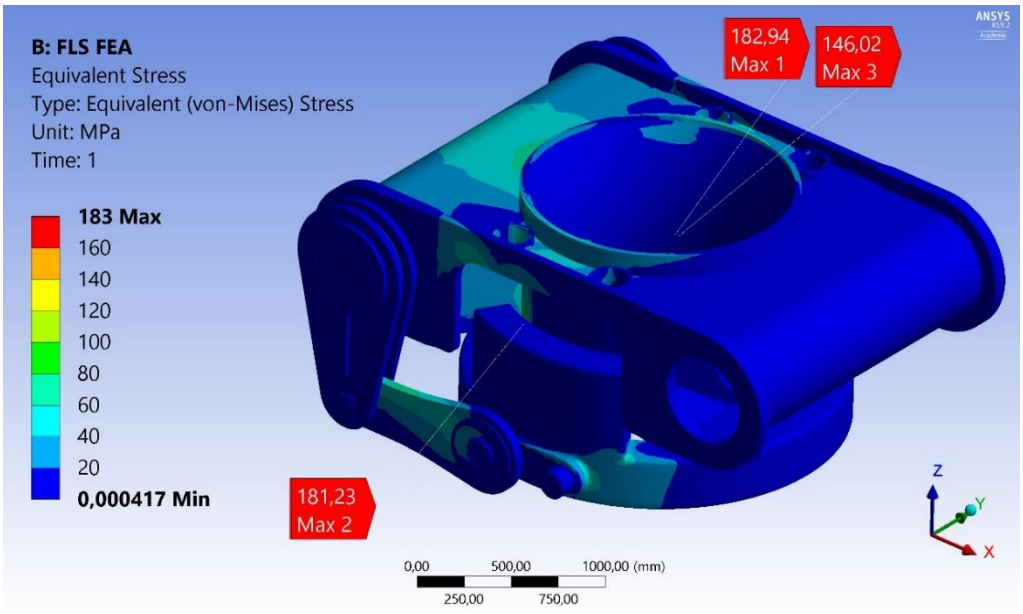

(a)

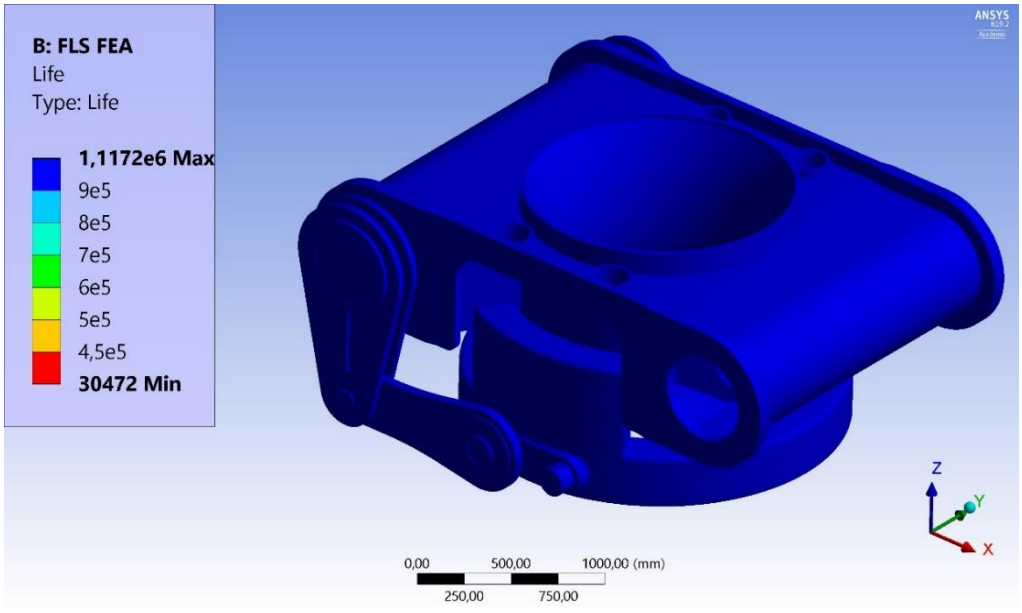

(b)

Figure 85 FLS FEA with (a) equivalent stress and (b) fatigue life.

Most of the torque transfer system seems to have "infinite" life since fatigue life mostly are above 1.12e6 cycles. By further examining, all components have "infinite" life except the defined reinforcement plate for ALS described in *Chapter 4.4*. *Figure 86 (a)* and *(b)* shows the

critical region with respect to equivalent stress and fatigue life, not showing the weld in the torque transfer structure.

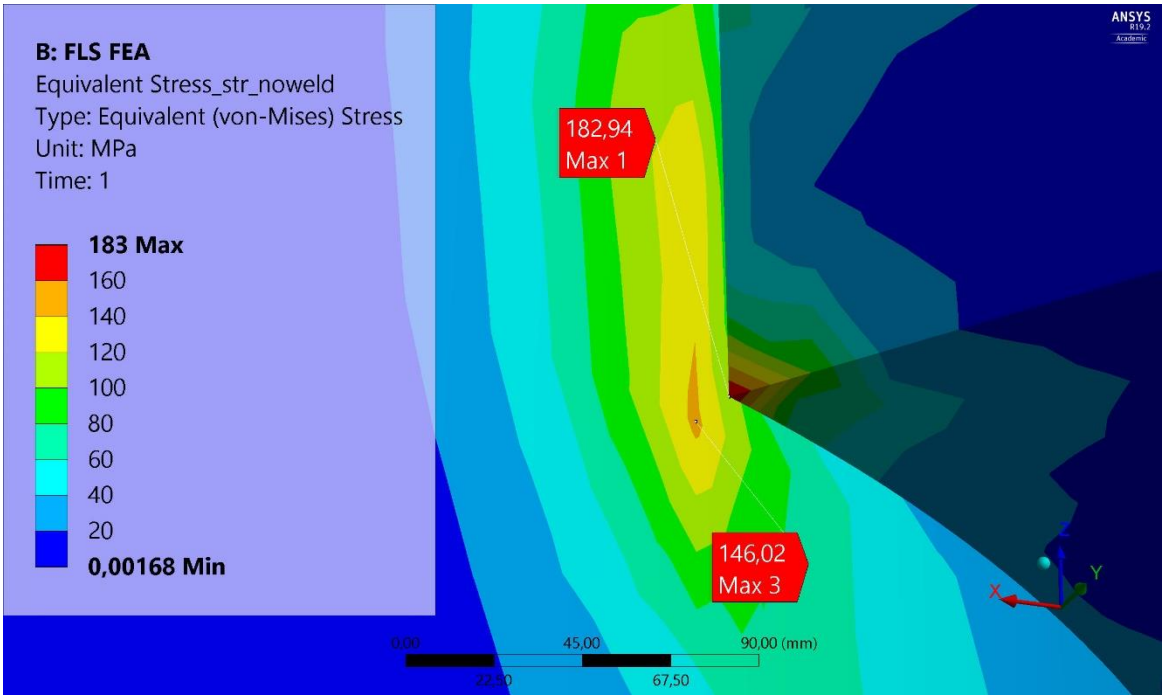

(a)

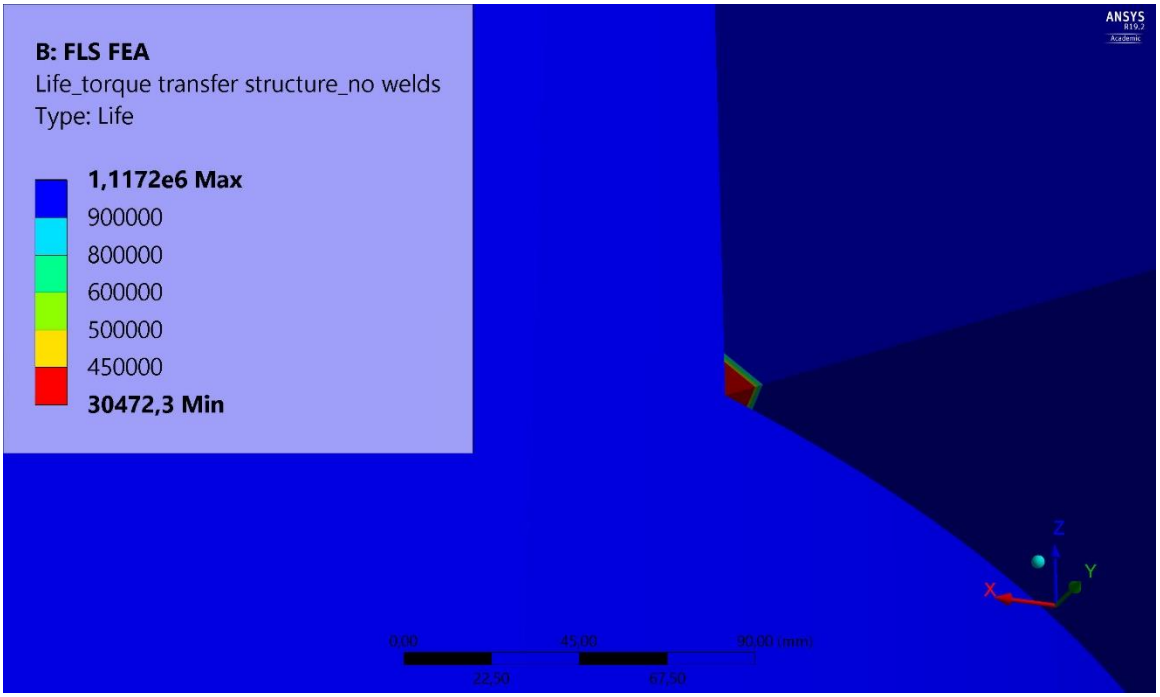

(b)

Figure 86 FLS FEA critical region showing (a) equivalent stress and (b) fatigue life.

Figure 86 (b) show minimum fatigue life to be slightly above 30,000 cycles in the corner region of the reinforcement plate for ASL. Given the structural requirement of 450,000 cycles to

fatigue failure, it is considered to fail. Only about 10 mm of the corner are considered to fail. Endurance limit for the material are 151.7 MPa and maximum stress are 183 MPa. However, based on discussion under *Chapter 7.1.2* and *7.1.3* this peak stress region is negligible and thus also its resulting fatigue life. Thus, fatigue failure will not occur in the structure. *Figure 87* shows the safety factor distribution for FLS condition.

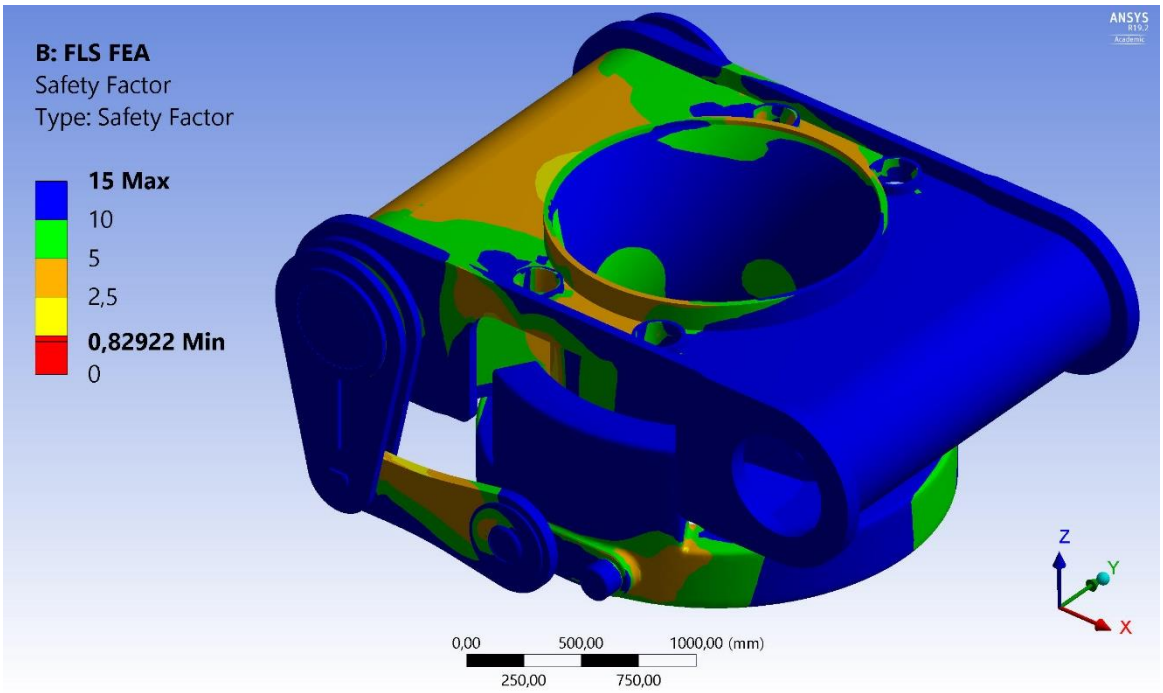

Figure 87 FLS FEA safety factor.

Except the negligible maximum stress region, safety factor is mostly above 2.5 and present throughout the structure.

7.2.1 Fatigue Limit State conclusion

Based on assumptions for fatigue and the utilized S-N curve, the torque transfer system shall fulfill FLS condition and not experience fatigue failure during its lifetime. The system is expected to experience 450,000 full loading cycles, and the analyses show that the system will have “infinite” fatigue life.

7.3 Accidental Limit State

Equivalent stress and deformation are examined under ALS condition for the torque transfer system. Based on results under *Chapter 7.1*, several regions containing stress concentrations are negligible due to sharp geometrical change, “bad” mesh quality and/or being able to redistribute stress further into the structure. Several loads were tested, to identity the believed to be maximum applied load that the torque transfer system can withstand during ALS condition.

A test case of same applied torque as for ULS were ran to observe structural behavior during ALS condition. Applied torque is 2,400 kNm, i.e. loading magnitude factor of 1.0. Welds applied in geometry optimization are present but hidden when examining results to observe structural behavior of the plates themselves in the torque transfer structure. From *Figure 88* it is observed that the torsion ring naturally experiences more stress than during ULS condition.

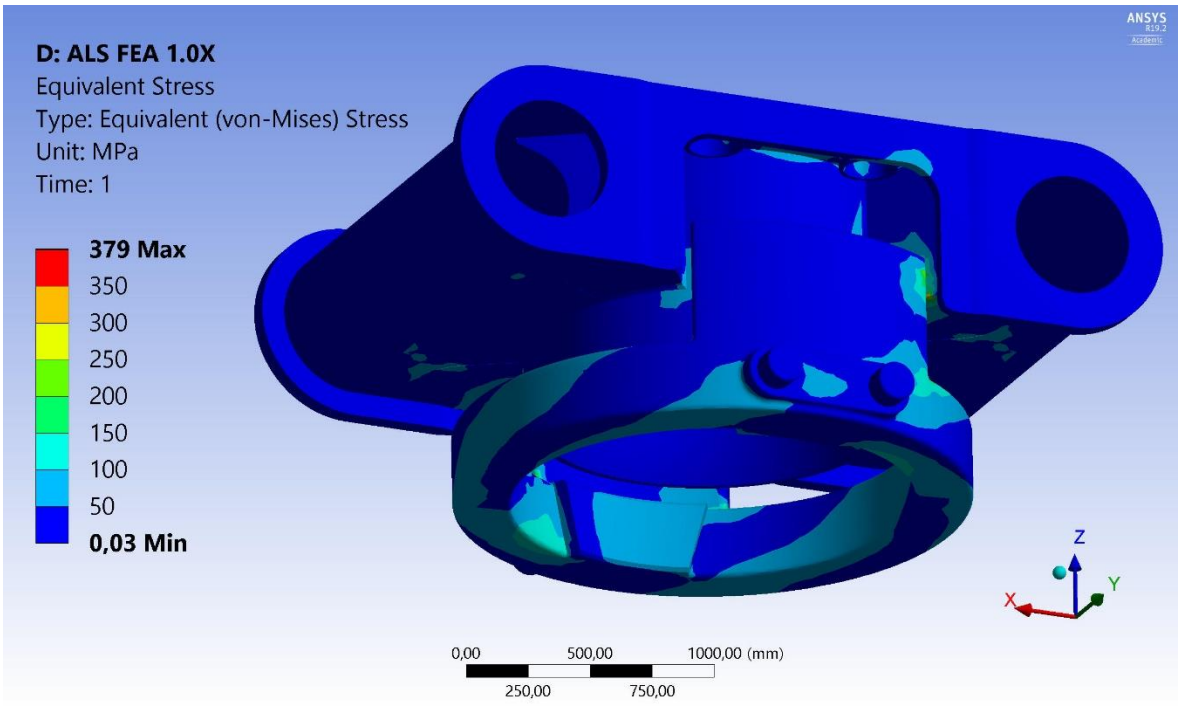

Figure 88 ALS FEA 1.0X loading.

Maximum stress of 379 MPa occurs in the torque transfer structure as viewed in *Figure 89 (a)*. However, based on *Chapter 7.1.2* and *7.1.3* it is believed that this stress concentration region is negligible and that the surrounding stress are governing. *Figure 89 (b)* show the torsion ring stress distribution, where the contact face and torsion ring extrusion see most stress.

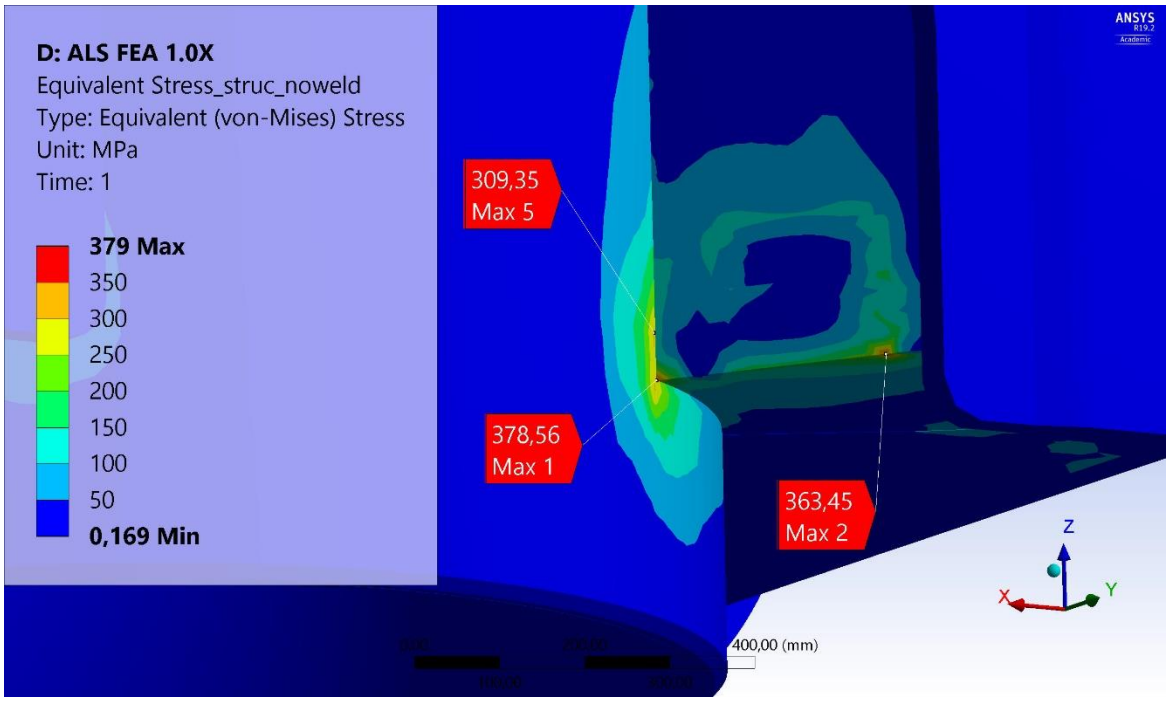

(a)

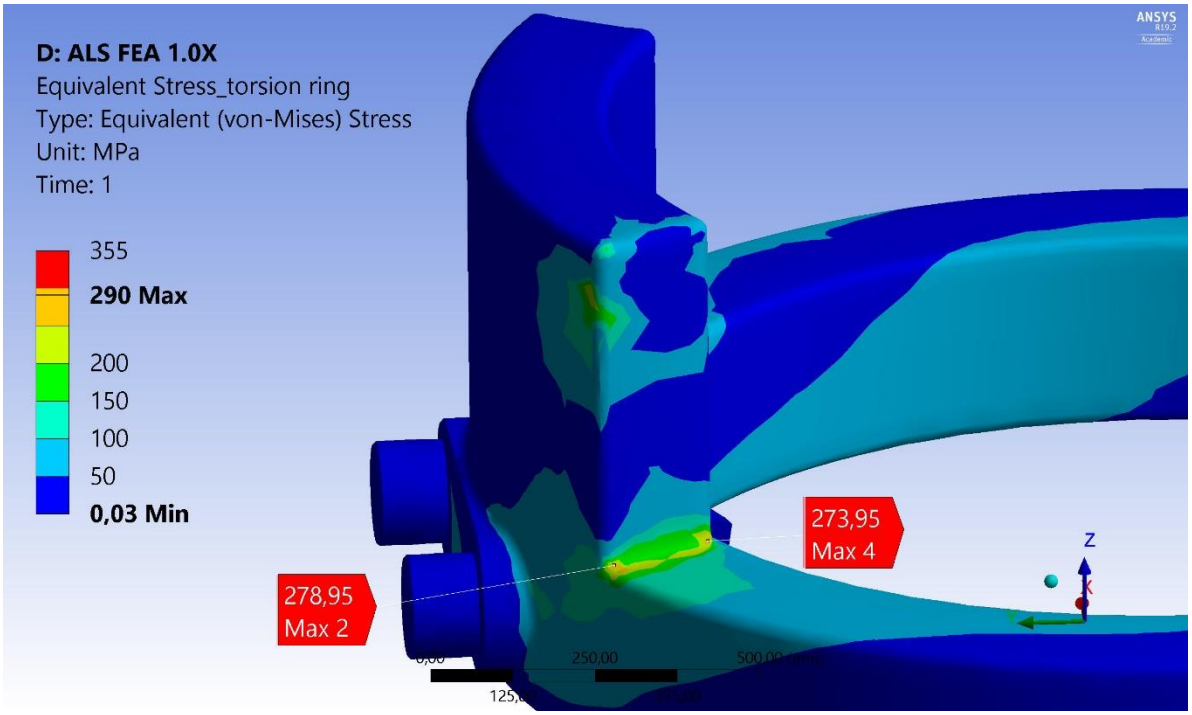

(b)

Figure 89 ALS FEA loading magnitude factor of 1.0 for (a) torque transfer structure and (b) torsion ring.

It seems like the torque transfer structure mostly experience stress around 200 MPa when neglecting peak stresses. As for the torsion ring, 200 MPa appear across the extrusion angle while 279 MPa are maximum. Due to material thickness in the region, stress shall redistribute

further into the torsion ring extrusion. Outer edge of contact face at the top of torsion ring extrusion also sees about 200 MPa of stress.

Figure 90 shows cross-section of the torque transfer structure to observe the internal stress distribution behind the contact face for the torsion ring.

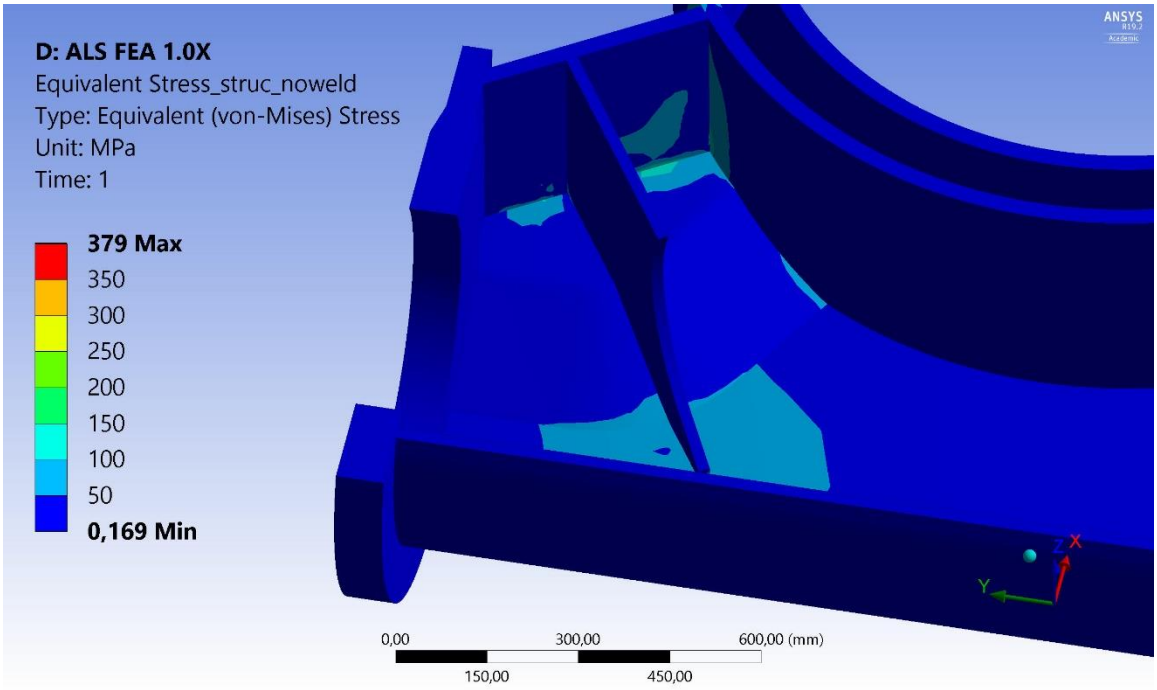

Figure 90 ALS FEA loading magnitude factor of 1.0 inside torque transfer structure.

Mostly stress of around 50-100 MPa appears at the back of the contact plate, top of the reinforcement plate and around the stiffener plate. This region will not be most critical.

Figure 91 (a), (b) and *(c)* show stress distribution in the torque transfer structure with 1.5X, 1.75X and 2.0X loading magnitude factors, respectively. Red regions show surpassing material yield strength of 355 MPa.

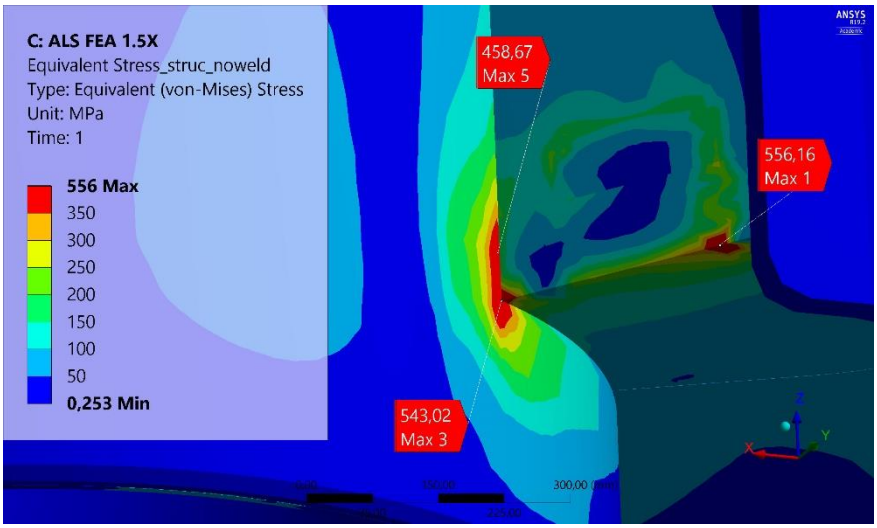

(a)

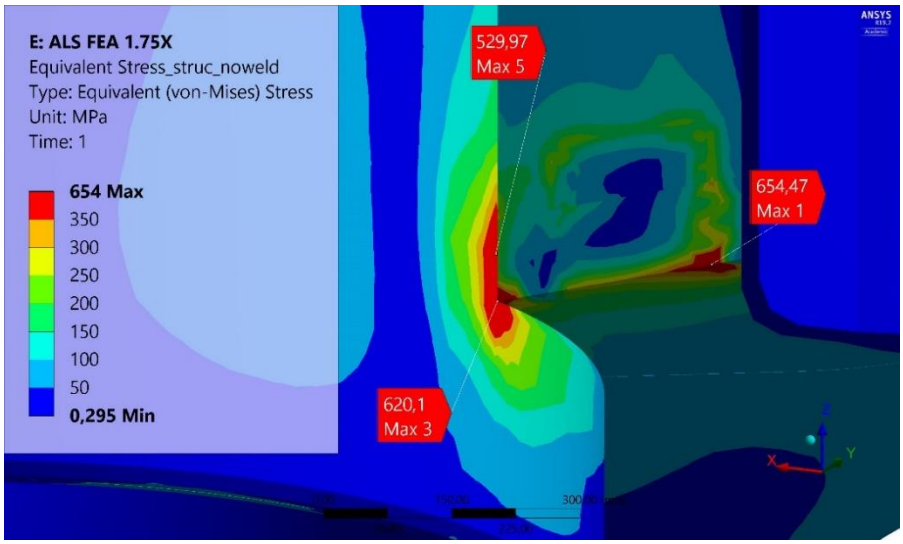

(b)

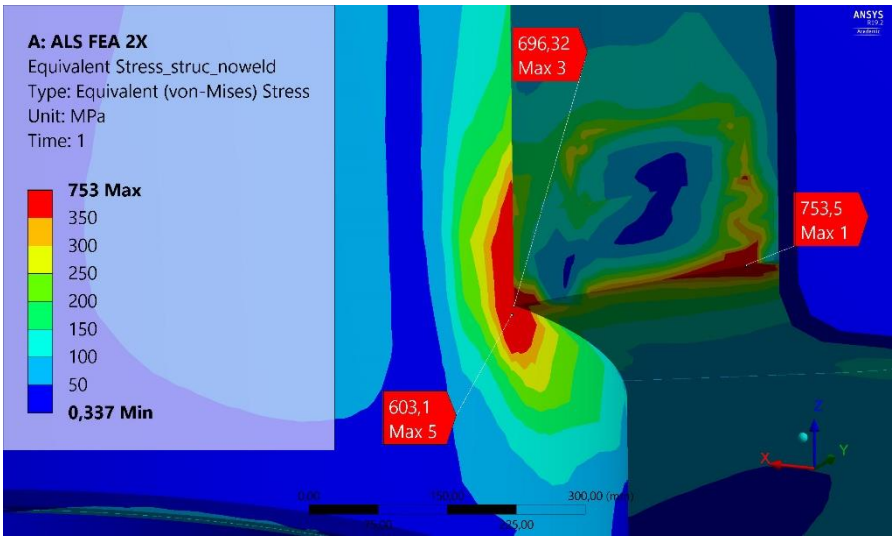

(c)

Figure 91 ALS FEA torque transfer structure stress distribution with loading magnitude factors of (a) 1.5X (b) 1.75X and (c) 2.0X.

It is somewhat unclear at what stage of resulting stress distribution, one can state that the system will fulfill ASL condition. Conducting elastic-plastic FEA for ALS is a relevant option for further work. As (DNV GL, 2019) states, the structure are only required to hold the ALS load, not necessarily withstand yielding, if redundancy and alternate redistribution of force path is possible.

For loading magnitude factor of 1.5, it seems that around 300-350 MPa appears in the torque transfer structure. For 1.75 and 2.0, a relatively large region sees stresses above material yield strength. *Figure 92 (a), (b)* and *(c)* show stress distribution in the torsion ring with 1.5X, 1.75X and 2.0X loading magnitude factors, respectively.

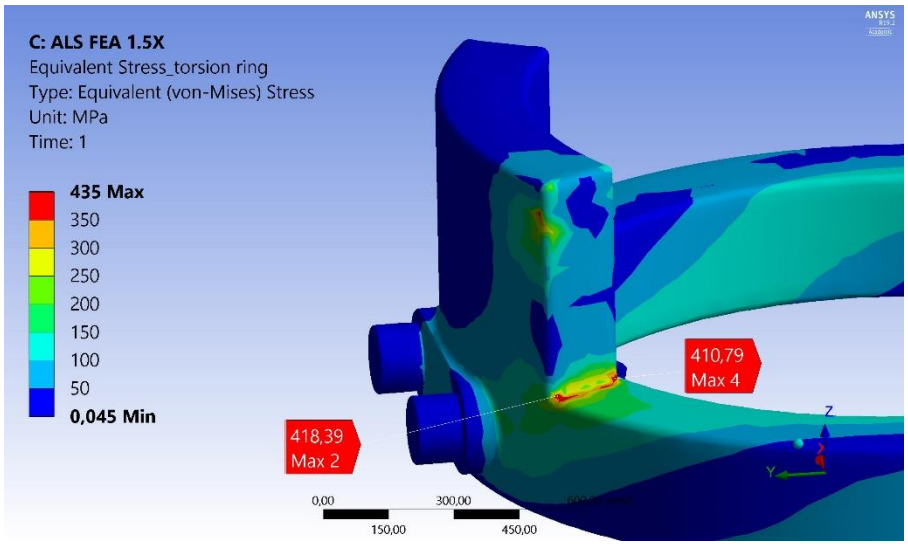

(a)

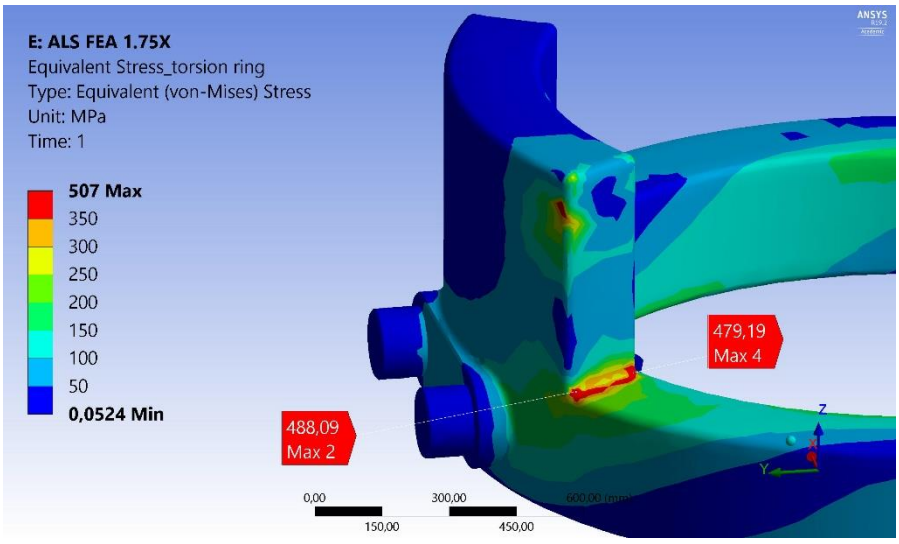

(b)

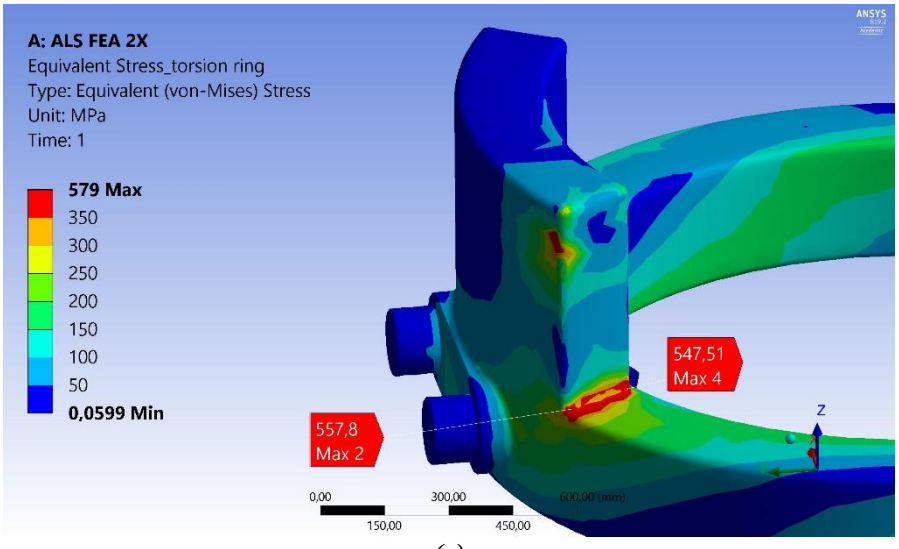

(c)

Figure 92 ALS FEA torsion ring stress distribution with loading magnitude factors of (a) 1.5X (b) 1.75X and (c) 2.0X.

In stress distribution for loading magnitude of 1.5, around 300-350 MPa seems to be present in the most exposed regions. Maximum peak values of 418 MPa are present, but it is believed to redistribute further into the extrusion part of the torsion ring. Once again, for loading magnitude factor of 1.75 and 2.0, it seems like stress above yield strength is present in relatively large regions. Above 400 MPa for 1.75 loading magnitude factor and around 450 MPa for 2.0.

Some local plastic deformation occurs during ALS condition. To be conservative, it is believed that loading magnitude factor of 1.5, are maximum ALS loading for the current geometry optimized torque transfer system. Both the 1.75 and 2.0 loading magnitude factors, seems to provide too much stress and plastic deformation to the system's critical regions. However, it is recommended to conduct elastic-plastic FEAs in order to verify the ALS conditions more accurately and determinately.

Running ALS loading with 3.0 times the design torque as seen in *Figure 93 (a)* and *(b)*, result is excessive stress well above material yield strength in several regions. Red distribution represents stress above material yield strength of 355 MPa.

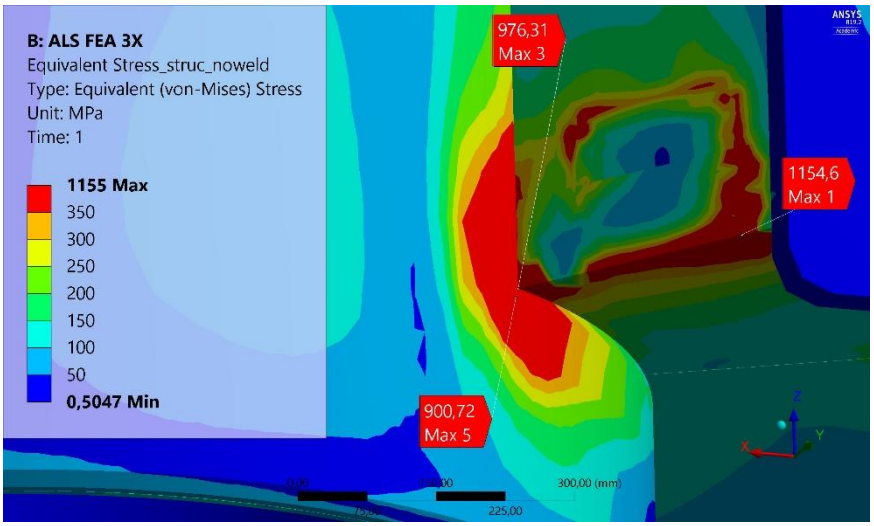

(a)

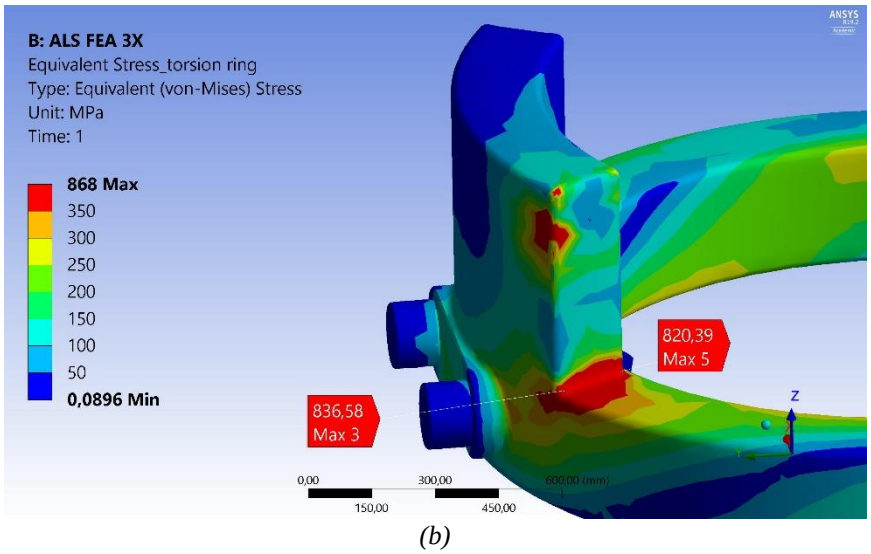

(b)

Figure 93 ALS FEA loading magnitude factor of 3.0 for (a) torque transfer structure and (b) torsion ring.

It seems like the current torque transfer system with implemented geometry optimization will fail during loading magnitude factor of 3.0 during ALS condition. These stress distribution results show that the system must be significantly strengthened to fulfill ALS condition under 3.0 times the applied torque if that is desirable. Around 600 MPa occurs in central regions.

Table 18 present results from all loading cases under ALS condition.

Table 18 ALS FEA results.

Loading magnitude factor	Applied torque [kNm]	Max. deformation [mm]	Max. negligible stress [MPa]	Max. realistic stress [MPa]
1.00	2,400	3.0	379	200
1.50	3,600	4.5	556	350
1.75	4,200	5.3	654	400
2.00	4,800	6.0	753	450
3.00	7,200	9.0	1,155	600

Deformation results show an increase of exactly the magnitude loading factor applied in a loading case. Intuitive for what to expect from increasing applied load. Stress regions also increase approximately linearly for increasing loading magnitude factor.

It is desirable to have an ALS loading condition as high as possible. Loading magnitude of 1.5 times the applied design torque is somewhat low in this relation. For further development of the most exposed stress regions in torque transfer system, material quality and/or thickness shall be increased to achieve a desirable ALS load.

7.3.1 Accidental Limit State conclusion

The current torque transfer system with implemented geometry optimization shall resist 1.5 times the applied ULS design torque during ALS condition. It means that 3,600 kNm will become the maximum allowable ALS loading. To increase the ALS loading, both material quality and thickness in the most exposed regions shall be increased. Additionally, elastic-plastic FEAs shall be conducted in the future since there are no requirement for avoiding yielding if structural integrity remains fulfilled.

7.4 Sensitivity study

Equivalent stress and deformation are examined to determine structural behavior under unsymmetrical loading condition. Deformation of 4.0 mm (with load factor) are present in the side the torsion ring is positionally adjusted to, as viewed in *Figure 94*. There are less deformation present in sensitivity study than for ULS FEA.

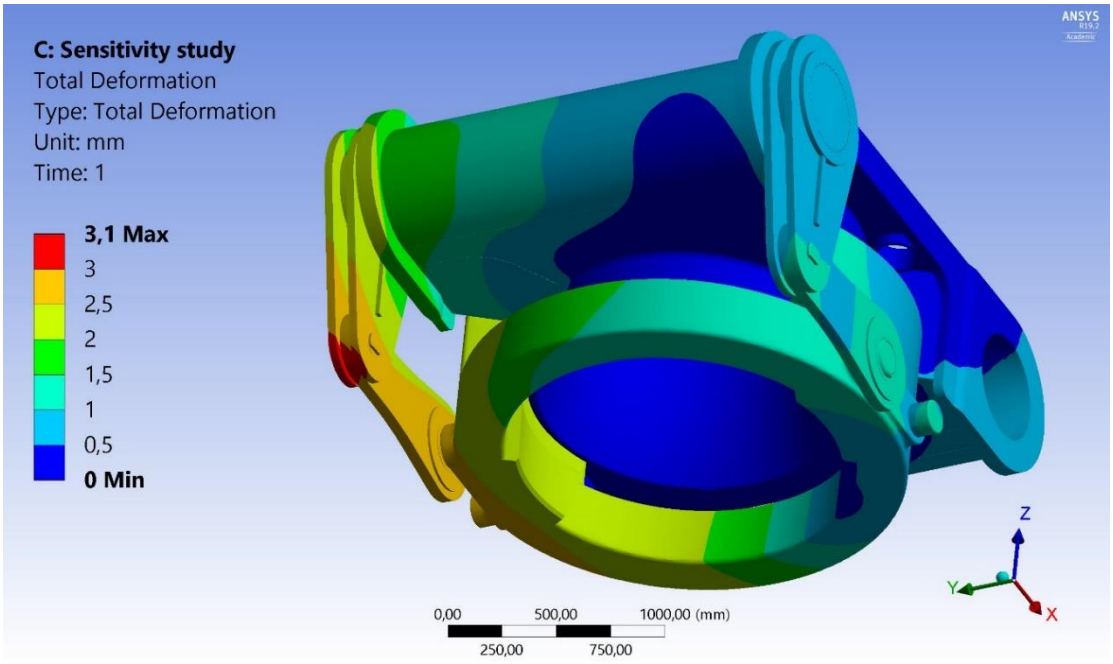

Figure 94 Sensitivity study deformation.

It is intuitive that the side the torsion ring is positionally adjusted to, will see more deformation and stress concentrations. *Figure 95 (a)* and *(b)* show increased stress distribution from ULS loading vs. sensitivity study.

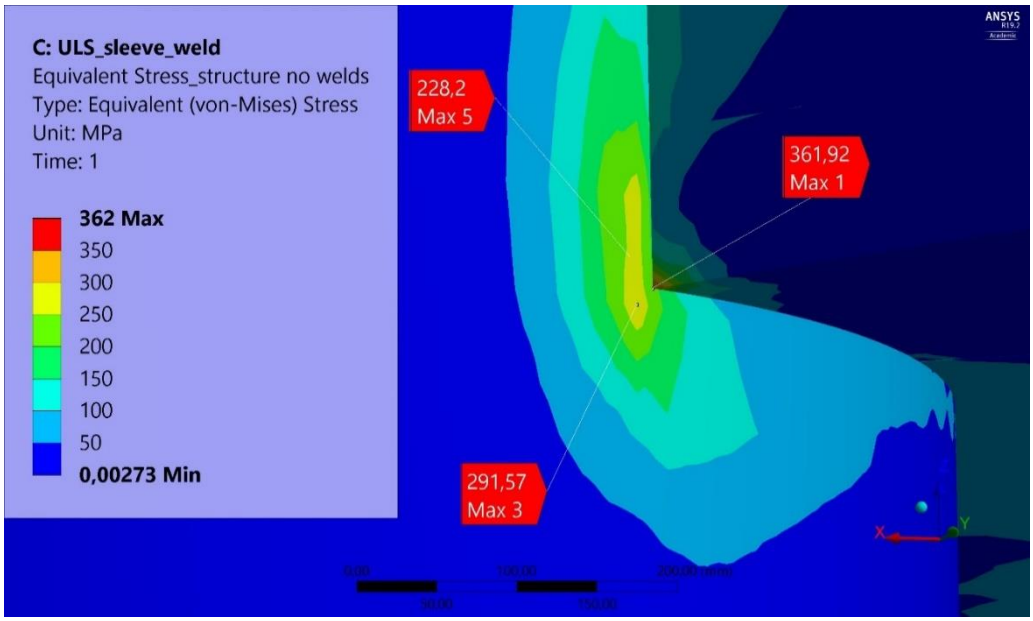

(a)

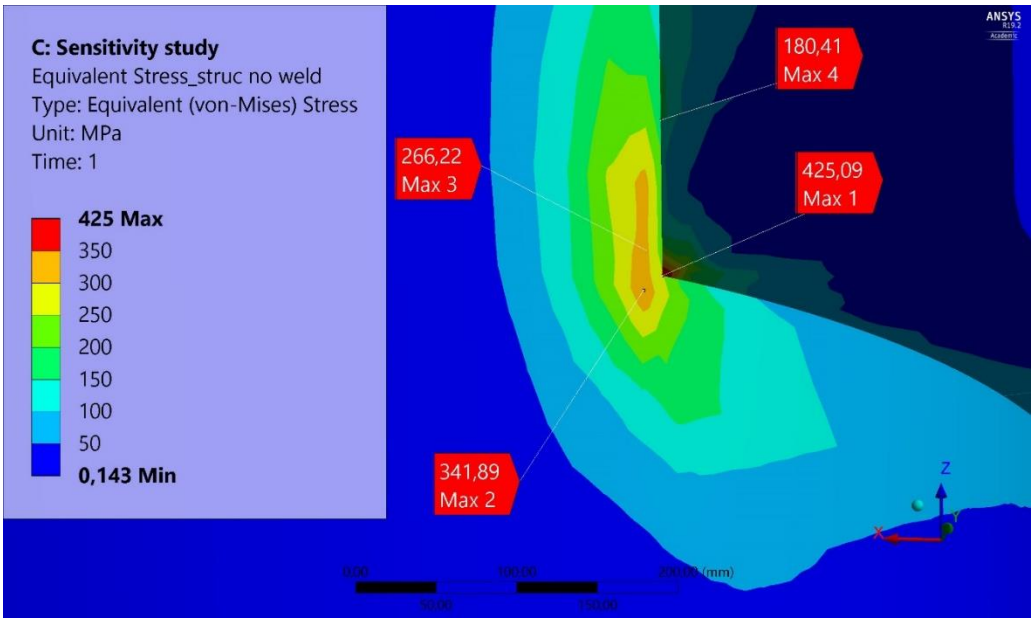

(b)

Figure 95 Comparison of stress concentration region for (a) ULS and (b) sensitivity study.

Based on reasoning from *Chapter 7.1.2* and *7.1.3*, maximum peak stresses in the reinforcement plate region are negligible. Only the surrounding stress region are considered to occur in real loading conditions. For ULS, around 250 MPa appeared in the region, whereas for sensitivity study around 300 MPa appears (both with load factor). *Figure 96* show that up to 100 MPa (with load factor) appears at the outer torque transfer structure, in the side which the torsion ring is positionally adjusted to.

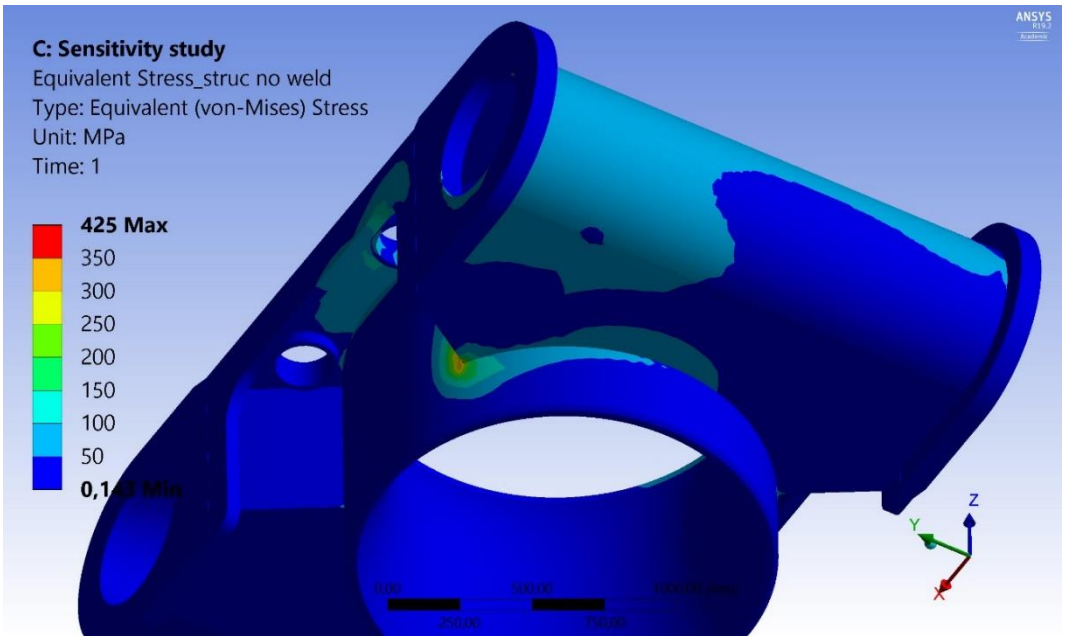

Figure 96 Sensitivity study stress in positionally adjusted side.

Larger positional adjustment sensitivity studies shall be conducted in the future to observe structural behavior under such circumstances. Also, for identifying maximum positional adjustment for the torsion ring while still be able to fulfill ULS condition.

Horizontal arms experience more stress than for symmetrical ULS condition. *Figure 97 (a)* shows stress distribution for ULS condition and *Figure 97 (b)* for sensitivity condition.

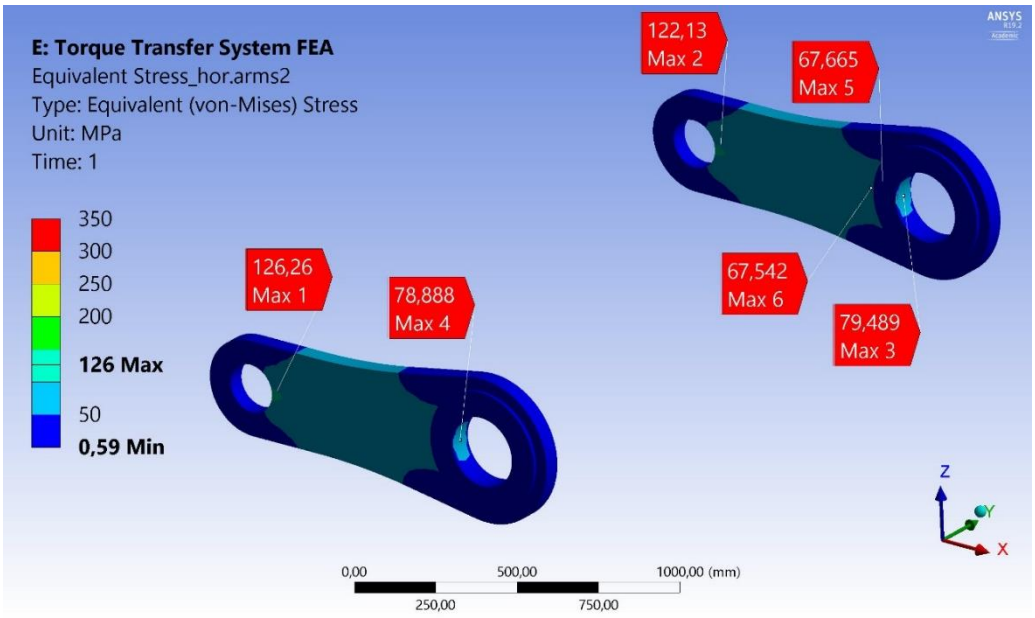

(a)

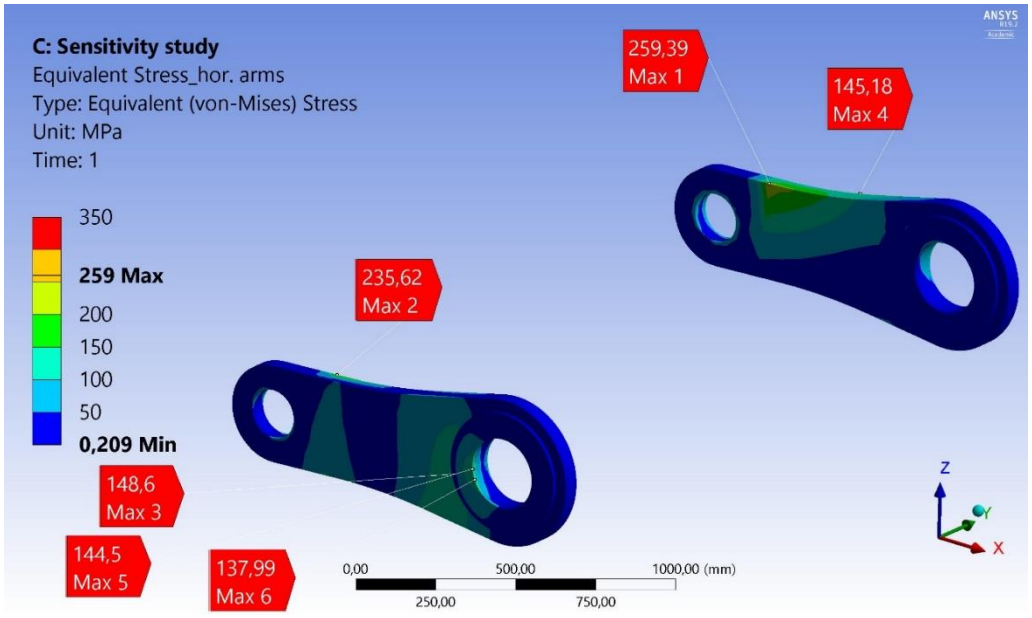

(b)

Figure 97 Comparison of stress in horizontal arms for (a) ULS and (b) sensitivity study.

Horizontal arms are designed to be pure tension/compression members. Peak stress values are negligible and surrounding stress region of about 250 MPa (with load factor) is assumed to be governing. For sensitivity condition, the horizontal arms experience around 80 MPa of more stress than in symmetric ULS condition. Stress distribution become unsymmetrical and are also shifted to more regions of the horizontal arms as moments are introduced to the component. Nevertheless, stress is below material strength capacity of 308.7 MPa.

Table 19 show comparison of results in similar regions for the sensitivity study vs. ULS FEA. Geometry optimized torque transfer structure are used for both comparison cases.

Table 19 Sensitivity study vs. ULS FEA.

Placement	Type	Sensitivity study	ULS FEA
Torsion ring	Deformation [mm]	4.0	5.3
Torque transfer structure, optimized	Equivalent stress [MPa]	300	250
Horizontal arms	Equivalent stress [MPa]	250	164

7.4.1 Sensitivity study conclusion

FEA show that the torque transfer system will fulfill ULS condition, even when the torsion ring is positionally adjusted in all directions and the system become unsymmetrical. Deformation will be reduced, whereas stress concentration was observed to increase in certain regions in the system.

Conclusion

This thesis aimed to determine if structural integrity is fulfilled for the torque transfer system for offshore turret production system in a FPSO. Detailed principal and technical description of the system were initially conducted, in order to recognize the functionality and requirements for the system. Benefits of the torque transfer system were presented, while comparing other mooring solutions for FPSOs formed comprehensive background knowledge. Strength calculations involving FEA and supporting hand calculations were performed, based on applicable rules and regulations considering ULS, FLS and ALS conditions. To conduct the FEA analysis Ansys Workbench R19.2 was used.

ULS condition is fulfilled by the torque transfer system, with 2,400 kNm of applied design torque. Stress concentration of about 300 MPa appears in the two most critical regions in the initial torque transfer system, slightly below material strength capacity of 308.7 MPa. After implementing geometry optimization, resulting stress concentration was reduced to about 250 MPa and 150 MPa, respectively. Implemented geometry optimization also improved FLS, ALS and sensitivity study condition. All other main components of the torque transfer system fulfill ULS condition. Hand calculations also resulted in similar values as obtained in ULS FEAs, thus supporting the analyses validity.

The torque transfer system fulfills FLS condition and will not experience fatigue failure during its lifetime.

Maximum loading that the torque transfer system manages to resist, is 3,600 kNm while still fulfilling ALS condition. The maximum ALS loading is 1.5 times the design torque as for ULS condition.

When components are exposed to positional movement and thus unsymmetrical applied torque on the system, it still proves to fulfill ULS condition. Stress concentration was observed to increase but remained below material strength capacity.

More examinations on material fatigue tests shall be conducted in the future to improve reliability of the S-N curve used in the FLS analysis. Both material quality and thickness shall be increased in the critical regions to increase allowable ALS loading if desirable. Elastic-plastic FEAs shall also improve reliability of ALS analyses. Several sensitivity studies shall also be conducted to identify the maximum allowable positional adjustment, while still fulfilling ULS condition.

By implementing the proposed geometry optimization to the torque transfer system, it shall fulfill all limit state conditions.

Further work

It is recommended to implement the proposed geometry optimization to assure all limit state conditions to be fulfilled. As proved in the thesis, the corrective actions will reduce stress concentrations.

The torque transfer system is currently a concept system which is yet to be produced and put into operation and thus be exposed to real loading conditions. More information regarding realistic stress and deformation will not be available until that stage. Strain gauges shall be place on relevant components to examine structural behavior, where one can determine if design torque is ever reached. Based on these examinations, calibrated input torque shall be applied for analyses in further development of the torque transfer system.

Regarding fatigue, reliability of the number of cycles and magnitude of cyclic loading shall be improved before the system is set into operation. It is heavily dependent on environmental conditions and are quite different from field to field, and further examinations are recommended. In order to get a S-N curve as valid as possible, it is also desirable to receive material specification data for fatigue specimen tests on the exact material batch of NVD36 and NVE36 used for the torque transfer system. As fatigue tests on standard specimens vary some, even for equivalent materials.

To increase maximum ALS load for the system, it is recommended to reinforce the contact region for the torsion ring and torque transfer structure. Both material quality and thickness shall be increased to improve stress distribution.

Positional adjustment of the torsion ring showed increasing stress concentrations relative to the symmetric ULS condition. Even larger positional adjustments analyses shall be conducted, to find the structure’s maximum allowed positional adjustment while still fulfilling ULS condition.

References

AST® BEARINGS LLC. 2020. *GE160XT-2RS Metric Series Steel on PTFE Fabric Material Spherical Plain Bearing* [Online]. Available: https://www.astbearings.com/catalog.html?page=product&id=GE160XT-2RS [Accessed 10.03.2020].

BLUEWATER. n.d. *What is an FPSO?* [Online]. Available: https://www.bluewater.com/fleet-operations/what-is-an-fpso/ [Accessed 17.02.2020].

BUDYANS, R. G. & NISBETT, J. K. 2015. *Shigley's Mechanical Engineering Design, Tenth Edition in SI Units*, McGraw-Hill Education.

BW OFFSHORE. 2019a. *BW Offshore turret, mooring, swivel, SURF & installation group* [Online]. Available: https://www.bwoffshore.com/tms/ [Accessed 28.01.2020].

BW OFFSHORE. 2019b. *E&P* [Online]. Available: https://www.bwoffshore.com/business/ep/ [Accessed 17.02.2020].

BW OFFSHORE 2020. Annual report 2019. BW Offshore Ltd.

CHAKRABARTI, S. K. 2005. *Handbook of Offshore Engineering*, Elsevier Ltd.

COLLINS, J. A., BUSBY, H. R. & STAAB, G. H. 2010. *Mechanical design of machine elements and machines: a failure prevention perspective, second edition*, Hoboken, New Jersey, Wiley.

CORUS CONSTRUCTION & INDUSTRIAL 2004. European structural steel standard EN 10025 : 2004, Explanation and comparison to previous standards. Corus Construction & Industrial.

DIN 2006. DIN 5480-1 Splined connections with involute splines based on reference diameters – Part 1: Principles. DIN (Deutsches Institut für Normung).

DNV GL 2019. Offshore Standards DNVGL-OS-C101 Design of offshore steel structures, general - LRFD method. DNV GL.

FATCHURROHMAN, N. & CHIA, S. T. 2017. Performance of hybrid nano-micro reinforced mg metal matrix composites brake calliper: simulation approach. *IOP Conference Series: Materials Science and Engineering*, 257.

HELLAND ANDERSEN, L. K. 2015. *Subsea Tie-in, design solutions and optimisation methods.* M.Sc. thesis, University of Stavanger.

KOREN, I. & KRISHNA, C. M. 2007. Fault-tolerant systems. Elsevier Science & Technology.

LANCASTER, J. 2005. *Engineering Catastrophes, Third Edition*, Woodhead Publishing Limited.

LEMU, H. G. 2016. *Dimensjonering av maskinelementer*, Stavanger.

LIBERTY STEEL DALZELL 2017. Premium Quality Steel Plate Brochure. Liberty House Group.

LIN, Y., YANG, Q. & GUAN, G. 2019. Scantling optimization of FPSO internal turret area structure using RBF model and evolutionary strategy. *Ocean Engineering*, 191.

MALM ORSTAD AS. 2020. *MO21 - With Spherical Bearings* [Online]. Available: https://malmorstad.com/products/cylinders/mo21-with-spherical-bearings- [Accessed 02.03.2020].

MILOVANOVIĆA, V., ŽIVKOVIĆA, M., JOVIČIĆA, G. & DIŠIĆA, A. 2019. Experimental determination of fatigue properties and fatigue life of S355J2+N steel grade. *Materials Today*.

MODEC INC. 2020. *About an FPSO* [Online]. Available: https://www.modec.com/fps/fpso_fso/about/index.html [Accessed 07.02.2020].

MYHRE BØE, M. E. 2014. *Analysis of mooring wire rope termination with respect to bending fatigue.* M.Sc. thesis, University of Stavanger.

NORSK STÅL AS 2001. Tabeller og standarder. Norsk Stål AS.

NOV APL 2020. APL Smarter Turret Mooring Brochure. 2 ed.: National Oilwell Varco.
SBM OFFSHORE 2020. Turret & Mooring Systems Supply Record Brochure. SBM Offshore.
SOFEC INC. 2020. Internal Turret Mooring System Brochure. SOFEC Inc.
WALØEN, Å. Ø. 1989. *Maskindeler Bind 1*, Trondheim, Tapir Forlag.

Appendix

Information regarding matters that naturally not belong directly in the thesis are included in this appendix. Supplements and support documentation are also listed in this section.

A.1 Status reports

All status reports in this thesis is written on a monthly basis. Each status report is written in the beginning of each month, and describes the progress and tasks conducted in the previous month.

January

Written on the 4th of February 2020.

The thesis started with kick-off meeting January 6th at BW Offshore in Arendal. In this meeting several CAD-files and drawings was handed over by the company.

It was agreed that it was important to fully understand and prove the theoretical aspect behind the torque transfer system. Basic hand calculations were to be conducted to prove static equilibrium of the system when exposed to torque. This proved to be more demanding than first anticipated, but after correction and discussion meetings by telephone and at the office, at the 20th and 27th of January, static equilibrium was proven. Static equilibrium is a central part of the principal description of the thesis.

Alongside the hand calculations, preliminary investigations of several subjects of the task was conducted. A couple of meetings with UiS supervisor was held for guidance. The pre-study report was one part of the work and discussion in this period. The pre-study report is an elaboration of the task description agreed upon before Christmas. Among other things, the report involves a Gantt chart, WBS, structure of report (table of content) and temporary list of references of the entire project. The pre-study report was not finished in January but is expected to be completed in early February. Hand in is due on the 15th of February. In later status reports, progress and deviations can be compared towards the Gantt chart.

More formal matters, such as document formatting, software licenses and endnote configuration, have also been conducted. Quite some time of literature studies in relevant areas have been examined and listed for later use.

For February, I expect to finish introduction, theory and principal description of the thesis. It will form the basis for the FEA.

February

Written on the 2nd of March 2020.

Throughout February a couple of meetings with UiS supervisor have been conducted. Mostly regarding the pre-study report that was due on the 15th of February, but also some formatting questions and more specific on the FEAs.

Introduction, literature study and principal description is finished. Technical description has been started, but still requires some work. This part will be in focus in the beginning of March

and is expected to be finish within mid-March. Some simple analyses have been tested in Ansys but will be in full focus after finishing the technical description. These first written parts will be handed over to BW Offshore when finished, for verification and comments.

Time have also been awarded CAD work, to make transparent visual figures when explaining specific areas or functions of the structure. This will also probably be the case for the technical description.

When the FEAs are fully started, several meetings with BW Offshore are probably required to keep them involved in the process.

For March, I expect to finish the technical description and getting a good start on the strength calculations.

March

Written on the 1st of April 2020.

In March I finished the parts prior to the strength calculations. In mid-March I got thorough feedback from Espen Holm in BW Offshore on these parts. After the telephone meeting we decided that I should perform refinements in certain sections, some section removals and some change on chaptering. Some rephrasing and reexplanation were also necessary on certain sections. A week or so afterwards more technical questions were discussed with Vidar Berg Pedersen in BW Offshore. Thus, more refinement and additions in certain sections were conducted.

March month will always be remembered as the time of the covid-19 virus fully came into Europe and shut down the society in ways not seen since wartime. With respect to this thesis, it involved closing of the University and not accessing more powerful computers with full Ansys Workbench license. However, with great efforts from different people at the University I was allowed to get the equivalent license on my personal computer. Without this, it would have proved difficult to continue the initial set objectives. A huge thanks to the IT department and especially Chief Engineer Adugna Deressa Akessa, for assisting me in these special times.

Some theory on FEA were conducted before starting the analyses themselves. A lot of different mesh generation settings were tested and exploring of the Ansys software. It was early on discovered that a few plates in the torque transfer structure had to be changed to be able to generate an acceptable mesh. Exploration of possible fatigue analyses have also been examined.

For April I expect to have most of the ULS FEA completed and got a good start on fatigue analyses. More involvement of BW Offshore is probable in these sections, as well as opinions on how to structure the presentation of results. As of this date, the covid-19 virus will probably continue to claim restrictions on everyday life. However, if I am allowed to keep a license of Ansys software it should not slow down my work noticeably. Telephone meetings and not physical meetings, with both BW Offshore and university supervisor, are likely to

continue in the following weeks. Easter holiday in week 15 is expected to prevent a few days of work in April.

An overall milestone is to finish most of the thesis before June, and only conduct minor changes, write conclusion, preface and abstract, in the last two weeks before hand-in. An A to Z read through should also be conducted in this period.

April

Written on the 1st of May 2020.

Home office were still required for the month of April. Thankfully, the license on my personal computer have worked smoothly and I have been able to conduct analyses work in the software. During April nearly the entire ULS FEA have been completed. Throughout April I had several discussions with UiS supervisor Hirpa Gelgele Lemu over telephone. I also decided to change some of the chaptering regarding the FEAs, to improve the presentation of the approach and results. Therefore, the structure of the FEA sections will be presented differently than originally planned. More refinements on presentation of the findings must probably be conducted in the next month in consultation with BW Offshore.

Thesis progress is on schedule. In June the fatigue, accidental and sensitivity FEA must be completed. After conducting those tasks, the thesis will have answered the set objectives. Hopefully, it will highlight some key areas of interest in the torque transfer system with respect to structural integrity, that BW Offshore should be made aware of.

I still expect to finish most of the thesis before June, and only conduct minor refinements and write conclusion, preface and abstract in the two last weeks before hand-in. I have also planned in consultation with UiS supervisor, to deliver a final draft to him in the last week of May. He will go through the thesis and provide feedback.

The final stage of the master thesis project is now entered. I must keep my work spirit up for the last weeks, and I hope and believe the final draft will be of great quality.

May

Written on 1st of June 2020.

The entire thesis is now written except from preface. Progress is on schedule as the final draft of the thesis now are delivered to UiS supervisor for feedback. In May, several discussions with both UiS supervisor and BW Offshore were conducted. I now feel that most of the thesis are in place, but I expect to conduct refinements and changes after getting final feedback.

In June, I will read through the entire thesis, check and refine sections based on my findings. Special focus on abstract and conclusion are of importance, as these sections are some of the most important ones in the master thesis.

Hopefully, I will finish and deliver a few days prior to deadline on the 15th of June at 14.00 (CEST).

A.2 Mathcad calculations

Mathcad sheets are included in the next pages to prove knowledge in typical engineering software for calculations. All these calculations are also included in the thesis itself. Mathcad is powerful for changing input values and effectively see the change in output values. Hence, only the calculations containing specific values are included and not the general proven formulas.

Torque Transfer System for offshore Turret Production System - hand calculations Mathcad

The purpose of this document is to conduct hand calculations for load cases in the torque transfer system and evaluate them in relation to FEAs. Hand calculations are arranged chronologically according to what is presented in the thesis document.

Friction moment from support bearing

$\mu := 0.006$	friction coefficient
$M_k := 0$	resulting tilting moment (neglected)
$W_{gm} := 4750.0\ kN$	weight geostationary module
$W_s := 1619.0\ kN$	weight swivel core
$F_a := W_{gm} + W_s = 6369.0\ kN$	axial load
$D_L := 3.6\ m$	bearing race diameter
$F_r := 0$	radial load (neglected)

Starting torque for the support bearing is defined as follows:

$$M_r = \frac{\mu}{2} \cdot \left(4.1 \cdot M_k + F_a \cdot D_L + 2.2 \cdot F_r \cdot D_L \cdot 1.73\right)$$

$$M_r := \frac{\mu}{2} \cdot \left(F_a \cdot D_L\right) = 68.8\ kN \cdot m$$

Friction moment from the support bearing will be slightly below 70 kNm. However, BW Offshore sets it to 200 kNm, just in case.

Reaction forces

Reaction forces from applied torque is based on torsional transmission principle.

$M_{z\_D} := 2400\ kN \cdot m$ design torque applied to the system

$x_A := 900\ mm$ x-distance between connection joints of horizontal arm

$y_B := 150\ mm$ y-distance between shaft bearings and round bars (spline connections)

$y_S := 1950\ mm$ y-distance between shaft bearings

$y_{TR} := 2250\ mm$ y-distance between torsion ring connection joints

$z_A := 805\ mm$ z-distance between connection joints of vertical arm

Reaction forces from applied torque to the system:

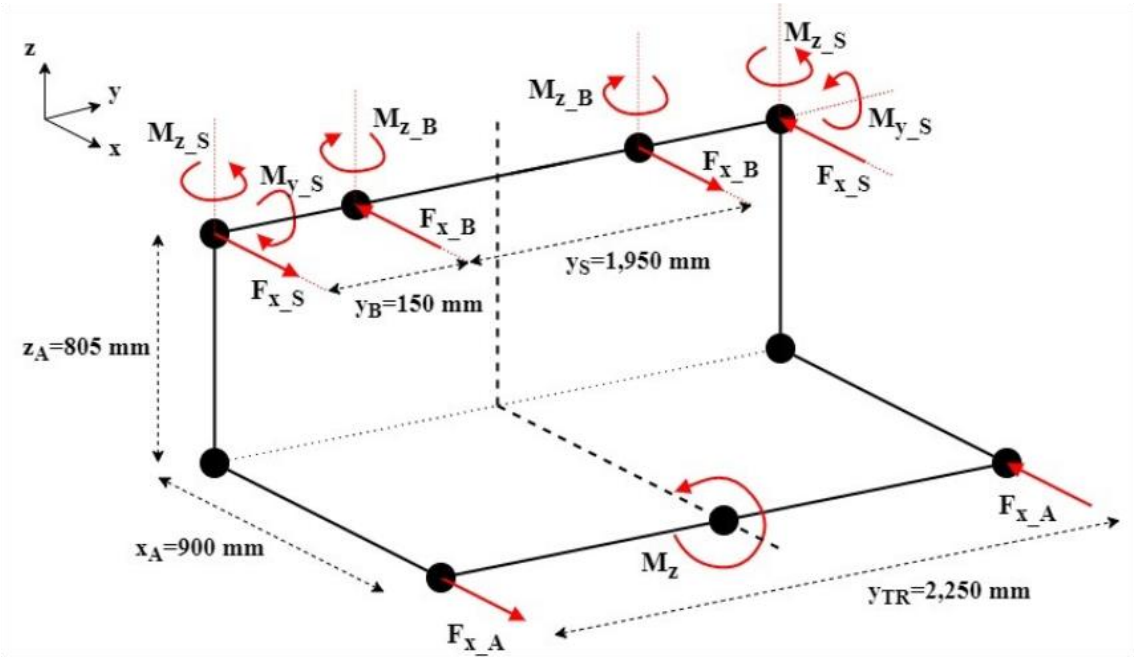

$F_{x\_A} := \frac{M_{z\_D}}{y_{TR}} = 1066.7\ kN$ reaction x-force at horizontal arms

$F_{x\_B} := \frac{M_{z\_D}}{y_S} = 1230.8\ kN$ reaction x-force shaft bearings

$F_{x\_S} := F_{x\_B} - F_{x\_A} = 164.1\ kN$ resultant x-force at round bars (spline connections)

$M_{z\_B} := F_{x\_B} \cdot y_B = 184.6\ kN \cdot m$ reaction z-moment in shaft bearings

$M_{z\_S} := M_{z\_B} = 184.6\ kN \cdot m$ reaction z-moment in round bars (spline connections)

$M_{y\_S} := F_{x\_A} \cdot z_A = 858.7\ kN \cdot m$ reaction y-moment in round bars (spline connections)

Hydraulic cylinders

$P_{HC} := 210\ bar = 21.0\ MPa$ specified capacity of hydraulic cylinders

Hydraulic cylinder capacity is based on internal bore diameter where the stroke arm can operate:

$d_{HC} := 125\ mm$ hydraulic cylinder internal bore stroke diameter

$A_{HC} := \pi \cdot \left(\frac{d_{HC}}{2}\right)^2 = 12272\ mm^2$ hydraulic cylinder internal stroke area

Total capacity of hydraulic cylinders:

$n_{HC} := 4$ number of hydraulic cylinders

$F_{g\_HC} := n_{HC} \cdot P_{HC} \cdot A_{HC} = 1030.8\ kN$ total capacity of hydraulic cylinders

$F_{g\_HC\_tons} := \frac{F_{g\_HC}}{g} = 105.1\ tonne$ total capacity of hydraulic cylinders in metric tons

Applied pressure - torsion ring

$d_{TR} := 1504\ mm$ inner diameter of contact face in torsion ring (conservative)

$F_{TR} := \frac{M_{z\_D}}{d_{TR}} = 1595.7\ kN$ applied load in torsion ring

$A_{CF} := 19708\ mm^2$ contact face area in torsion ring (found in Inventor)

$P_{TR} := \frac{F_{TR}}{A_{CF}} = 81.0\ MPa$ applied pressure at contact face in torsion ring

FLS

$P_{TR\_FLS} := 0.5 \cdot P_{TR} = 40.5\ MPa$ applied pressure at contact face in torsion ring under FLS condition

$\sigma_{UTS} := 460$ material ultimate tensile strength (not considering units)

$k_a := 4.51 \cdot \sigma_{UTS}^{-0.265} = 0.888$ surface modification factor (machined/cold-drawn)

$d := 100$ size of member exposed to fatigue (not considering units)

$k_b := 1.51 \cdot d^{-0.157} = 0.733$ size modification factor

$k := k_a \cdot k_b = 0.651$ combined modification factor

$DFF := 3.0$ design fatigue factor

$n_{YR} := 7500$ number full loading cycles per year

$t_{YR} := 20$ number of design years of operational service

$n_d := DFF \cdot n_{YR} \cdot t_{YR} = 4.5 \cdot 10^5$ fatigue design cycles

Material capacity

Material capacity in both equivalent stress and shear stress are based on material yield strength and take into account material factor.

$\sigma_{YS} := 355\ MPa$ NVD36/NVE35 material yield strength

$\gamma_M := 1.15$ material factor for plated structure and tubular members based on (DNV GL, 2019)

$\sigma_{cap} := \frac{\sigma_{YS}}{\gamma_M} = 308.7\ MPa$ equivalent stress capacity

$\tau_{cap} := \frac{\sigma_{YS}}{\gamma_M \cdot \sqrt{3}} = 178.2\ MPa$ shear stress capacity based on Von Mises criterion

Angle of twist - shaft

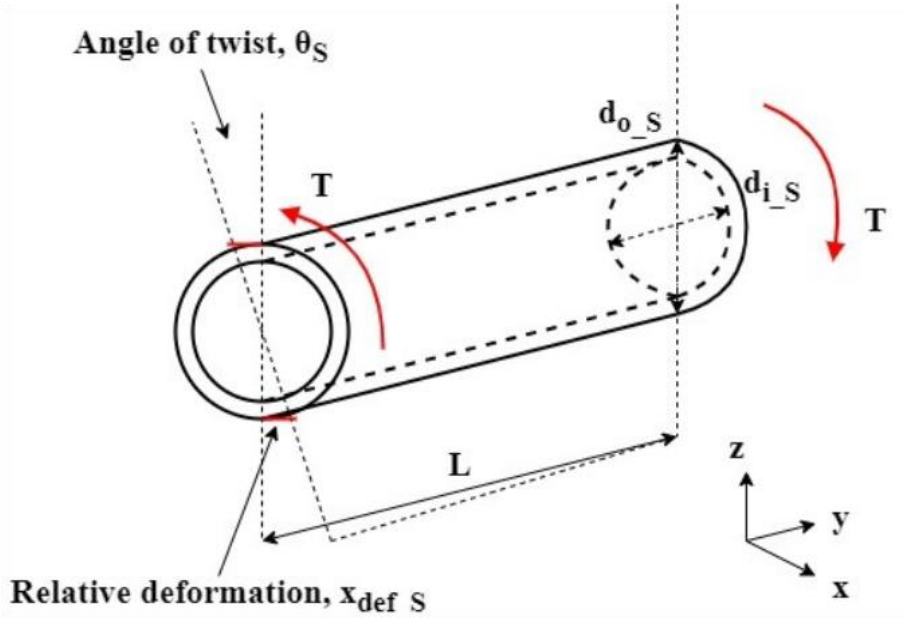

$E := 200\ GPa$ — Young's modulus or modulus of elasticity

$v := 0.3$ — Poisson's ratio

$G := \frac{E}{2 \cdot (1+v)} = 76.9\ GPa$ — shear modulus or modulus of rigidity

$T := M_{y\_S} = 858.7\ kN \cdot m$ — applied torque (reaction y-moment at round bars/spline connections)

$L := 2 \cdot y_B + y_S = 2250.0\ mm$ — length of shaft exposed to torque

$D_S := 455\ mm$ — outer diameter of central pipe section of shaft

$d_S := 387.4\ mm$ — inner diameter of central pipe section of shaft

$J_S := \frac{\pi}{32} \cdot \left(D_S^4 - d_S^4\right) = \left(2 \cdot 10^9\right)\ mm^4$ — polar second moment of area in shaft

$\gamma_f := 1.3$ — load factor for ULS condition

$\theta_S := \gamma_f \cdot \frac{T \cdot L}{G \cdot J_S} = 0.937\ deg$ — angle of twist in shaft (incl. load factor)

$x_{def\_S} := \frac{D_S}{2} \cdot \sin\left(\theta_S\right) = 3.7\ mm$ — relative deformation in shaft

Torsion ring

In pure shear, a member will have limit shear stress based on yield strength and Von Mises criterion:

$d_{TR\_A} := 160\ mm$ diameter of torsion ring connection joint to horizontal arms

$A_{TR\_A} := \pi \cdot \left(\frac{d_{TR\_A}}{2}\right)^2 = 20106\ mm^2$ cross-section area of torsion ring connection joint to horizontal arms

$\tau_{TR\_A} := \gamma_f \cdot \frac{F_{x\_A}}{A_{TR\_A}} = 69.0\ MPa$ shear stress in torsion ring connection joint to horizontal arms (incl. load factor)

$u_{TR\_A} := \frac{\tau_{TR\_A}}{\tau_{cap}} = 0.39$ utilization of shear stress capacity in torsion ring

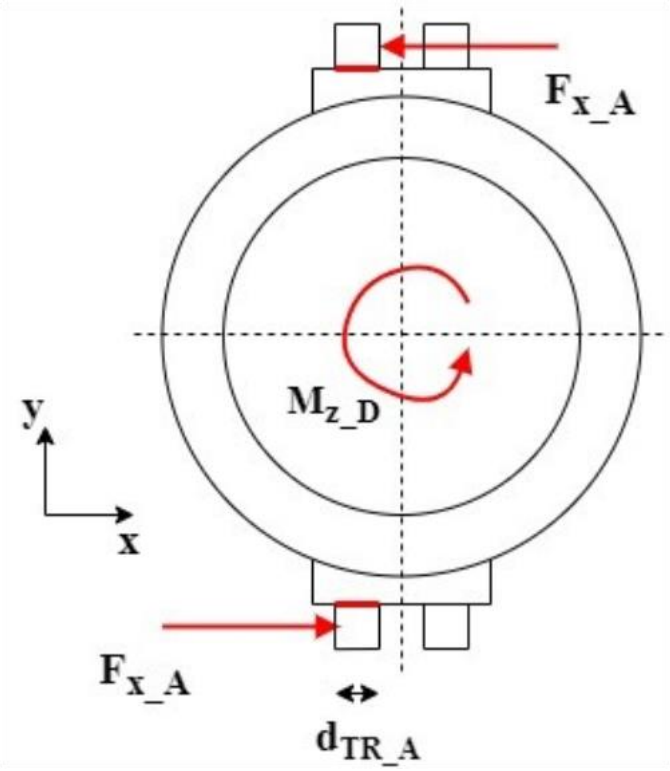

Horizontal arms

Tear-out of spherical bearing and axle in the rear end of the horizontal arms seems to be the critical condition.

$R_{HA\_r} := 160\ mm$ outer radius of rear horizontal arms

$t_{HA} := 55\ mm$ thickness of horizontal arms

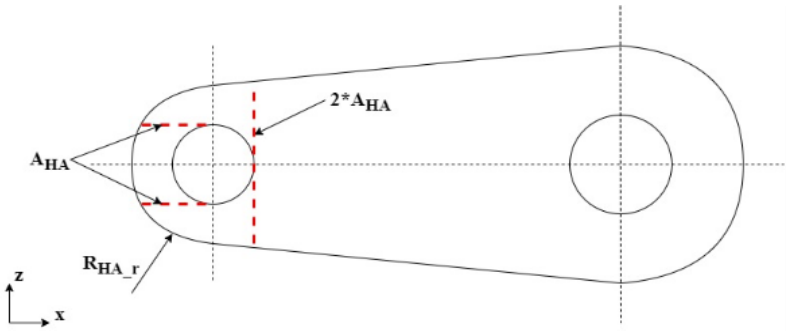

Tear-out area:

$A_{HA} := t_{HA} \cdot R_{HA\_r} = 8800\ mm^2$ tear-out and axial cross-sectional area

$\tau_{HA} := \gamma_f \cdot \frac{F_{x\_A}}{2 \cdot A_{HA}} = 78.8\ MPa$ tear-out shear stress (incl. load factor)

$u_{HA} := \frac{\tau_{HA}}{\tau_{cap}} = 0.44$ utilization of tear-out shear stress capacity in horizontal arms

Axial stress:

$\sigma_{HA} := \gamma_f \cdot \frac{F_{x\_A}}{2 \cdot A_{HA}} = 78.8\ MPa$ axial stress (same as for shear stress)

$u_{HA\_a} := \frac{\sigma_{HA}}{\sigma_{cap}} = 0.26$ utilization of axial stress capacity in horizontal arms

Axle

In the same manner as for the horizontal arms, the axles are checked for tear-off from pure shear stress.

$d_A := 110\ mm$ diameter of axle

$A_A := \pi \cdot \left(\frac{d_A}{2}\right)^2 = 9503\ mm^2$ cross-sectional area of axle

$\tau_A := \gamma_f \cdot \frac{F_{x\_A}}{2 \cdot A_A} = 73.0\ MPa$ tear-off shear stress of axle (incl. load factor)

$u_A := \frac{\tau_A}{\tau_{cap}} = 0.41$ utilization of tear-off shear stress capacity in axle

Vertical arms - hub

The hub are checked for equivalent stress based on the two resulting moments from reaction forces found in *3.3.1 Specific values*. This calculation is also quite conservative.

$M_{z\_S} = 184.615\ kN \cdot m$

bending moment applied to the hub

$M_{y\_S} = 858.667\ kN \cdot m$

torsion applied to the hub

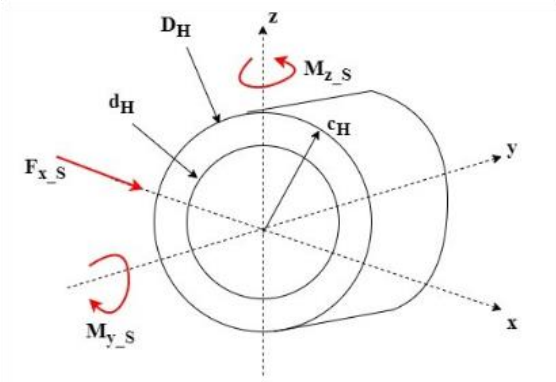

$F_{x\_S} = 164.1\ kN$ shear force applied to the hub

$D_H := 540\ mm$ outer diameter of hub (female spline connection) in vertical arms

$d_H := 420\ mm$ inner diameter (reference) of hub (female spline connection) in vertical arms

$c_H := \frac{D_H}{2} = 270\ mm$ max. distance to outer surface

$A_H := \pi \cdot \left(\left(\frac{D_H}{2} \right)^2 - \left(\frac{d_H}{2} \right)^2 \right) = 90478\ mm^2$ cross-sectional area of central pipe section of shaft

$I_H := \frac{\pi}{64} \cdot \left({D_H}^4 - {d_H}^4 \right) = \left(2.6 \cdot 10^9 \right)\ mm^4$ second-area moment of hub in vertical arms

$J_H := \frac{\pi}{32} \cdot \left({D_H}^4 - {d_H}^4 \right) = \left(5.3 \cdot 10^9 \right)\ mm^4$ polar second moment of area in hub of vertical arms

$\sigma_{max\_H} := \frac{M_{z\_S} \cdot c_H}{I_H} = 18.8\ MPa$ max. bending stress in hub of vertical arms

$\tau_{max\_H} := \frac{M_{y\_S} \cdot c_H}{J_H} = 43.8\ MPa$ max. shear stress from applied torsion in hub of vertical arms

$\tau_H := \frac{F_{x\_S}}{A_H} = 1.8\ MPa$ shear stress from shear force in hub of vertical arms

$\sigma_{VM\_H} := \gamma_f \cdot \sqrt{{\sigma_{max\_H}}^2 + 3 \cdot \left(\tau_{max\_H} + \tau_H \right)^2} = 105.6\ MPa$ equivalent Von Mises stress in hub of vertical arms (incl. load factor)

$u_H := \frac{\sigma_{VM\_H}}{\sigma_{cap}} = 0.34$ utilization of equivalent stress capacity in hub of vertical arms

Vertical arms - section

The section below the hub are checked for equivalent stress based on bending moment and shear force. This calculation is also somewhat conservative.

$B_{VA} := 596\ mm$

width of vertical arm cross-section

$b_{VA} := 2 \cdot 283\ mm = 566\ mm$

combined flange width (no web) of vertical arm cross-section

$H_{VA} := 150\ mm$

height of vertical arm cross-section

$h_{VA} := 70\ mm$

height between flanges of vertical arm cross-section

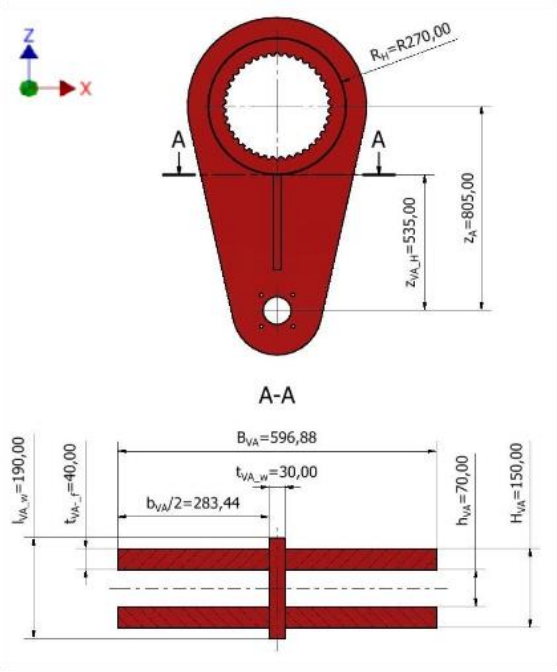

$R_H := \frac{D_H}{2} = 270\ mm$ hub radius

$z_{VA\_H} := z_A - R_H = 535\ mm$ distance from load to max. stress location in cross-section in vertical arm

$l_{VA\_w} := 190\ mm$ web length of vertical arm cross-section

$t_{VA\_w} := 30\ mm$ web thickness of vertical arm cross-section

$t_{VA\_f} := 40\ mm$ flange thickness of vertical arm cross-section

From the reaction force in x-direction in the horizontal arms the cross-section just below the hub will experinece both resulting bending moment and shear stress.

$$A_{VA} := t_{VA\_w} \cdot l_{VA\_w} + 4 \cdot \left(t_{VA\_f} \cdot \frac{b_{VA}}{2} \right) = 50980\ mm^2$$

Cross-sectional area of vertical arm below hub

$\tau_{VA} := \frac{F_{x\_A}}{A_{VA}} = 20.9\ MPa$ shear stress in vertical arm below hub

$$w_{y\_VA} := \frac{{B_{VA}}^2 \cdot (H_{VA} - h_{VA})}{6} + \frac{(B_{VA} - b_{VA})^3 \cdot h_{VA}}{6 \cdot B_{VA}} = (4.74 \cdot 10^6)\ mm^3$$

section modulus of cross-section of vertical arm below hub

$\sigma_{VA} := \frac{F_{x\_A} \cdot z_{VA\_H}}{w_{y\_VA}} = 120.5\ MPa$ bending stress in vertical arm below hub

$\sigma_{VM\_VA} := \gamma_f \cdot \sqrt{\sigma_{VA}^2 + 3 \cdot \tau_{VA}^2} = 163.6\ MPa$ equivalent Von Mises stress in vertical arm below hub (incl. load factor)

$u_{VA} := \frac{\sigma_{VM\_VA}}{\sigma_{cap}} = 0.53$ utilization of equivalent stress capacity in vertical arm below hub

Shaft bearing

$l_B := 90\ mm$ length of shaft bearing

$d_B := 455\ mm$ inner diameter of shaft bearing

$F_{x\_B} = 1230.8\ kN$ force applied radially to shaft bearing

$\sigma_B := \gamma_f \cdot \frac{F_{x\_B}}{l_B \cdot d_B} = 39.1\ MPa$ bearing pressure in shaft bearing (incl. load factor)

Shaft

Applied moments and force to the shaft are quite conservative to assume to act in the described matter. The two solid spline connection ends should also lead to significantly reduced stress in real loading conditions. This aspect were proved when calculating angle of twist.

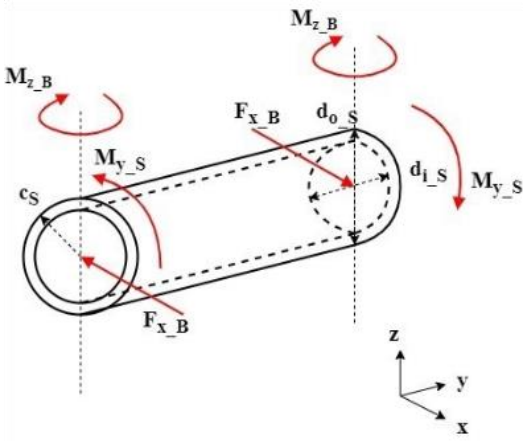

$M_{z\_B} = 184.6\ kN \cdot m$

applied bending moment on shaft

$M_{y\_S} = 858.7\ kN \cdot m$ applied torsional moment on shaft

$F_{x\_B} = 1230.8\ kN$ applied shear force on shaft

$D_S = 455\ mm$ outer diameter of central pipe section in shaft

$d_S = 387.4\ mm$ inner diameter of central pipe section in shaft

$c_S := \frac{D_S}{2} = 227.5\ mm$ max. distance to outer surface of shaft

$J_S = (2.0 \cdot 10^9)\ mm^4$ polar second moment of area in central pipe section of shaft

$I_S := \frac{\pi}{64} \cdot (D_S^4 - d_S^4) = (10.0 \cdot 10^8)\ mm^4$ second-area moment of central pipe section of shaft

$\tau_{max\_S} := \frac{M_{y\_S} \cdot c_S}{J_S} = 97.8\ MPa$ shear stress from torsional moment

$\sigma_{max\_S} := \frac{M_{z\_B} \cdot c_S}{I_S} = 42.1\ MPa$ equivalent stress from bending moment

$\sigma_{VM\_S} := \gamma_f \cdot \sqrt{\sigma_{max\_S}^2 + 3 \cdot \tau_{max\_S}^2} = 227.0\ MPa$ combined equivalent stress in shaft (incl. load factor)

$u_S := \frac{\sigma_{VM\_S}}{\sigma_{cap}} = 0.74$ utilization of equivalent stress capacity

A.3 Work Breakdown Structure and Gantt

A pre-study report was delivered to UiS supervisor in the beginning of the thesis work. Most of the sections are included in the introduction of this thesis. Hence, only the Work Breakdown Structure (WBS) and Gantt from the pre-study report are added in this appendix.

The project execution plan consists of an overview of the activities, constructed as a WBS and a Gantt chart for time-based distribution of the activities. WBS and Gantt chart are located in the next pages.

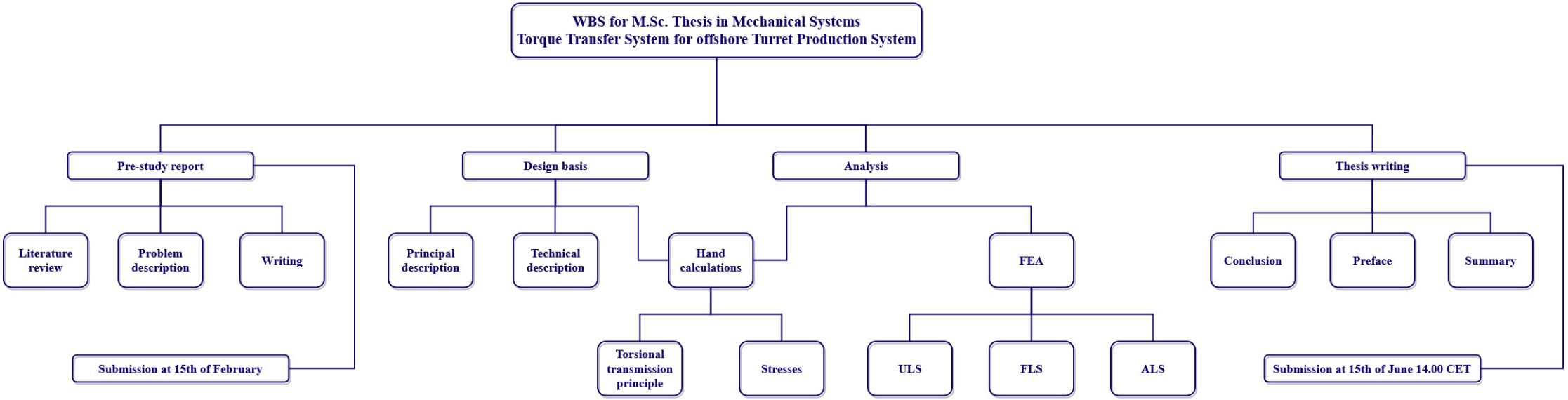
WBS for M.Sc. Thesis in Mechanical Systems
Torque Transfer System for offshore Turret Production System
Pre-study report
Literature review
Problem description
Writing
Submission at 15th of February
Design basis
Principal description
Technical description
Hand calculations
Torsional transmission principle
Stresses
Analysis
FEA
ULS
FLS
ALS
Thesis writing
Conclusion
Preface
Summary
Submission at 15th of June 14.00 CET

BW OFFSHORE

Gantt chart for M.Sc. in Mechanical Systems
Torque Transfer System for offshore Turret Production System

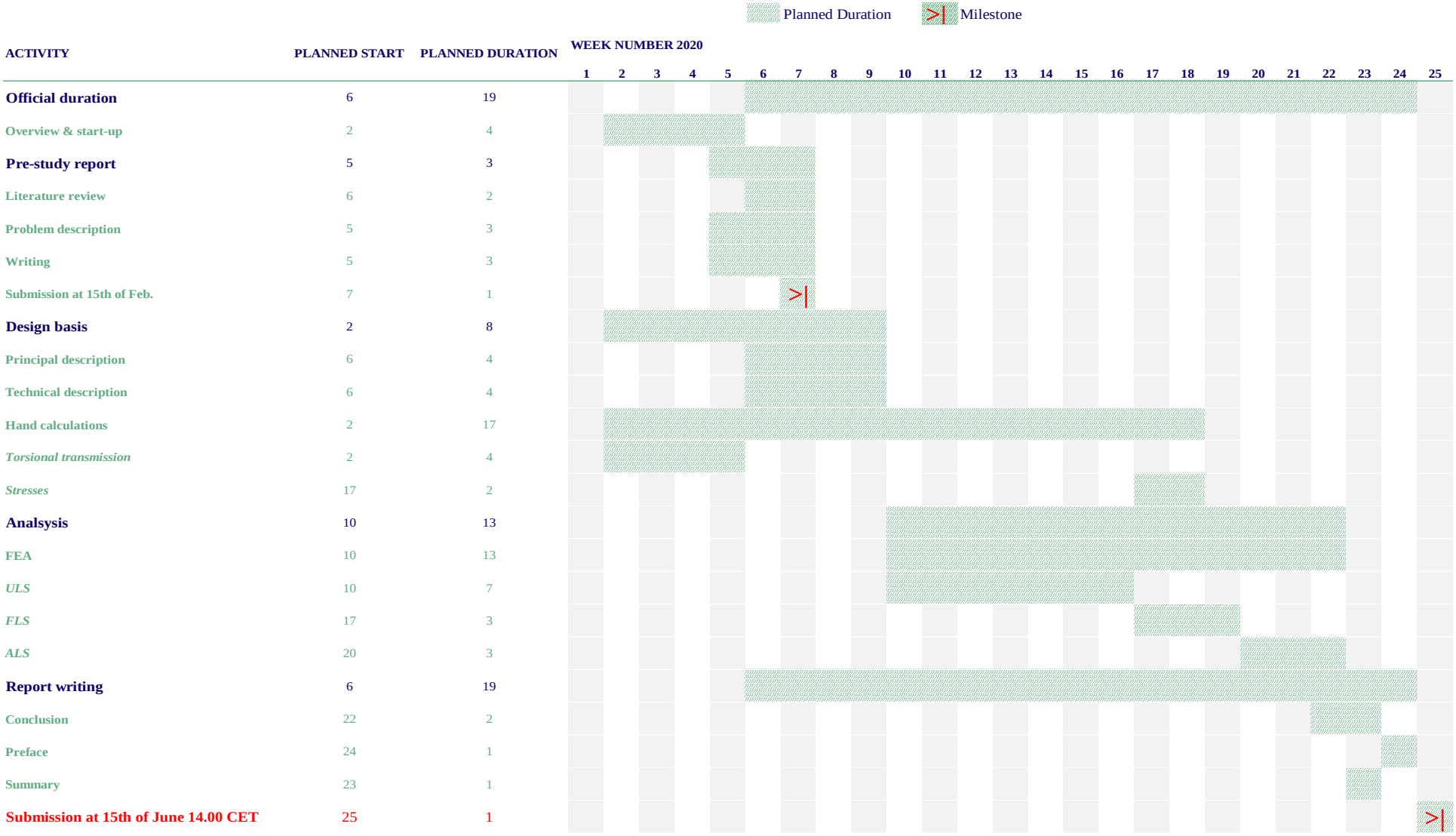

A.4 Drawing

The assembly drawing of the torque transfer system is added in the following page.

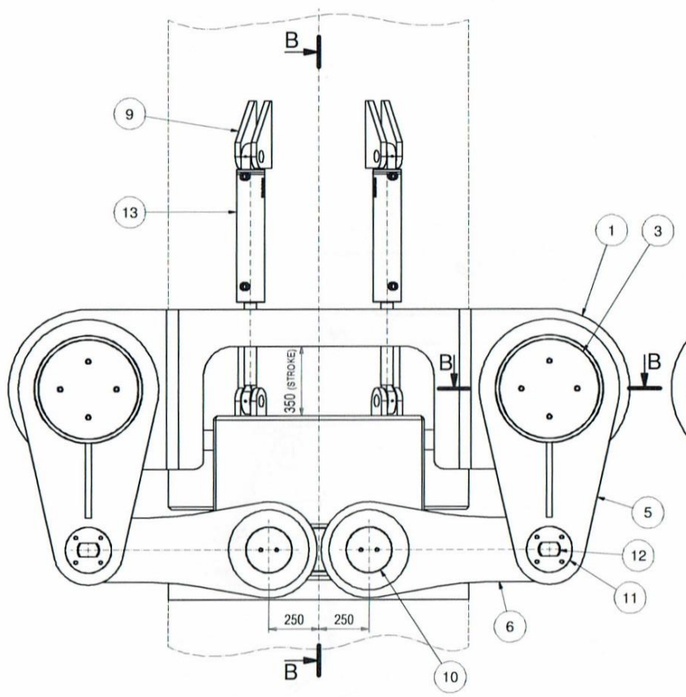

SIDE VIEW
SCALE (1 : 15)

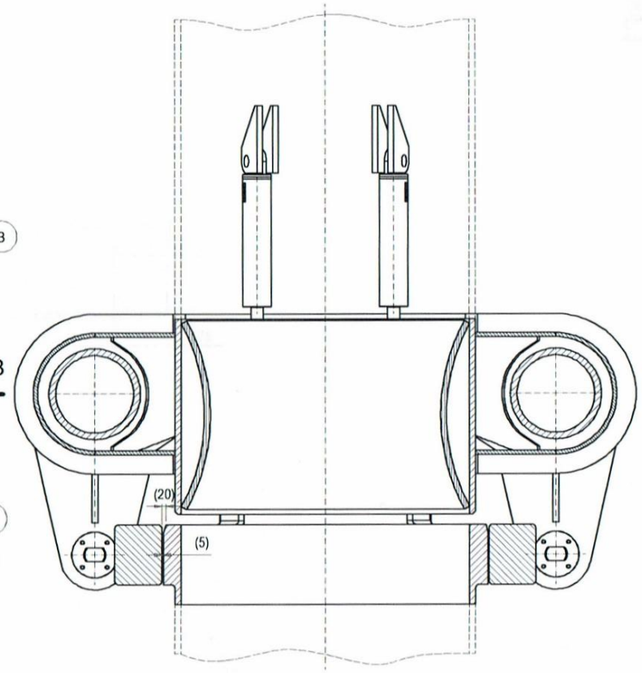

SECTION A-A
SCALE (1 : 15)

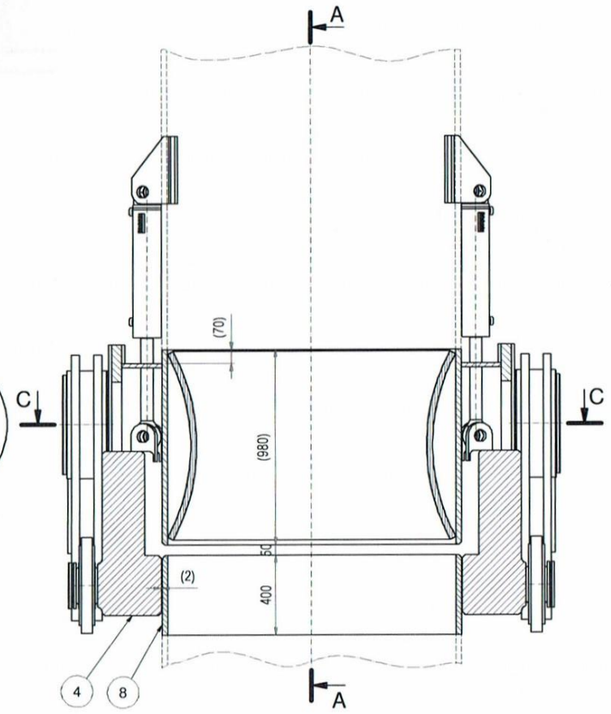

SECTION B-B
SCALE (1 : 15)

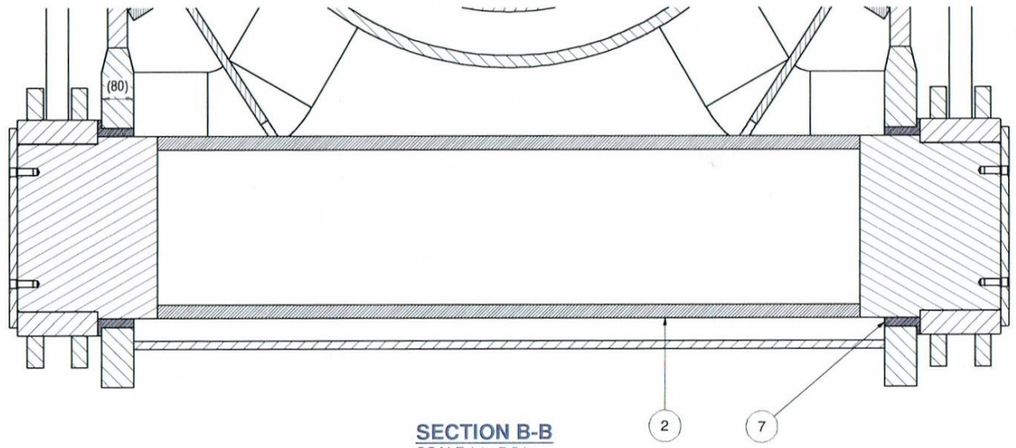

SECTION B-B
SCALE (1 : 7,5)

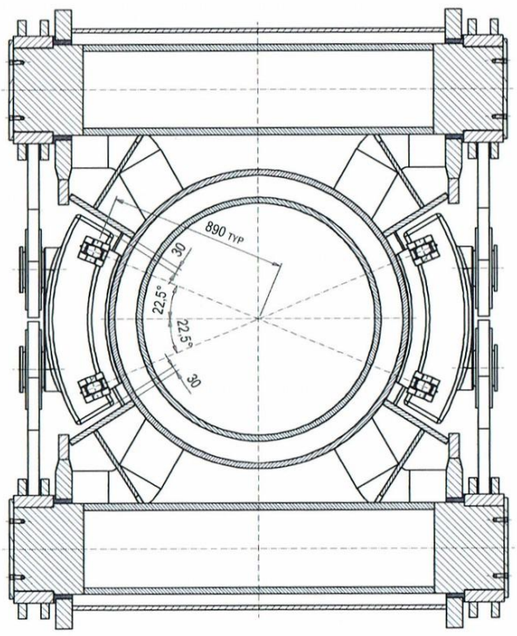

SECTION C-C
SCALE (1 : 15)

PRELIMINARY COPY

REFERENCE DRAWINGS:

Reference	Drawing Title	Drawing Number

1. FOR GENERAL INFORMATION SEE BW OFFSHORE DWG. No. XXXX-XX-00000000.00
2. ALL WELDS SHALL HAVE INSPECTION CATEGORY I UNO
3. ALL WELDS SHALL HAVE FULL PENETRATION UNO
4. ALL SHARP EDGES TO BE ROUNDED min. 2mm

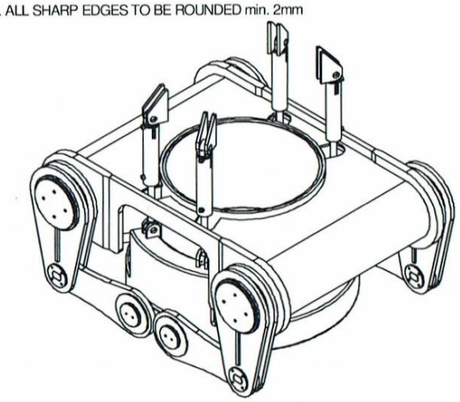

ISOMETRIC VIEW
N.T.S.

Item	Qty	Decription	Standard	Material	Dimension	Kg/Each
13	4	HYDRAULIC CYLINDER 125/60x200/526			Malm Orstad as	51 kg
12	4	BOLT Ø110 x 180	DNV	NVD 36		13 kg
11	8	REAR LOCKING PLATE	DNV	NVD 36		4 kg
10	4	FOREMOST LOCKING PLATE	DNV	NVD 36		5 kg
9	4	PADEYE FOR HYDRAULIC CYLINDER	DNV	NVD 36		22 kg
8	1	TORQUE TUBE, LOWER PART			SEA LION FEED_SKETCH-08	953 kg
7	4	TORQUE TRANSFER SHAFT BEARING			SEA LION FEED_SKETCH-07	30 kg
6	4	TORQUE TRANSFER HORIZONTAL ARM			SEA LION FEED_SKETCH-06	207 kg
5	4	TORQUE TRANSFER VERTICAL ARM			SEA LION FEED_SKETCH-05	434 kg
4	1	TORQUE TRANSFER, TORSION RING			SEA LION FEED_SKETCH-04	5359 kg
3	4	TORQUE SHAFT LOCKING PLATE			SEA LION FEED_SKETCH-03	31 kg
2	2	TORQUE TRANSFER SHAFT			SEA LION FEED_SKETCH-03	1410 kg
1	1	TORQUE TRANSFER STRUCTURE, ASSEMBLY			SEA LION FEED_SKETCH-02	5285 kg

Parts List

Surface roughness: ISO / IS 1302 Ra (µm)
Remove all burrs
Tolerance when not specified: WELDING NS-EN ISO 13920 BF; MACHINING NS-EN ISO 2768-mK; CASTING NS-EN ISO 8062-CT13
Fabrication Specification No.:
Standard Reference: Weld symbols: NS-ISO 2553
Coated According to:
Replacement For:
Replaced By:
Modified by: 103920anli Date: 02.12.2019
Total weight: N/A

Rev	Reason for Issue	Date	Drawn	Issued	Checked	Approved
A	ISSUED FOR INFORMATION	05.12.2019	ANLI		VIB1	ESHO

Discipline:	System No.:	Area/ Module:	IMO No.:	Project No.:	Scale:	Format Size:
				4430	AS NOTED	A1

Client: SEA LION PROJECT
Unit/ Field: SEA LION PHASE 1 FPSO
Subject: TORQUE TRANSFER DEVICE, ASSEMBLY
BWO Doc. No.: SEA LION FEED, SKETCH-01 Rev.: A Sheet:
Client Doc. No.:
Ref. Doc. No.: